Dynamic Modeling and Optimization of Cryogenic Air Separations Units

Dynamic Modeling and Optimization of Cryogenic Air Separations Units: Design and Operation Strategies

by

Yanan Cao, B.Eng.Mgt., M.A.Sc.

A Thesis
Submitted to the School of Graduate Studies
in Partial Fulfillment of the Requirements
for the Degree of
Doctor of Philosophy

McMaster University

DOCTOR OF PHILOSOPHY (2016) McMaster University
(Chemical Engineering) Hamilton, Ontario, Canada

TITLE:	Dynamic Modeling and Optimization of Cryogenic Air Separations Units: Design and Operation Strategies
AUTHOR:	Yanan Cao
	B.Eng.Mgt. (McMaster University, Hamilton, Ontario, Canada)
	M.A.Sc. (McMaster University, Hamilton, Ontario, Canada)
SUPERVISOR:	Dr. Christopher L.E. Swartz
NUMBER OF PAGES:	xv, 134

Abstract

In the air separation industry, cryogenic distillation is the dominant technology for separating large quantities of air into individual high purity component products. Due to the complexity of the process, in addition to significant energy input, air separation units (ASUs) also have high degrees of material and thermal integration and low process agility. As markets become more competitive and dynamic, especially after electricity market deregulation, ASUs can no longer practice mostly stationary operations, and are in need for design and control strategies to achieve high adaptability. In this study, we address such issues through a dynamic optimization framework. The use of rigorous dynamic models is important for developing economically beneficial designs and operating practices.

The first part of this study focuses on the modeling aspect. For the column section of the plant, a full-order stage-wise model and a collocation based reduced order model are proposed. Model size, simulation time and predication accuracy are compared. For the primary heat exchanger, a novel moving boundary model is derived to handle the phase change in such a multi-stream heat exchanger. Simulation results demonstrate the capability of the proposed model in tracking the boundary points of the phase change occurrence, as well as the potential pinch point, along the length of the heat exchanger.

The second part of the study addresses the operation aspects of ASUs through conducting dynamic optimization studies with collocation based dynamic models. We first performed a comprehensive analysis for a storage-then-utilization strategy on a nitrogen plant, following a two-tier multi-period formulation. As the parameter varies with time, the plant collects liquid, either directly from liquid product or by liquefaction of overproduced gas product, and then redistributes it for meeting gas product demand or as additional reflux. Effects of electricity price and demand profiles, additional operation costs, as well as product specifications are explored. Then we investigated the economic incentive for employing preemptive actions on a super-staged argon system, which allows the plant to take actions before external

changes arrive. In the evaluation, changes are in the gas oxygen product demand. During the preemptive period, the plant takes either a single set or multiple sets of control actions. In the demand increase case, operation degrees of freedom are introduced to or removed from the set of decision variables. The demand decrease scenarios are explored with an under-supplied or saturated liquid oxygen market.

Acknowledgments

I wish to express my gratitude first to my supervisor, Dr. Christopher Swartz, for his continued support, advice and guidance throughout the course of this research. This thesis would certainly not be possible without his vision and direction.

I would also like to thank Dr. Thomas Adams and Dr. Antoine Deza for being on my doctoral committee. Their questions, comments, and suggestions during our meetings have triggered my thoughts and enhanced the quality of this research.

I wish to acknowledge everyone in McMaster Advanced Control Consortium and the Department of Chemical Engineering at McMaster University. Their encouragement, support and friendship over the years are invaluable.

Thanks also go to the industrial partner, Praxair, Inc., for graciously providing the key motivation for and continued participation in this project. Special thanks go to Jesus Flores-Cerrillo, Jingran Ma and Sujit Jogwar for their insights and suggestions.

This thesis is dedicated to my family. I am grateful for the personal sacrifice they have made to provide me an environment where I could pursue my goal. This work is as much a product of their efforts as mine.

Table of Contents

1 Introduction **1**

1.1 Motivation and Goals 1

1.2 Main Contributions 4

1.3 Thesis Outline 5

References 6

2 Dynamic Modeling and Collocation-Based Model Reduction of Cryogenic Air Separation Units **11**

2.1 Introduction 12

2.2 Literature Review 14

2.3 Cryogenic Distillation Model 18

2.4 Multi-stream Heat Exchanger Model with Phase Change 25

2.5 Results and Discussion 30

2.6 Conclusions 43

References 44

3 Optimal Dynamic Operation of a High Purity Air Separation Plant under Varying Market Conditions **51**

3.1 Introduction 52

3.2 Process Model 56

3.3 Optimization Problem Formulation 59

3.4 Case studies: scheduling under time-varying prices and demand 68

3.5 Conclusion 86

References 87

4 Reactive and Preemptive Responses in the Operation of Cryogenic Air Separation Units **91**

4.1 Introduction 92

4.2 Operational Studies on Air Separation Units 95
4.3 Process Model 97
4.4 Optimization Problem Formulations 99
4.5 Results and Discussion 104
4.6 Conclusion 124
References 125

5 Conclusions and Future Work **129**
5.1 Concluding Remarks 129
5.2 Future Work 131

Notation **133**

List of Figures

1.1 Process diagram for a cryogenic air separation plant that produces argon, oxygen and nitrogen. PHX = Primary Heat Exchanger; LC = Lower Column; UC = Upper Column; LRC = Lower-Ratio Column; SSC = Super-Staged Column. The dashed line highlights the cold box section of the process. 3

2.1 Collocation grid 22

2.2 Collocation profile 22

2.3 O_2 liquid phase composition profile in the lower column. 25

2.4 Graphical illustration of the moving boundary approach 26

2.5 Illustration of segment numbering and stream flow directions in MSHX model 27

2.6 Temperature and pressure profiles of the upper column in the integrated column model after the model validation: measurements–OTS (- -) and predictions–gPROMS (—). 32

2.7 Steady-state vapor phase N_2 composition profile in the collocation section of the lower column: full order stage-wise model (—) vs. collocation model (•). The N_2 composition is scaled relative to that on the bottom tray of the collocation section ($y^B_{N_2}$). 34

2.8 Parts per million oxygen (PPMO) level in the liquid argon product in response to an increase in the vapor inlet flow rate with the SSC model only: full order stage-wise model (—) vs. collocation model (•). 35

2.9 Temperature profiles of hot air (—) and boiling O_2 (- •-) from stage-wise (left) and fractional length (right) views. Locations of the boundary points in the fractional length view are defined by the value of f_{SH}, f_{TP}, and f_{SC}. 36

2.10 Hot air stream temperature profile with stage-wise model (—) and collocation based model (•). 37

2.11 Dynamic response to a negative step change in the gas O_2 stream: (a) O_2 content in the crude argon feed with: the column section only model (—) and with the integrated cold-box model (...); (b) fractional length of the superheated section in the heat exchanger. 39
2.12 Dynamic response to a positive step change in the waste N_2 stream: (a) O_2 content in the crude argon feed; (b) fractional length of the superheated section in the heat exchanger. 40
2.13 Dynamic response to a positive pulse change in the gas O_2 stream flow rate: (a) N_2 content in the crude argon feed (—) and crude argon flow rate (...); (b) fractional length of the superheated section in the heat exchanger. 42
2.14 Dynamic response of upper column N_2 and temperature profile to a positive pulse change in the gas O2 stream flow rate 43
2.15 Dynamic response of O_2 content in the waste nitrogen stream in response to a negative step change in the vapor air feed to the LC. 44

3.1 Case study ASU configuration (solid lines are existing streams with the base case plant design and dashed lines are streams available with design modifications). 60
3.2 Illustration of the control profile 62
3.3 Different approximations for piecewise constant input profile. 67
3.4 Example electricity and demand profile for the operational planning study. Two different sets of times, $\mathbf{t} = [t_0, t_1, t_2, t_3, t_4]$, are used in the study. The demand has a 10 % increase during the second change period unless otherwise specified. Starting from a nominal value ($P_{\text{elec}}^{\text{nominal}}$), the electricity price first decreases to ($P_{\text{elec}}^{\text{min}}$) then increases to ($P_{\text{elec}}^{\text{peak}}$) before returning to the nominal value. 69
3.5 Optimal trajectories for selected variables in scaled values for Scenario S1.2 using economic objective function (tier 1). 72

3.6 Optimal solution for Scenario S1.2 after move suppression (tier 2). Corresponding tier 1 solution is presented in Fig. 3.5. 73
3.7 Optimal trajectories for selected variables in scaled values Scenario S1.3. . . . 77
3.8 Optimal trajectories for selected variables in scaled values for Scenario S1.4. . 78
3.9 Reboiler drain flow rate and reboiler level for S1.3 (subfigs. a and b) and S1.4 (subfigs. c and d). 79
3.10 Optimal trajectories for selected variables in scaled values for Scenarios S2.1 and S2.2. 83
3.11 Optimal trajectories for selected variables in scaled values for Scenarios S2.4 and S2.5. 84
3.12 Optimal trajectories for selected variables in scaled values for Scenario S2.6. . 86

4.1 Simplified process diagram with system inputs and outputs used in the optimization study. Detailed argon plant configuration is shown in Fig. 1.1. 99
4.2 Input action categorization and lead-time definition. 105
4.3 Trajectories of selected variables for the reactive case under a 10 % GO_2 demand increase, reported in scaled values. 107
4.4 Improvement in the profitability with increasing lead time. Single action - one set of sustained preemptive actions regardless of the length of the lead time. Multiple actions - multiple actions with one set of control actions per Δt during the preemptive period. Lead time = 0 represents the result from the reactive controls (Benchmark Scenario 1). 110
4.5 Trajectories of selected variables for the preemptive case with LT $= 5\Delta t$ under a 10 % GO_2 demand increase, reported in scaled values. SA = single set of preemptive actions; MA = multiple sets of preemptive actions; LB = lower bounds; UB = upper bounds. 111
4.6 Improvement in the profitability with increasing lead time, with and without inventory set-point manipulation. Lead time = 0 represents the result from the reactive controls (Benchmark Scenario 1). 113

4.7 Trajectories of selected variables for the preemptive case (MA with LT $= 2\Delta t$) under a 10 % GO_2 demand increase, reported in scaled values. The optimal solution is indicated by the solid line (–). The dashed line (- -) shows the simulation result with the optimal solution except for use of constant liquid level set-points. 114
4.8 Trajectories of selected variables for reactive case under a 10 % GO_2 demand increase, reported in scaled values with and without feed rate changes. Liquid split = without feed flow rate changes. 118
4.9 Trajectories of selected variables for preemptive cases under a 10 % GO_2 demand increase without feed flow rate change, reported in scaled values. . . 119
4.10 Trajectories of selected variables with preemptive controls (LT = $6\Delta t$) in response to a 10 % GO_2 demand decrease (under-supplied liquid market), reported in scaled values. 121
4.11 Trajectories of selected variables with reactive and preemptive control in response to a 10 % GO_2 demand decrease (saturated liquid market), reported in scaled values. 123

List of Tables

2.1 Product purities in the integrated column model after the model validation. . 31

2.2 Liquid inventories in the integrated column model after the model validation. 31

2.3 Model reduction results with the collocation based method (simulations are performed in gPROMS). 34

2.4 Average percent errors in the stream outlet temperature (in Kelvin) after model validation. 37

3.1 Potential decision variables. 61

3.2 Piecewise constant control profile setup. 61

3.3 Constraints in the study. 63

3.4 Scenarios with different values of process parameters used in the vaporization study (Case 1) 71

3.5 Optimization results for the vaporization scenarios with different values of process parameters compared to the corresponding reference cases (Table 3.4). 80

3.6 Scenarios with different values of process parameters used in the reflux study (Case 2) 81

3.7 Optimization results for the reflux scenarios with different values of process parameters compared to the corresponding reference cases. 82

4.1 Optimization Problem Constraints 104

4.2 Profitability vs Lead Time for 10 % Increase in GO_2 Demand without Feed Flow Rate Changes 117

4.3 Profitability vs Lead Time for 10 % Decrease in GO_2 Demand in Under-Supplied LO_2 Market 120

4.4 Profitability vs Lead Time for 10 % decrease in GO_2 demand in Saturated Liquid Market 124

Chapter 1

Introduction

1.1 Motivation and Goals 1
1.2 Main Contributions 4
1.3 Thesis Outline 5
References 6

This chapter outlines and defines the research problem and further highlights the solution path taken. The research goals and contributions are also stated.

1.1 Motivation and Goals

Air separation based on cryogenic distillation technology is the primary choice for producing large qualities of high purity oxygen, nitrogen and argon products in both liquid and gaseous forms. These products have critical roles in a variety of industries, which impact our daily life either directly (e.g. portable oxygen therapy system in healthcare) or indirectly (e.g. CO_2 capture through oxy-fuel combustion in coal-derived power generation) [1–3]. In order to separate ambient air into different components, air intake needs to go through compression, purification, cooling and distillation steps as shown in Fig. 1.1: a complex and power-intensive process. The consequence of such a plant configuration is that air separation units (ASUs) suffer from three operational issues:

- Costly compression – A significant amount of energy is required to compress air to a high pressure for the downstream separation. The total energy consumed in 2010 by the U.S. industrial gas suppliers was 19.4 TWh, approximately equivalent to an

electricity bill of $ 1 billion dollars or a year-round electricity usage of 1.77 million homes [4].

- Low flexibility – Since separation of air components occurs at extreme cold temperature (i.e. -190 to -170 ^{o}C), refrigeration recovery is achieved through heat exchange of different process streams. Such thermal integration removes operational degrees of freedom and makes the already complex flow network even less flexible.

- Inadequate agility – When the impurity in the end product is required to be at parts per thousand or million levels, large distillation columns with significant numbers of stages are needed. The liquid holdup in these columns introduces prolonged delays in the response dynamics.

Due to the above mentioned process characteristics, ASUs favor production with infrequent changes. However, such an operation strategy is challenged by the increasingly transient and competitive market [5, 6]. The changing landscape in power generation, distribution and management is one of the key drivers for ASUs to seek for adaptability in the process. Under the circumstances of time-sensitive electricity pricing, ASUs are motivated to practice demand response (DR) operations, such as voluntarily adjusting the production schedule and using liquid inventory as a buffer or cryogenic energy storage in accordance to the forecasted or negotiated electricity price pattern [7–9]. In addition to variation on the supply side, demands of different products are also more volatile in a dynamic market. In other words, the transition to agile and flexible processes is an inevitable trend in ASUs or more general, the entire manufacturing industry.

The desired agility and flexibility, on the other hand, can be achieved through either improving operations or re-engineering the process [10]. In the field of air separation, to assist the transition towards a highly adaptable process, several studies have been conducted to understand the dynamic behavior, to optimize operation strategies, and to evaluate design modifications. Studies on process agility illustrate the importance of process dynamics on

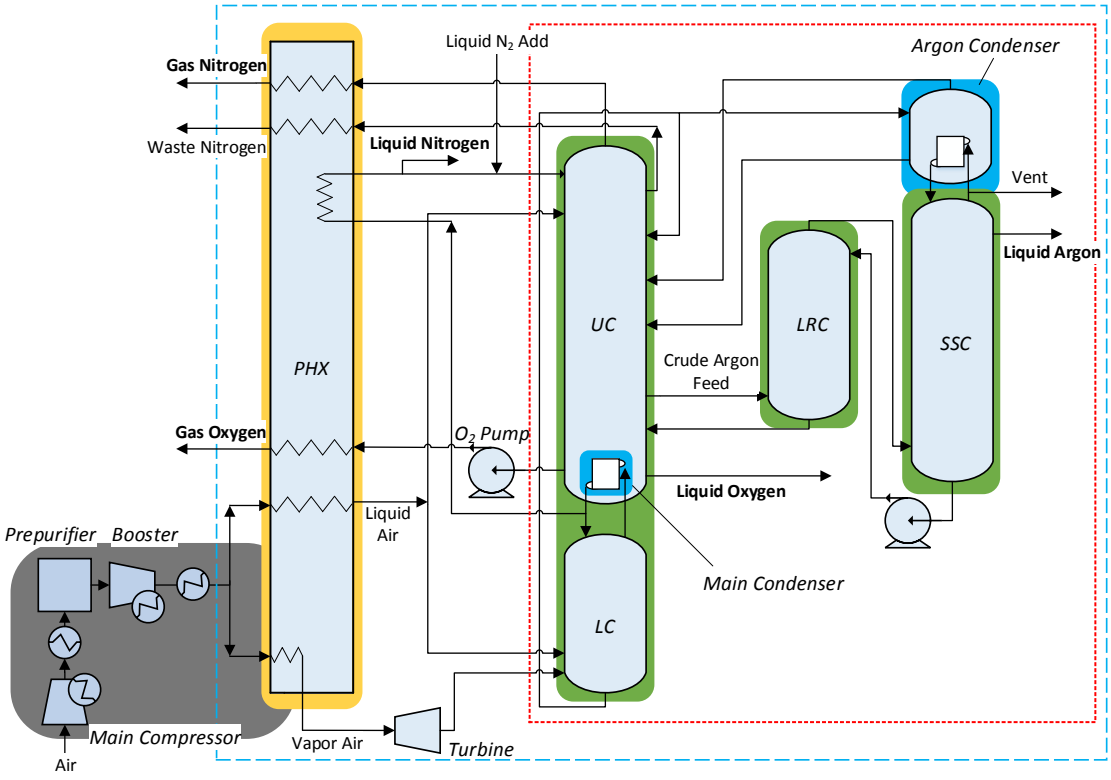

Figure 1.1: Process diagram for a cryogenic air separation plant that produces argon, oxygen and nitrogen. PHX = Primary Heat Exchanger; LC = Lower Column; UC = Upper Column; LRC = Lower-Ratio Column; SSC = Super-Staged Column. The dashed line highlights the cold box section of the process.

determining the best practice to operate the plant involving single transitions, including analyzing process switchability [11], speeding up plant startup [5] and debottlenecking limiting factors for plant operations [12]. Design modifications proposed in these studies include using a storage vessel for collecting and redistributing liquid for startup [5] and introducing liquid as additional reflux during transitions [12]. Meanwhile, scheduling and planning problems typically introduce multiple time steps with time-sensitive process parameters (i.e. electricity price and/or product demand). The main focus of these studies is typically DR type of operations under time-of-use or real-time electricity pricing [8, 13–16]. Discrete operation events, such as plant startup and shutdown, are considered only in the long term planning studies due to the transition time and effort involved [14–16]. A few of the studies consider dynamic and uncertain market conditions: electricity price [14], product

demand [2, 13, 17] or energy reserve demand, when liquid storage acts as cryogenic energy storage (CES) [9]. Design modifications evaluated include using liquid storage to buffer variations in liquid demand [2, 9] and gas demand [8, 9], or to act as CES so that ASU can sell electricity back to the energy reserve market [9]. However, except in the work done by Pattison and co-workers [8], process dynamic behavior, identified as critical in the agility studies, are commonly not accurately captured in the scheduling and planning studies.

This research is motivated by the need in the air separation industry to transition towards agile and flexible processes while considering limitations due to process dynamics. This requires understanding not only where to go (i.e. future optimal operation points defined based on certain criteria), but also how to get there (i.e. inclusion of accurate representation of process dynamics) and what needs to be done to assist (i.e. design retrofit). Our work aims to provide insights on dynamic operations of the ASU, and towards closing the gap between the current process status and the inevitable trend in the manufacturing industry. Our proposed approach involves systematically solving dynamic optimization problems to address subjects of short term scheduling and intentionally dynamic operations. The foundation of the project is developing a rigorous mathematical representation of the process that is suitable for the proposed framework.

1.2 Main Contributions

The main novel contributions of this work include:

1. High fidelity dynamic models for cryogenic distillation columns in air separations units using stage-wise and collocation based formulations - a foundation for the proposed optimization framework
2. Moving boundary model for multi-stream heat exchanger with one process stream undergoing phase change - a novel approach for handle phase change in

a multi-stream heat exchanger

3. Short term scheduling with the storage-then-utilization strategy under varying market conditions - a comprehensive analysis on economic incentives for practicing such an operation policy

4. Preemptive action in the operation of air separation units - a motivating study on the subject of intentional dynamic operations of ASUs

Additional, three different formulations are proposed and compared for solving move suppression problems using the sequential approach of dynamic optimization.

1.3 Thesis Outline

This thesis is organized according to the following chapters:

In Chapter 2, we present our first two contributions focusing on developing rigorous dynamic models for multi-product air separation units with a plant configuration shown in Fig. 1.1. The focus is on the cold box section of the plant, including PHX, LC, UC, LRC, SSC, main condenser, argon condenser, turbine and O_2 pump. Identified modeling challenges together with proposed solutions are explained. For the column section of ASUs, vapor liquid equilibrium based, first principles dynamic model are developed in stage-wise form. A multi-stream heat exchanger with phase change is represented through a moving boundary approach. Model size reductions are conducted through a multiple finite element collocation approach. Dynamic simulation studies are conducted to verify the accuracy of the proposed model.

In Chapter 3, we present our third contribution. The focus is on evaluating the storage-then-utilization strategy in the operation of ASUs through a two-tiered approach: economic based optimization followed by move suppression. An ASU that produces only N_2 products is used here. The plant configuration is similar to the one in Fig. 1.1. However, instead of the multi-

column arrangement, the process has only a single cryogenic distillation column. Detailed mathematical representations for compressor, turbine, PHX, column and integrated-reboiler condenser are included. The PHX and column models used here are reduced order dynamic models following the collocation approach proposed in Chapter 2. Dynamic optimization problems are formulated in order to determine the economically optimal operations policy under time-sensitive electricity and product demand, considering the process dynamics. Three formulations, trajectory tracking, hyperbolic function approximation and approximation using valve dynamics, are proposed for the move suppression layer.

In Chapter 4, we present our last contribution which focuses on evaluation of the intentionally dynamic operation strategy for an argon plant (Fig. 1.1) subject to demand changes in both positive and negative directions. The integrated cold box model developed in Chapter 2 is embedded in the optimization study. Preemptive actions are evaluated under various operation principles, leveraging full or partial sets of the current system inputs or introducing additional ones, and different assumptions of market conditions, under-supplied or saturated liquid market.

In Chapter 5, we highlight the major findings and emphasize the main contributions to this area of study. Furthermore, future directions are discussed and our proposed next steps are laid out.

Bibliography

[1] A. R. Sirdeshpande et al. “Process synthesis optimization and flexibility evaluation of air separation cycles”. In: *AIChE Journal* 51.4 (2005), pp. 1190 –1200 (cit. on p. 1).

[2] Y. Zhu, S. Legg, and C. D. Laird. “Optimal operation of cryogenic air separation systems with demand uncertainty and contractual obligations”. In: *Chemical Engineering Science* 66.5 (2011), pp. 953 –963 (cit. on pp. 1, 4).

[3] J. D. Figueroa et al. “Advances in CO_2 capture technology - The U.S. Department of Energy’s Carbon Sequestration Program”. In: *International Journal of Greenhouse Gas Control* 2.1 (2008), pp. 9 –20 (cit. on p. 1).

[4] U.S. Energy Information Administration. *Manufacturing energy consumptionsurvey*. Online. Available at: http://www.eia.gov/consumption/data.cfm. 2012 (cit. on p. 2).

[5] J. Miller et al. “Improving agility of cryogenic air separation plants”. In: *Industrial & Engineering Chemistry Research* 47.10 (2008), pp. 394 –404 (cit. on pp. 2, 3).

[6] G. Y. Zhu, M. A. Henson, and L. Megan. “Low-order dynamic modeling of cryogenic distillation columns based on nonlinear wave phenomenon”. In: *Separation and Purification Technology* 24 (2001), pp. 467 –487 (cit. on p. 2).

[7] US Department of Energy. *Benefits of demand response in electricity markets and recommendations for achieving them*. A Report to the United States Congress Pursuant to Section 1252 of the Energy Policy Act of 2005. 2006 (cit. on p. 2).

[8] R. Pattison et al. “Optimal process operations in fast-changing energy markets: Framework for scheduling with low-order dynamic models and an air separation application”. In: *Industrial & Engineering Chemistry Research.* 55.16 (2016), pp. 4562 –4584 (cit. on pp. 2–4).

[9] Q. Zhang et al. “Air separation with cryogenic energy storage: Optimal scheduling considering electric energy and reserve markets”. In: *AIChE J.* 61.5 (2015), pp. 1547–1558 (cit. on pp. 2, 4).

[10] T. Backx, O. Bosgra, and W. Marquardt. “Towards intentional dynamics in supply chain conscious process operations”. In: *Proceedings of Third International Conference on Foundations of Computer-Aided Process Operations*. Ed. by J. F. Pekny, G. E. Blau, and B. Carnahan. American Institute of Chemical Engineers. Snowbird, Utah, 1998, pp. 5–20 (cit. on p. 2).

[11] V. White, J. D. Perkins, and D. M. Espie. “Switchability analysis”. In: *Computers & Chemical Engineering* 20.4 (1996), pp. 469 –474 (cit. on p. 3).

[12] Y. Cao et al. “Optimization-based assessment of design limitations to air separation plant agility in demand response scenarios”. In: *Journal of Process Control* 33 (2015), pp. 37 –48 (cit. on p. 3).

[13] Y. Zhu, S. Legg, and C. D. Laird. “A multiperiod nonlinear programming approach for operation of air separation plants with variable power pricing”. In: *AIChE Journal* 57.9 (2011), pp. 2421 –2430 (cit. on pp. 3, 4).

[14] M. G. Ierapetritou et al. “Cost minimization in an energy-intensive plant using mathematical programming approaches”. In: *Industrial & Engineering Chemistry Research* 41.21 (2002), pp. 5262 –5277 (cit. on p. 3).

[15] M. H. Karwan and M. F. Keblis. “Operations planning with real time pricing of a primary input”. In: *Computers & Operations Research* 34.3 (2007), pp. 848 –867 (cit. on p. 3).

[16] S. Mitra et al. “Optimal production planning under time-sensitive electricity prices for continuous power-intensive processes”. In: *Computers & Chemical Engineering* 38 (2012), pp. 171 –184 (cit. on p. 3).

[17] S. Mitra, J. M. Pinto, and I. E. Grossmann. “Optimal multi-scale capacity planning for power-intensive continuous processes under time-sensitive electricity prices and demand uncertainty. Part I: Modeling”. In: *Computers & Chemical Engineering* 65.0 (2014), pp. 89 –101 (cit. on p. 4).

Chapter 2

Dynamic Modeling and Collocation-Based Model Reduction of Cryogenic Air Separation Units

2.1 Introduction 12
2.2 Literature Review 14
2.3 Cryogenic Distillation Model 18
2.4 Multi-stream Heat Exchanger Model with Phase Change 25
2.5 Results and Discussion 30
2.6 Conclusions 43
References 44

High purity distillation columns and multi-stream heat exchangers are critical units in cryogenic air separation plants. This chapter focuses on modeling approaches for the primary section of a super-staged argon plant. A full-order stage-wise model (FOSM) for distillation columns in air separation units (ASUs) that considers key process phenomena is presented, followed by a reduced-order model using a collocation approach. The extent of model reduction that can be achieved without losing significant prediction accuracy is demonstrated. A novel moving boundary model is proposed to handle multi-stream heat exchangers with phase change. Simulation results demonstrate the capability of the proposed model for tracking the phase change occurrence along the length of the heat exchanger. Dynamic simulation studies of the integrated plant show that the thermal integration between the feed and product streams captured in the primary heat exchanger is critical to accurately capture the behavior of ASUs.

Note, portions of this chapter were published in the journal article:

Y. Cao, C.L.E. Swartz, J. Flores-Cerrillo and J. Ma "Dynamic Modeling and Collocation-Based Model Reduction of Cryogenic Air Separation Units". In: *AIChE Journal*, 2016. 60 (9), 1602–1615.

2.1 Introduction

Cryogenic air separation plants are used to produce large quantities of high purity nitrogen, oxygen and argon products in both gaseous and liquid forms for various industries [1]. The cold-box section of such plants, comprising distillation columns operating at -170 to -190 ^{o}C, multi-stream heat exchangers, and ancillary equipment, forms the core of the process. An air separation plant producing multiple products (Fig. 1.1) usually has double or triple column arrangements. As in ordinary distillation processes, the cryogenic distillation separates air components utilizing differences in components' boiling points. Air drawn from the atmosphere goes through compression and purification prior to being introduced at different locations of the upper and lower columns (UC and LC). These columns operate at different pressures (i.e. at approximately 0.13-0.14 MPa and 0.68-0.69 MPa, respectively). Along the path, necessary refrigeration and expansion are provided according to the feed location. As N_2 is the most volatile component, it is concentrated in the overhead products of both the UC and LC. The oxygen product stream is drawn from the bottom of the UC. The boiling point of Ar is between that of O_2 and N_2, and is recovered in the argon columns operating around 0.13 MPa. To achieve this, a vapor side stream is drawn from the UC, close to the composition peak of argon, and is supplied to the argon section [2, 3]. As shown in Fig. 1.1, the multi-product cryogenic air separation process exhibits high degrees of thermal and material integration, primarily through the double-effect distillation columns and the primary heat exchanger. This integration, together with the the high purity requirements, makes operation and design of air separation units (ASUs), especially argon plants, challenging tasks.

ASUs suffer from high operating costs due to energy usage during feed air compression and product liquefaction. Although the total electricity consumption of industrial gas producers reduced from 31,460 million kWh in 1998 to 19,401 million kWh in 2010, it still accounted for more than 2.6 % of the electricity consumption of the entire manufacturing industry in the U.S., which translates into an annual electricity cost of approximately $ 1 billion [4]. In recent decades, fluctuations and uncertainty in electricity price and demand, resulting from electricity price deregulation, has triggered fundamental changes in the operation of ASUs. Being able to respond to the dynamic market conditions in a rapid and economically optimal manner is of significant importance, as small improvements can translate into substantial savings. Meanwhile, advances in CO_2 capture technologies, such as pre-combustion and oxy-fuel systems in coal-derived power generation, also rely on improvements in air separation processes. Cost effective operation to produce large quantities of high purity O_2 products with the capability of compensating for potential demand changes is essential to fully capture the economic benefit of these technologies [5]. These factors motivate research on design and operation of ASUs with detailed first-principles dynamic models, toward seizing the above mentioned opportunities. Since ASUs are subject to frequent load changes under the above described operating environment, roles of such models are to not only accurately represent steady-state operation, but also capture the dynamic behavior of the plant. As observed in a previous study, certain operational constraints are active only during transitions and can be revealed only with detailed dynamic models [6, 7].

This chapter focuses on modeling and simulation of the cold-box section of an argon plant, including 4 distillation columns, a multi-stream heat exchanger, 2 integrated reboiler/condenser systems, a turbine and a pump. The column and heat exchanger models will be described in detail. This work is the foundation for our long-term objective of performing optimization studies to explore design and operation of ASUs. Key contributions include (i) construction of a highly accuracy stage-wise model for the column section of an argon plant that accounts for key process phenomena, (ii) development of reduced-order distillation column and heat

exchanger models through collocation on finite finite element approaches, and (iii) proposal of a moving boundary approach for modeling multi-stream heat exchangers with phase change.

The remainder of this chapter is organized as follows. First, we briefly review studies conducted on modeling and simulation of ASUs appearing in the literature. This is followed by proposed stage-wise and reduced order distillation column models and a moving boundary heat exchanger model. Model validation and simulation results are documented in the result section. Finally, concluding remarks on our current work that highlights the benefits of the proposed model approaches and future research plans are presented.

2.2 Literature Review

2.2.1 Distillation Column Modeling in ASUs

Equation oriented distillation column models used in studies on ASUs, including N_2 and multi-product plants, can be classified into three categories: simplified, detailed first-principles and reduced-order models. Empirical/surrogate models belong to the first group. Such models have been playing an important role in design and operation studies of ASUs. These include Trierweiler and Engell's investigation on control structure selection [8], Li and coworkers's proposal on applying a real time optimization technique to improve ASUs' profit margin [9], Ierapetritou and coworker's study on operation and planning under electricity price uncertainty with operation mode switching [10], Sirdeshpande and coworker's research on flowsheet synthesis for flexibility over a range of operation conditions [11], Miller and coworkers' evaluation of intermittent operation policy under different peak-to-minimum electricity price ratios [12], as well as Mitra and coworkers' exploration in the area of capacity/design and operation planning under hourly varying electricity price with deterministic and stochastic demands [13, 14]. The empirical/surrogate models used in these studies are

typically derived from simulation results or historical data and are in the form of linear or nonlinear correlations between the selected system input and output variables. The simplified models are cost-effective while making high-level strategic decisions. However, their accuracy and information availability may limit their application in areas such as operation bottleneck identification and fundamental equipment design. In addition, these models are not able to capture accurate dynamic behavior of the process, even though in some cases, additional logic or constraints are introduced to handle operation mode transitions [10, 12–14].

An alternative way of modeling distillation columns in ASUs follows the conventional full-order stage-wise model (FOSM) approach [2, 3, 7, 15]. FOSMs usually consist of material and energy balances, tray hydraulics, thermodynamic correlations, pressure drop profiles and other physical properties. FOSMs can either be steady state or dynamic. The dynamic version includes stage-by-stage dynamic material balances in the form of ordinary differential equations (ODEs) with either dynamic or pseudo steady-state energy balances. When dynamic energy balances are used, depending on the modeling assumptions, the resulting differential algebraic equation (DAE) system could be of high-index, making the column simulation even more challenging [1, 16, 17]. When a high-index distillation column model is obtained, index reduction procedures are available and have been successfully demonstrated in ASUs studies [16, 17]. FOSMs have been adopted in design, control and operation studies of ASUs. Subjects that have been addressed include (1) design retrofit and corresponding operation strategies [3, 7], (2) control structure analysis including multivariable and model predictive control [15, 16], (3) operation bottleneck identification [7], (4) design and operation under uncertainty [2, 18, 19], as well as (5) flowsheet optimization [20]. Despite its capability, for a column of N_{tray} stages and N_{comp} components, a FOSM generally consists of $N_{\text{tray}} \times N_{\text{comp}}$ differential material equations. When dynamic energy balances are used, additional N_{tray} ODEs are introduced. Hence, detailed models of ASUs are high-order in nature and typically lead to large-scale optimization problems, which are challenging to solve and not readily amenable to incorporation of situations such as equipment start-up

or shutdown [13]. In addition, the thermal coupling captured in FOSMs of ASUs, such as through the integrated reboiler/condenser at the bottom of the UC and in the argon section, amplifies the complexity and simulation difficulty of the distillation model in ASUs [21].

Considering the limitations of simplified models and FOSMs, researchers have been exploring alternatives to reduce the model complexity without losing steady-state and dynamic prediction accuracy. Wave theory, compartmentalization and collocation methods are three popular modeling techniques that have been investigated [22]. Among the three approaches, to the best of our knowledge, only nonlinear wave theory and compartmentalization have been applied to ASUs. Studies using reduced-order models of ASUs have mainly focused on concept demonstration and the control/operation side of the process, such as nonlinear model predictive control (NMPC) design [1, 23] and switchability analysis [24]. The nonlinear wave theory (NWT) approach approximates the concentration and/or temperature profile of a column using a moving wave front with a constant pattern [25]. Distillation models following NWT generally assume constant molar overflow, molar holdups and relative volatility [25, 26]. The wavefront profile moves with respect to time in response to changes in column conditions. For a column of N_{comp} components, such a model requires only $N_{\text{comp}} - 1$ dynamic equations. However, modeling assumptions, such as constant wave pattern are invalid for non-ideal mixtures [26]. Noticeable dynamic and steady-state prediction errors are observed in studies on ASUs [22, 23, 25]. The second model reduction technique, compartmentalization, was proposed in 1980s by Benallou and coworkers [27]. Order reduction following this approach is achieved based on subdividing the distillation column into a number of compartments containing one or multiple trays. When the number of trays within a compartment is large, the dynamics of the individual tray are much faster than the compartment. Due to this time scale separation, dynamic balances are only required for each compartment and balances for individual trays can be reduced to algebraic equations (AEs). Compared with the stage-by-stage approach, this method can result in significantly fewer ODEs [22, 28, 29]. Applications to ASUs show satisfactory steady-state prediction

accuracy with noticeable reduction in model complexity, i.e. fewer ODEs [1, 22]. However, Bian and coworkers [22] concluded that dynamic simulation prediction accuracy depends on the number of compartments selected and there is no guarantee of simulation time reduction. The last model reduction method, the collocation approach, was first applied to staged separation processes in the 1980s [30–33], with more recent applications including [34–36]. It has also been used to represent columns with a change in the number of liquid phases [36, 37]. The basic concept is to approximate states within the column as low-order polynomials whose coefficients are determined by setting the balance equation residuals to zero at a prescribed number of collocation points within the spatial domain. This method is discussed further in later sections of this chapter.

2.2.2 Multi-stream Heat Exchanger Model

The primary heat exchanger in ASUs is a multi-stream heat exchanger (MSHX) where multiple hot and cold streams simultaneously exchange heat in a single compact unit. Such heat exchangers usually have a high-density heat transfer area, require a small temperature driving force and often involve process streams that undergo phase changes. Despite their popularity in many energy-intensive and cryogenic processes, limited work on modeling MSHXs has been reported in the literature, especially for those involving phase change. Due to condensation or vaporization, the temperature and enthalpy correlations of a stream undergoing phase transitions are highly nonlinear, and the correlation changes noticeably as the stream state changes, for example, from liquid to two phases and then to vapor [38, 39]. One way to model MSHXs is to follow a rigorous physicochemical approach involving, for example, fluid dynamics [40]. However, the computationally intensive and time-consuming nature of such models limits their applications in optimization studies [38]. Alternatively, simpler models can be developed with limited knowledge of physical details of the heat exchanger (HX). Typically, such models treat MSHXs as heat exchanger networks with no hot or cold utility inputs and use binary variables or disjunctive models for detecting the

state of the process stream [38, 39, 41]. More recently, Pattison and Baldea[42] proposed a pseudo-transient model based on temperature-enthalpy composite composite curves. The original algebraic model is transformed into a DAE system to facilitate the model convergence, with the solution to the original model recovered at steady state. Implicit discontinuities due to phase change during simulations are handled by the DAE solver.

2.3 Cryogenic Distillation Model

In this section, two modeling approaches investigated by the authors in modeling the column section of the super-staged argon plant (demarcated by the outer dashed box in Fig. 1.1) will be explained. The goal is to develop a model that will ultimately be used within an optimization framework; thus, the desired model should be accurate and robust, and at the same time, be manageable in size.

2.3.1 Full-order Stagewise Model

The proposed dynamic FOSM is based on tray-by-tray component material and energy balances with the following assumptions:

- ternary column with components N_2, O_2 and Ar,
- negligible vapor holdup, and
- perfect mixing, with saturated liquid on each tray.

Key modeling equations include

- dynamic material balances,
- pseudo steady-state energy balances (to reduce the model complexity),

- vapor-liquid equilibrium, using the Modified Raoult's Law and the Antoine equation,
- activity coefficient estimation, using the Margules equation,
- tray efficiency and hydraulics,
- varying pressure drop,
- vapor and liquid density calculation, and
- level controllers for the liquid inventory.

The model is very similar to dynamic first-principles ASU models described in the literature [3, 15]. The reader can refer to our previous work for details on the full equation set [17]. The vapor pressure drop is a function of the vapor velocity and the liquid head at the tray above [43]

$$P_n - P_{n+1} = \alpha f(\rho_n^v, \mathbf{y}_n, V_n) + \beta f(\rho_{n+1}^l, \mathbf{x}_{n+1}, M_{n+1}) \tag{2.1}$$

where P_n is the pressure at tray n, α and β are lumped pressure parameters, $\mathbf{y}_n$ and $\mathbf{x}_n$ are the component mole fractions in the vapor and liquid phases, ρ_n^v and ρ_n^l are the molar density of the vapor and liquid phase, V_n is the molar flow rate of the vapor stream leaving tray n, and M_n is the amount of liquid holdup on tray n. The trays are numbered from bottom to top.

To accurately represent the plant, two critical process phenomena, heat leakage and stream pressure effects, are also included. The heat leakage between the surroundings and the cold box are captured in the energy balance. This is important for later studies when ambient temperature fluctuation is considered as one of the main sources of disturbances. This introduces an additional term in the typical pseudo steady-state energy balances,

$$V_n = V_{n-1}\left(\frac{h_{n-1}^v - h_n^l}{h_n^v - h_n^l}\right) + L_{n+1}\left(\frac{h_{n+1}^l - h_n^l}{h_n^v - h_n^l}\right) + UA_{\text{leak}}(T_a - T_n)\left(\frac{1}{h_n^v - h_n^l}\right) \tag{2.2}$$

The term $UA_{\text{leak}}(T_a - T_n)$ represents the amount of heat transferred into stage n due to

the temperature gradient between the ambient surroundings and the column. In Eqn. 2.2, L_n is the liquid flow rate leaving tray n, h_n^v and h_n^l are the vapor and liquid stream molar enthalpies, UA_{leak} is the product of heat transfer coefficient and heat transfer area, and T_a and T_n are the ambient and tray n temperatures. In addition, pressure effects in some of the streams, such as the liquid stream from the LC sump to the UC, due to pressure loss during transportation, are accounted for in the model. When such streams reach the entrance point, they are partially vaporized and immediately separate into two phases after being introduced into the column/reboiler. Flash calculations are performed for these streams. This involves a vapor-liquid calculation similar to a column tray. For each component i [44, 45],

$$
\begin{aligned}
F z_i &= F_i^{\text{vap}} + F_i^{\text{liq}} && (2.3)\\
(F_i^{\text{vap}}/\Sigma_{i=1}^{NC} F_i^{\text{vap}}) &= K_{\text{feed},i}(F_i^{\text{liq}}/\Sigma_{i=1}^{NC} F_i^{\text{liq}}) && (2.4)\\
K_{\text{feed},i} &= \frac{\gamma_{\text{feed},i} P_{\text{feed},i}^{sat}}{P_{\text{feed}}} && (2.5)\\
\ln(P_{\text{feed},i}^{sat}) &= A_i + \frac{B_i}{T_{\text{feed}} + C_i} && (2.6)\\
R_{gas} T_{\text{feed}} \ln(\gamma_{\text{feed},i}) &= \sum_{j=1}^{NC}\sum_{k=1}^{NC} \left(A_{ji}^{Margules} - \frac{1}{2} A_{jk}^{Margules} \right) \frac{F_j^{\text{liq}} F_k^{\text{liq}}}{(\Sigma_{i=1}^{NC} F_i^{\text{liq}})^2} && (2.7)
\end{aligned}
$$

where F, T_{feed} and P_{feed} are the stream flow rate, temperature and pressure at the feed location; z_i is component composition; F_i^{vap} and F_i^{liq} are component molar flow rates in vapor and liquid phases after flashing; $K_{\text{feed},i}$, $\gamma_{\text{feed},i}$ and $P_{\text{feed},i}^{sat}$ are the vapor/liquid equilibrium ratio, activity coefficient and saturated vapor pressure. The vapor portion leaves with the vapor stream leaving the stage and the liquid portion mixes with the liquid stream from the tray above. This set of equations is embedded in the overall column model.

The resulting FOSM for the column section of the argon plant is a large-scale DAE system of the general form,

$$
\begin{aligned}
\dot{\mathbf{x}}(t) &= \mathbf{f}(t, \mathbf{x}(t), \mathbf{y}(t), \mathbf{u}(t), \mathbf{p}) && (2.8)\\
\mathbf{0} &= \mathbf{g}(t, \mathbf{x}(t), \mathbf{y}(t), \mathbf{u}(t), \mathbf{p}) && (2.9)
\end{aligned}
$$

where $\mathbf{x}$, $\mathbf{y}$, $\mathbf{u}$ and $\mathbf{p}$ are differential state, algebraic state, control input and parameter vectors, respectively. The model size grows quickly with respect to the column size, with the combined FOSMs for the argon plant under consideration comprising approximately 1,000 differential variables and over 10,000 algebraic variables. In addition, since the super-staged argon plant operates at extremely high purity, the values of the modeling variables range from approximately 10^{-6} to 10^{3}, which makes the problem very ill-conditioned.

Remarks

The proposed integrated reboiler-condenser (IRC) model is also a vapor-liquid equilibrium based first-principles model. The basic modeling equation set for the reboiler side is very similar to a column tray, except that the negligible vapor holdup assumption is removed considering the size of a reboiler. The condenser side is assumed to have negligible material and energy holdups. The heat released from condensing the vapor stream in the condenser is used to heat up and boil the liquid on the reboiler side.

Proportional integral (PI) control logic is applied to regulate the liquid inventory at the reboiler side of the main and argon condenser, as well as the bottom liquid of the LC and SSC:

$$MV = MV_{\text{bias}} + K_c(CV_{\text{sp}} - CV) + \frac{K_c}{\tau_I} I \tag{2.10}$$

$$\frac{dI}{dt} = CV_{\text{sp}} - CV \tag{2.11}$$

where MV and MV_{bias} are the manipulated variable and its corresponding bias, K_c is the proportional gain, CV and CV_{sp} are the controlled variable and its set-point, τ_I is the integral time and I is the integral error. In the current version of the proposed model, control loop pairings are assigned according to those in an actual ASU with tuning parameter values based on available plant information.

2.3.2 Collocation Based Model

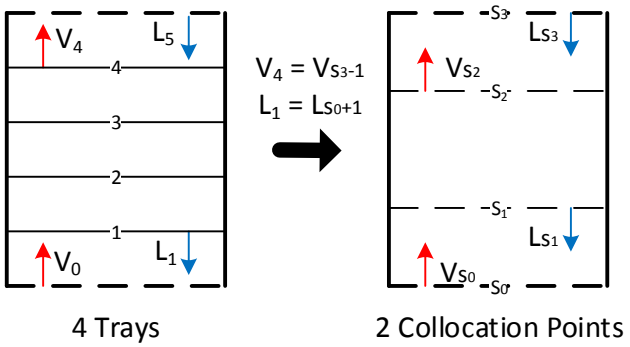

Figure 2.1: Collocation grid

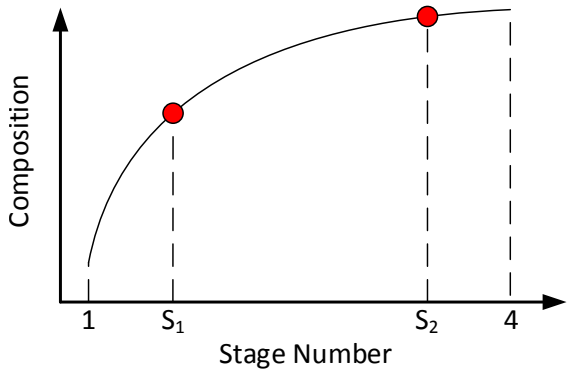

Figure 2.2: Collocation profile

Since the long term objective of our study is to conduct optimization studies, the high dimension of the FOSM is undesirable. To reduce the model size, a collocation approximation approach is followed, where system states are approximated with low-order polynomials at K pre-determined interior points, s_k, and 2 boundary points, s_0 and s_{K+1}. Modeling equation sets are only required at the collocation points instead of the column stages. The information at any location of the column can be interpolated using, for example, the Lagrange polynomial when needed. Hence, if $K \ll N_{\text{tray}}$, significant model reduction can be achieved. When K^{th} degree Hahn polynomial is used to determine the location of the collocation points s_k, the exact tray-by-tray model can be recovered when $K = N_{tray}$ [32]. Note that trays having side feed or withdrawal streams need to be treated in the same way as

in the FOSM. Figs. 2.1 and 2.2 show an example of using a 2^{nd} degree polynomial to capture the composition profile over 4 discrete trays. In this case, 2 sets of modeling equations are needed instead of 4 sets in the FOSM case.

Taking the component molar balances to illustrate the idea, in the FOSM, it is expressed as

$$\frac{dm_{n,i}}{dt} = x_{n+1,i}L_{n+1} + y_{n-1,i}V_{n-1} - x_{n,i}L_n - y_{n,i}V_n \tag{2.12}$$

With the collocation approach, Eqn. 2.12 is rewritten at each collocation points, s_k, as

$$\frac{dm_{s_k,i}}{dt} = \tilde{x}_{s_k+1,i}\tilde{L}_{s_k+1} + \tilde{y}_{s_k-1,i}\tilde{V}_{s_k-1} - \tilde{x}_{s_k,i}\tilde{L}_{s_k} - \tilde{y}_{s_k,i}\tilde{V}_{s_k} \tag{2.13}$$

where $\tilde{x}_{s_k+1,i}$ and $\tilde{L}_{s_k+1}$ are polynomial approximations of the indicated liquid stream variables evaluated at “one tray above" the collocation point, and $\tilde{y}_{s_k-1,i}$ and $\tilde{V}_{s_k-1}$ are polynomial approximations of the vapor stream variables evaluated at “one tray below" the collocation point. Using the Lagrange polynomial form for the approximating functions, the values are given by

$$\tilde{x}_{s_k+1,i} = \sum_{j=1}^{K+1} W_j^l(s_k+1)\tilde{x}_{s_j,i}, \quad \tilde{L}_{s_k+1} = \sum_{j=1}^{K+1} W_j^l(s_k+1)\tilde{L}_{s_j} \tag{2.14}$$

$$\tilde{y}_{s_k-1,i} = \sum_{j=0}^{K} W_j^v(s_k-1)\tilde{y}_{s_j,i}, \quad \tilde{V}_{s_k-1} = \sum_{j=0}^{K} W_j^v(s_k-1)\tilde{V}_{s_j} \tag{2.15}$$

with Lagrange polynomial basis functions,

$$W_j^l(s) = \prod_{\substack{z=1 \\ z\neq j}}^{K+1} \frac{(s-s_z)}{(s_j-s_z)}, \quad W_j^v(s) = \prod_{\substack{z=0 \\ z\neq j}}^{K} \frac{(s-s_z)}{(s_j-s_z)}. \tag{2.16}$$

In the above equations, $\tilde{x}_{s_{K+1},i}$ and $\tilde{L}_{s_{K+1}}$ are the liquid inlet variables at the upper boundary point (liquid from tray 5 in Fig. 2.1), while $\tilde{y}_{s_0,i}$ and $\tilde{L}_{s_0}$ are the vapor inlet variables at the lower boundary point (vapor flow from the bottom of the column into the 1^{st} tray in Fig. 2.1).

The stream leaving the section, such as the liquid leaving tray 1 (L_1), can be estimated as

$$L_1 = \tilde{L}_{s_0+1} = \sum_{j=1}^{K+1} W_j^l(s_0+1)\tilde{L}_{s_j}$$

More detailed descriptions of the collocation approach applied to staged separation systems can be found in [32, 33]. In the present application, Lagrange approximating functions are constructed in addition for the liquid density and molar holdup in the varying pressure drop equation (Eqn. 2.1), and the liquid and vapor molar enthalpies in the energy balance (Eqn. 2.2). A convenient feature of Lagrange polynomials is that the coefficients in the polynomial expressions for the variables correspond to the variable values at the collocation and boundary points (e.g. $\tilde{L}_{s_j}, j = 1, \ldots, K+1$, for the liquid molar flows).

Due to the extremely high purity separations in ASUs, the composition profiles have rapid changes at the bottom followed by a flatted tail towards the top as major separations only occur in a section of the column, with the rest responsible for refining the product. Low-order polynomials defined over the entire column section cannot accurately capture such profiles, especially when the trajectory flattens out [35]. Consequently, in our collocation approach, we subdivide column sections into multiple finite elements (FEs), with 2 collocation points (CPs) per FE. In addition, to improve the prediction accuracy, logarithmic transformations of the composition profile are used. This can be done for both the major and minor components. For a minor component, such as O_2 in the LC (Fig. 2.3), the logarithmic transformation can be performed as [17, 46]

$$\hat{x}_{O_2} = \ln(x_{O_2}) \Rightarrow x_{O_2} = \exp(\hat{x}_{O_2}). \tag{2.17}$$

Under this transformation, a composition of 1 part per million (ppm) for a minor component yields an $\hat{x}_i$ value of -13.8. In case of a major component, such as N_2 in the LC, the

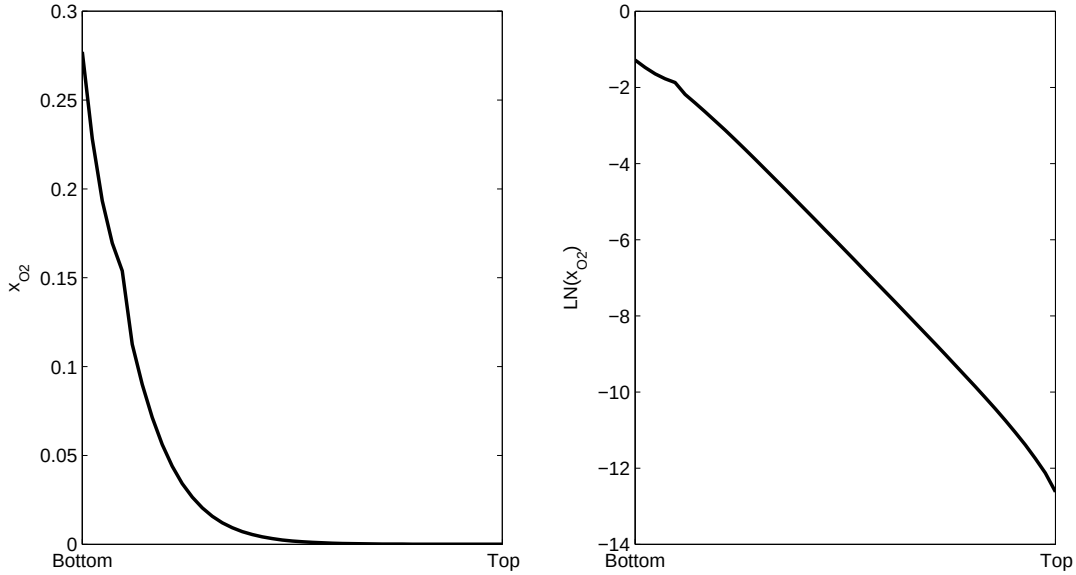

Figure 2.3: O_2 liquid phase composition profile in the lower column.

transformation is treated as

$$\hat{x}_{\mathrm{N}_2} = \ln(1 - x_{\mathrm{N}_2}) \Rightarrow x_{\mathrm{N}_2} = 1 - \exp(\hat{x}_{\mathrm{N}_2}) \tag{2.18}$$

After replacing x_i with $\hat{x}_i$, $\hat{x}_i$ is the variable set that is seen by the solver, which is better scaled than the original set. Moreover, it has less curvature, which is more desireable for applying the collocation approximation, as shown in Fig. 2.3.

2.4 Multi-stream Heat Exchanger Model with Phase Change

To model the MSHX with one stream (i.e. reference stream) experiencing an isothermal phase change, we propose a novel moving boundary approach. According to the condition of the stream, the heat exchanger can be divided into three regions: superheated (SH), two-phase (TP) and subcooled (SC), with each section occupying a fractional length of the heat exchanger as shown in Fig. 2.4. The basic concept is that for the reference stream, only

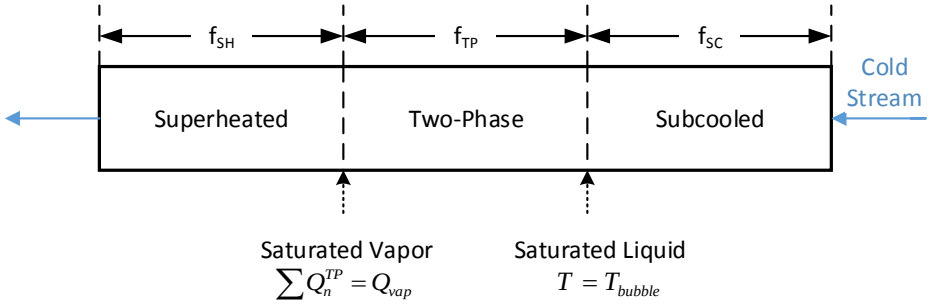

(a) Cold stream undergoing phase change

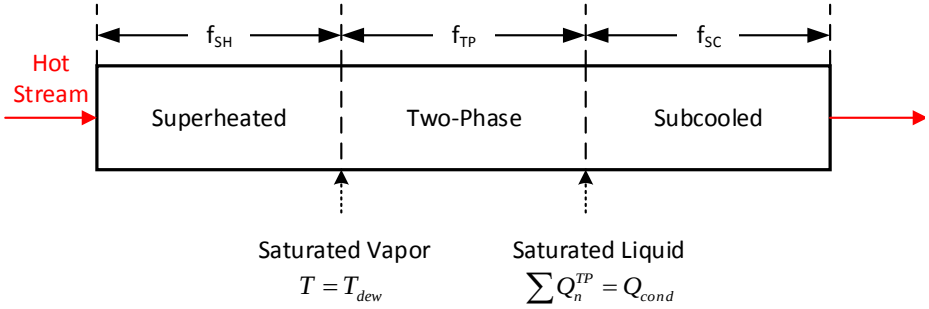

(b) Hot stream undergoing phase change

Figure 2.4: Graphical illustration of the moving boundary approach

latent heat is considered in the TP section and sensible heat is accounted for in the SH and SC sections [41]. For other process streams, sensible heat is considered in all regions. The phase change starts and completes at the boundary of different sections and not within a particular section. For a liquid to vapor phase change, the boundary between the TP and SC sections is tracked with a bubble point calculation, and the boundary between the SH and TP sections is defined when the heat absorbed by the stream equals the heat of vaporization. Corresponding boundary points for streams experiencing vapor to liquid phase transitions are captured with the dew point and heat of condensation, respectively. Hence, the locations of the starting and completion of the phase change, represented by the fractional length, are not specified but rather treated as calculated variables in the proposed model. As stream conditions vary, the regional heat transfer area expands and shrinks. A graphical illustration of the method is shown in Fig. 2.4. Each section in the HX further is divided into small

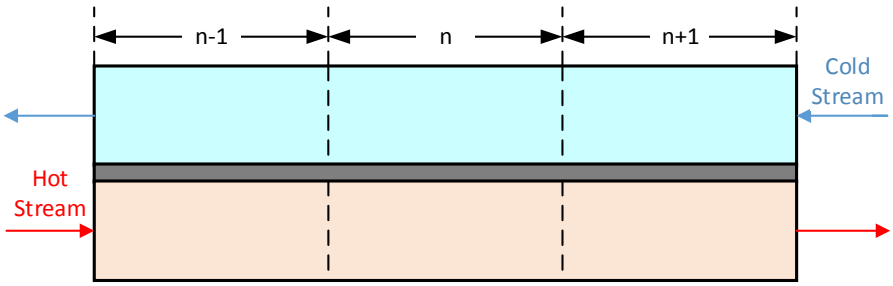

Figure 2.5: Illustration of segment numbering and stream flow directions in MSHX model

equally-spaced segments. Modeling assumptions include:

- well mixed streams within each segment,
- heat transfer between the process streams and the metal wall,
- linear pressure drop, and
- heat transfer area of each section proportional to its fractional length.

The modeling approach us illustrated using the cold stream as the reference stream (i.e. experiencing phase change). Fig. 2.5 illustrates the numbering of the segments, and the hot and cold stream directions that are used in the model formulation.

(a) Superheated region, considering sensible heat for the reference stream

$$0 = F_{\text{ref}}(h^{SH}_{n+1,\text{ref}} - h^{SH}_{n,\text{ref}}) + \frac{f_{SH} \cdot A_{HX}}{N_{SH}} U^{SH}_{\text{ref}} (T^{m,SH}_{n} - T^{SH}_{n,\text{ref}}) \tag{2.19}$$

In Eqn. 2.19, F_{ref} is the reference stream flow rate, $h^{SH}_{n,\text{ref}}$ is the molar enthalpy of the reference stream leaving segment n of the SH section, f_{SH} is the fractional length of the SH section, A_{HX} is the total heat transfer area of the HX, N_{SH} is the number of segments in the superheated region, and U^{SH}_{ref} is the sectional heat transfer coefficient. $T^{m,SH}_{n}$ and $T^{SH}_{n,\text{ref}}$ are metal wall and reference stream temperatures at segment n. Other process streams are

modeled in a similar manner. The energy balance on the metal wall is

$$0 = \sum_{j=1}^{N_s} \frac{f_{SH} \cdot A_{HX}}{N_{SH}} U_j^{SH} (T_{n,j}^{SH} - T_n^{m,SH}) \tag{2.20}$$

where N_s is total number of streams in the heat exchanger.

(b) Two-phase region, considering the latent heat for the reference stream

$$0 = -Q_n^{TP} + \frac{f_{TP} \cdot A_{HX}}{N_{TP}} U_{\text{ref}}^{TP} (T_n^{m,TP} - T_{n,\text{ref}}^{TP}), \quad T_{n,\text{ref}}^{TP} = T_{\text{in,ref}}^{TP} \tag{2.21}$$

Q_n^{TP} is the amount of heat absorbed by the liquid stream at segment n of the TP section. $T_{\text{in,ref}}^{TP}$ is the TP section inlet temperature of the reference stream, which has the same value as the corresponding exiting temperature from the SC region. Other variables in Eqn. 2.21 are defined in the same way as in Eqn. 2.19. In this section, other process streams and the metal wall are modeled as in Eqn. 2.19 and Eqn. 2.20, respectively.

(c) Subcooled region, considering sensible heat for the reference stream

$$0 = F_{\text{ref}} (h_{n+1,\text{ref}}^{SC} - h_{n,\text{ref}}^{SC}) + \frac{f_{SC} \cdot A_{HX}}{N_{SC}} U_{\text{ref}}^{SC} (T_n^{m,SC} - T_{n,\text{ref}}^{SC}) \tag{2.22}$$

The variables in Eqn. 2.22 are defined in the same way as in in Eqn. 2.19. In this section, other process streams are modeled in a similar manner, and the metal wall is modeled as in Eqn. 2.20. Since the stream changes phase from liquid to vapor, the boundary between the SC and TP section are defined by when the outlet temperature of the reference stream from the SC section reaches its bubble point temperature

$$T_{\text{out,ref}}^{SC} = T_{\text{bubble}} \tag{2.23}$$

which signals the starting point of the phase change. Note that T_{bubble} is a function of

reference stream conditions and is calculated in the model as in:

$$T_{\text{bubble}} = f(\mathbf{x}_{\text{ref}}, P^{SC}_{\text{out,ref}})$$

where $\mathbf{x}_{\text{ref}}$ is the composition of the reference stream. The prediction accuracy is assured through the use of the modified Raoult's law and the Antoine equation with the Margules equation for the non-ideality. When the accumulated heat absorbed by the stream equals the heat of vaporization, the phase change completes

$$\sum_{n=1}^{N_{TP}} Q_n^{TP} = Q_{\text{vap}} \tag{2.24}$$

This defines the boundary between the TP and SH sections. Similar to T_{bubble}, Q_{vap} is also stream condition specific, and is calculated as the product of the latent heat of vaporization and the stream molar flow rate. Finally, the summation of the fractional lengths should be 1.

$$f_{SH} + f_{TP} + f_{SC} = 1 \tag{2.25}$$

Remarks

In the case where the reference stream is the hot stream, a similar model can be developed following Eqns. 2.19 – 2.25. However, Eqns. 2.23 and 2.24 are now replaced by

$$T^{SH}_{\text{out,ref}} = T_{\text{dew}} \tag{2.26}$$

$$\sum_{n=1}^{N_{TP}} Q_n^{TP} = Q_{\text{cond}} \tag{2.27}$$

The moving boundary model, as proposed, can handle only one process stream undergoing a phase change, not multiple phase transitions simultaneously. However, this is adequate for the industrial system under consideration under the operating conditions of interest. The model retains the necessary process details without introducing binary variables/model disjunctions for handling the phase transitions, which is a desired property when combined

with the column model for optimization studies. Although the model presented here is a steady-state version, the moving boundary model can be readily converted into a dynamic model, as shown in our previous study [17] for single phase streams. In the present situation, the dynamics of the heat exchanger are expected to be much faster than the column section, thus the steady-state model will be used in our study.

2.5 Results and Discussion

2.5.1 Full-Order Distillation Column Model Validation

The proposed FOSMs for columns in the argon plant are coded in `gPROMS 4.0.0` [47]. To verify the prediction accuracy, the FOSM was validated against data consistent with industrial operation to ensure that the model accurately represents the plant. Operation data near design conditions were collected from Praxair's high fidelity operator training simulator (OTS) model. Data reconciliation was first completed for each individual unit, with re-fitting preformed after integrating different columns. In this project, model fitting was conducted using the parameter estimation feature in `gPROMS`, which solves an optimization problem to minimize the weighted sum of squared errors between the data and model prediction. Data supplied in this case are the flow information, pressure, temperature and compositions around the feed, withdrawal and product trays; as well as conditions of the product streams. Decision variables in the integrated column section model consist of lumped pressure parameters (in Eqn. 2.1) and tray efficiency for the columns, as well as heat transfer coefficients for the IRCs (between the reboiler and condenser) and the column section heat leakage term. In this study, it is assumed that efficiency values for a group of trays having a consistent design are identical. Due to its unique design, the UC has multiple stage efficiency values. Column parameters, i.e. weir height, length or active area, were adjusted when fitting individual models. The reason for introducing the geometric parameters is that the stage

Table 2.1: Product purities in the integrated column model after the model validation.

Variables	Absolute Error
ppm O_2 in LAr	0.3 ppm
ppm N_2 in LAr	1.0 ppm
ppm O_2 in GN_2	0 ppm
LO_2 Purity	0.2 %

Table 2.2: Liquid inventories in the integrated column model after the model validation.

Variables	Absolute % Error
Lower Column Bottom Liquid	0.36 %
Main Condenser Reboiler Liquid	0.68 %
Super-stage Column Bottom Liquid	0.11 %
Argon Condenser Reboiler Liquid	0.52 %

design in this case differs from that of typical valve or sieve trays.

Results of the model validation are presented in Fig. 2.6 and Tables 2.1 and 2.2. As shown, the proposed gPROMS model shows a high degree of consistency with the OTS model. The temperature and pressure profiles of the upper column, which has multiple feed and side-draw streams, based on the two models are almost identical. Predictions of product purity are also in close agreement, even at the ppm level. gPROMS model predictions of liquid inventory in the system, which affect the process dynamic response time, are also consistent with those from the OTS model. Absolute percent errors,

$$\text{Absolute \% Error} = \frac{|\text{Data} - \text{Prediction}|}{\text{Data}} \times 100\%, \tag{2.28}$$

of liquid holdup at the critical locations are reported in Table 2.2. Excellent prediction accuracy is observed. Using the FOSM, dynamic simulations of the integrated column section for a single step change in the system input can be completed in less than 30 s in gPROMS.

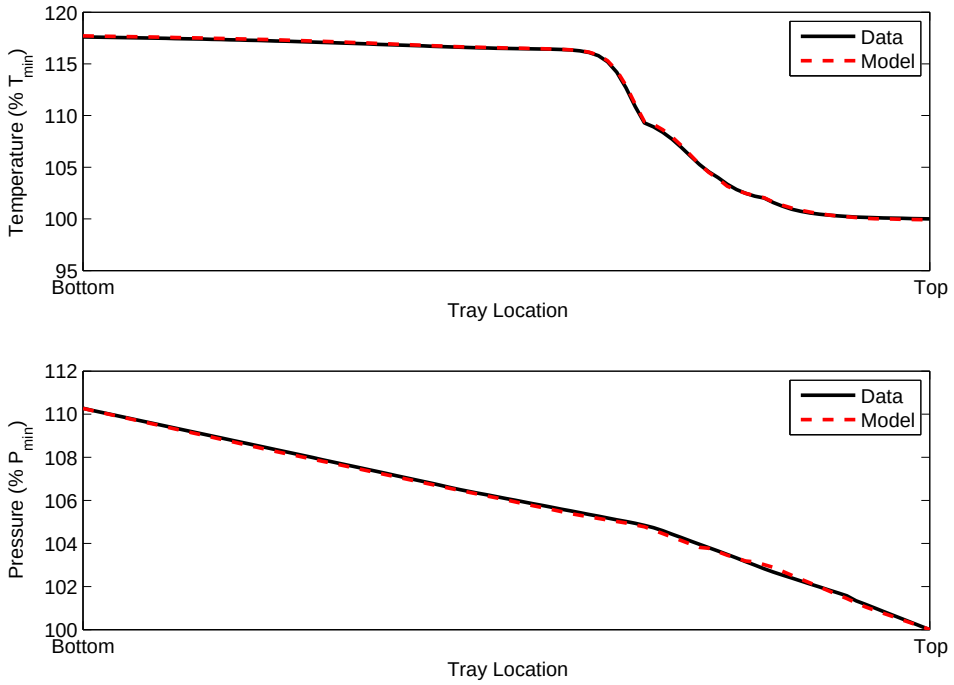

Figure 2.6: Temperature and pressure profiles of the upper column in the integrated column model after the model validation: measurements–OTS (- -) and predictions–gPROMS (—).

2.5.2 Collocation Model Reduction

The collocation approach was applied to the lower column (LC), lower ratio column (LRC) and super-staged argon column (SSC). Since the feed and side withdrawal trays need to be treated separately in this method, the upper column (UC) model was kept in the stage-wise form. A multiple finite element (FE) grid was utilized with 2 collocation points (CPs) per FE, as it was shown in simulations to be the most robust and stable for the high purity and tightly integrated system under consideration. For ASUs, particular attention is required on retaining the prediction accuracy, as a slight deviation in one variable value may cause significant accumulated impact on the overall system behavior.

Approaches for automatic adjustment of finite element breakpoint locations have been proposed, which for process systems applications includes work of Cuthrell and Biegler[48],

Vasantharajan and Biegler[49] and Damartzis and Seferlis[36]. These strategies incorporate an estimate of the approximation error within an optimization problem formulation. While Vasantharajan and Biegler[49] present a formulation for inclusion of the number of FEs in the search space through additional binary decision variables, most other studies require *a priori* specification of the number of FEs, the latter including applications to distillation systems[36]. Given the complexity of the system in our study, manual adjustment of the finite elements together with dynamic simulation evaluations are utilized. The number of stages contained in each section is determined based on observations of simulation trajectories. The prediction offset increases with the number of trays in the element. When the number of collocation points equals the number of trays in the section, $K = N_{\text{tray}}$, the collocation model takes the format of the original stage-wise model (i.e. zero prediction offsets). Our objective is to limit the prediction error in the critical variables (i.e. product purity, LC and LRC bottom composition and LRC bottom pressure) within a predetermined threshold. A value of 0.05 % is used as the threshold in our study. To do so, the following procedure has been adopted:

1. Decide an initial number of the trays to be contained in the element.
2. Replace the stage-wise model of the selected section with the collocation based model, while others remain unchanged.
3. Perform steady state and dynamic simulations.
4. If the predication error in the critical parameters is negligible, increase the finite element size to encompass more stages; otherwise, reduce the number of stages in the section and go back to step 3.
5. Proceed to the next section once desired trade-off between prediction accuracy and model reduction is achieved.

The procedure is repeated down the length of the column. If the overall error is within the prescribed tolerance, the next column is tackled; otherwise, the FE grid is re-adjusted.

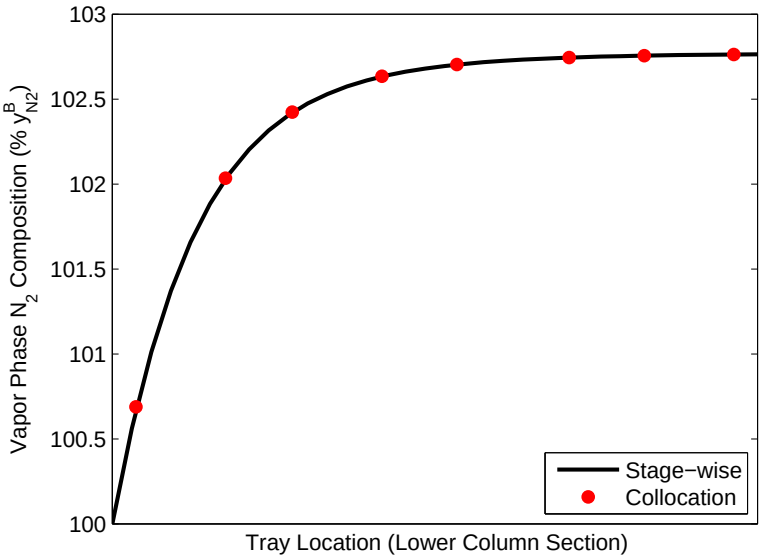

Figure 2.7: Steady-state vapor phase N_2 composition profile in the collocation section of the lower column: full order stage-wise model (—) vs. collocation model (•). The N_2 composition is scaled relative to that on the bottom tray of the collocation section ($y^B_{N_2}$).

Table 2.3: Model reduction results with the collocation based method (simulations are performed in gPROMS).

Column	Model Size Reduction	Simulation Time Reduction (CPU Time)
LC	58.6 %	52.7 %
LRC	59.2 %	50.1 %
SSC	72.2 %	63.0 %

Note that with this approach, the user has the flexibility of defining problem specific grids that best serve the application. The number of stages covered per FE can vary and the model can be partially based on the collocation approach. Following the proposed method, significant model reduction was achieved for each column, while both steady-state and dynamic predication errors were minimal as shown in Table 2.3 and Figs. 2.7 and 2.8. The overall prediction accuracy for the integrated column model also maintains a desired level while the model size is reduced by over 50 %. Further model reduction can be obtained if the prediction accuracy threshold is relaxed. The presentation of the dynamic simulation results in Fig. 2.8 uses a reference time scale (i.e. 1 unit = x hours; the value for x is not shown due to proprietary reasons) and applied to subsequent figures in this chapter.

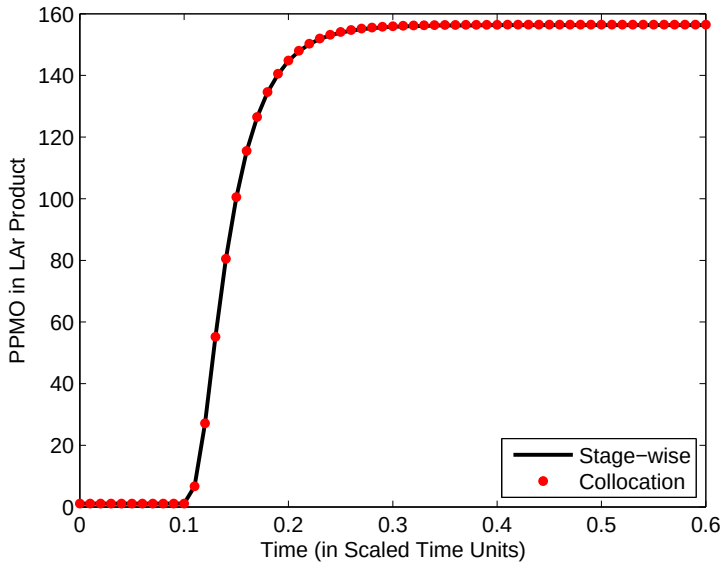

Figure 2.8: Parts per million oxygen (PPMO) level in the liquid argon product in response to an increase in the vapor inlet flow rate with the SSC model only: full order stage-wise model (—) vs. collocation model (•).

2.5.3 Moving Boundary Multi-stream Heat Exchanger Model

The proposed moving boundary model was applied for the portion of the primary heat exchanger having isothermal phase transitions. The process streams involved are:

- hot air stream (hot stream),
- boiling O_2 stream (cold stream; going through a liquid to vapor phase change to produce gas O_2 product),
- gas N_2 product stream (cold stream),
- and waste N_2 stream (cold stream).

In this example, the boiling O_2 is the reference stream. The SH, TP and SC sections were further divided into 10, 5 and 20 segments respectively. Note that segments within the same section are equally spaced, having a fractional length of f_{SH}/N_{SH}, f_{TP}/N_{TP} or f_{SC}/N_{SC}.

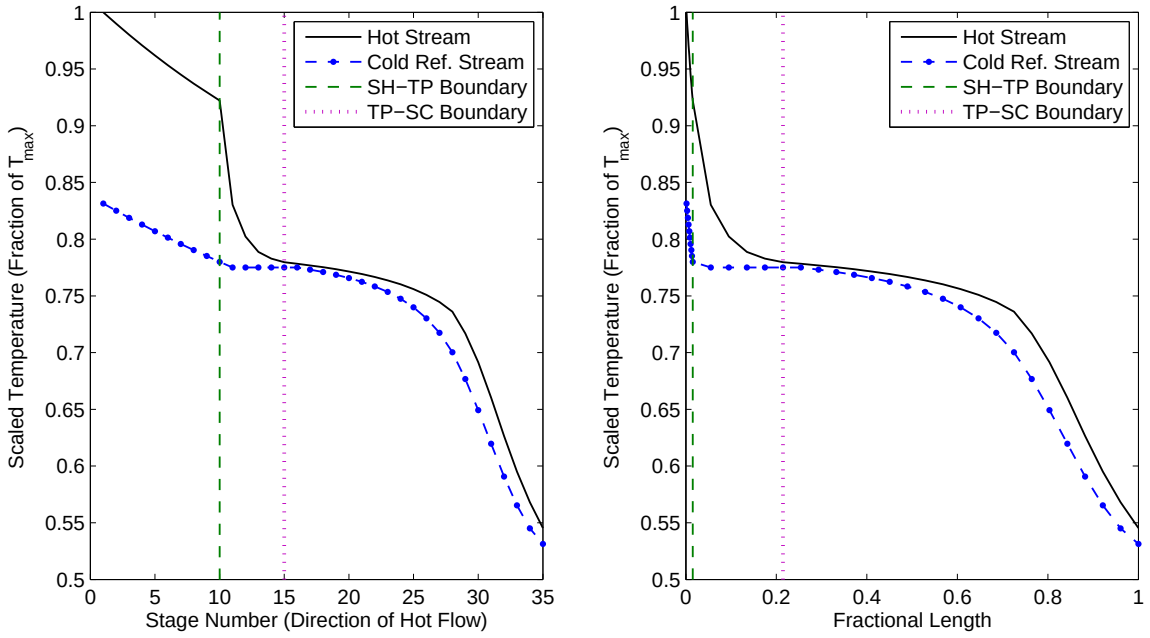

Figure 2.9: Temperature profiles of hot air (—) and boiling O_2 (- •-) from stage-wise (left) and fractional length (right) views. Locations of the boundary points in the fractional length view are defined by the value of f_{SH}, f_{TP}, and f_{SC}.

Segment lengths between different sections, e.g. TP and SC, are not necessarily the same. As shown in Fig. 2.9, the proposed method can successful track the boundary points between SC-TP and TP-SH sections. In addition, the result shows the potential pinch point along the length of the heat exchanger, which is useful design and operation information.

To validate the proposed model, 7 sets of data were collected from Praxair's OTS model. Data collected cover a wide range of gas O_2 production rate. The parameter estimation feature in `gPROMS` was used in this case. Sectional heat transfer coefficients were estimated so that errors between the data and model predictions are minimized. As shown in Table 2.4, excellent prediction accuracy can be achieved.

Remarks

Similar to the stage-wise column model, the collocation approach with multiple finite elements can be applied to reduce the size of the stage-wise moving boundary heat exchange

Table 2.4: Average percent errors in the stream outlet temperature (in Kelvin) after model validation.

	Average % Error in T_{out}
Hot Air (Hot Stream)	0.57 %
Boiling O_2 (Cold 1)	0.24 %
Gas N_2 Product (Cold 2)	0.43 %
Waste N_2 (Cold 3)	0.23 %

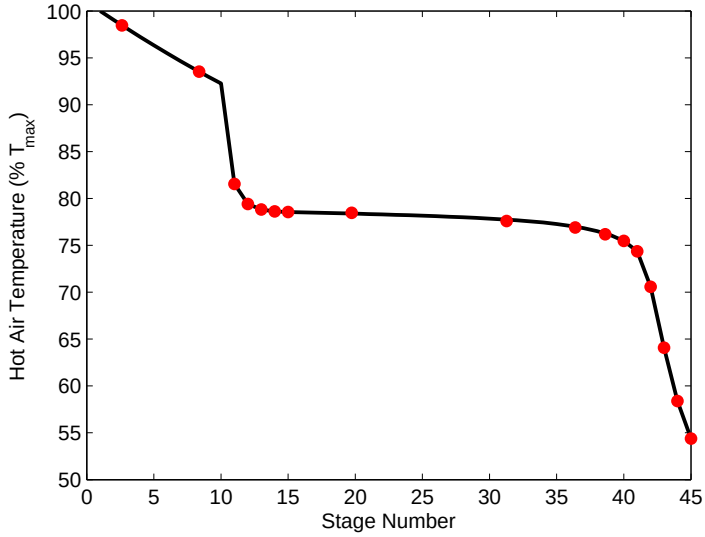

Figure 2.10: Hot air stream temperature profile with stage-wise model (—) and collocation based model (•).

model. As shown in Fig. 2.10, a customized grid was developed. Due to the sharp temperature profile of the hot air stream around the TP section (stages 11 – 15) and towards the end point of the SC section (above stages 40), we kept the model for these sections in a stage-wise manner (collocation points at the exact stage location). There are negligible differences between predictions with the partially collocated and the full stage-wise model. However, a solution time reduction of more than 50 % is achieved with the partially collocated model. Results shown here demonstrate that the collocation modeling approach is not limited to distillation columns, but is generally applicable to any systems that can be modeled in a stage-wise manner; its application to distributed parameter systems over continuous domains is well established [50, 51]. As mentioned previously, customized grids can be adopted for

specific problems/applications to maintain a desired prediction accuracy.

2.5.4 Dynamic Simulation of the ASU Cryogenic Section

A Negative Step Change in Gas Oxygen Stream Flow Rate

In this section, a negative step change is introduced to the gas O_2 stream flow rate. Two models are compared in this case: (1) the column section only model, shown in the dotted inner box in Fig. 1.1, and (2) integrated cold-box model, shown in the dashed outer box. Note that in the cold-box model, we also include mathematical representations of the turbine and the oxygen pump. We are interested in the composition of the crude argon feed stream (from the UC to the LRC) in response to such a change. Without the heat exchanger, changing the gas O_2 flow rate has no effect on other system inputs as there is no heat integration between the product and the system inputs. The liquid level at the bottom of the UC is regulated by adjusting the liquid O_2 flow rate. As a result, the O_2 content in the crude argon feed should remain constant. When the heat exchanger is included, a negative step change in gas O_2 flow rate will lead to an immediate decrease in the cold stream in the HX while other stream flow rates remain constant (e.g. waste N_2 stream). Consequently, air streams entering the system will be warmer. Hence, the O_2 profile in the UC is shifted upwards due to an increased amount of N_2 being boiled off, and the O_2 content in the argon feed stream should increase. Observations in the simulation results in Fig. 2.11 are consistent with expectation. In addition, as shown, the moving boundary heat exchange model for the HX is able to track the boundary movement in this case.

Remarks

Results shown here demonstrate the role of the primary heat exchanger (PHX) in accurately capturing the behavior of the ASU. Without the PHX, the thermal coupling between product and feed streams is absent. In simulation or optimization studies where either production rate

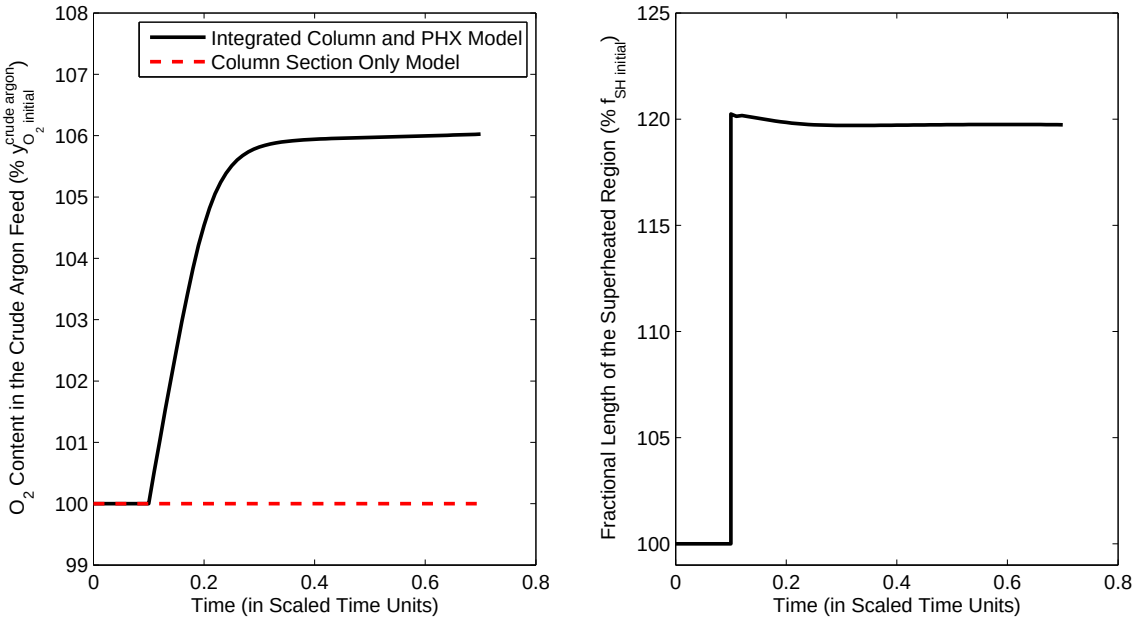

Figure 2.11: Dynamic response to a negative step change in the gas O_2 stream: (a) O_2 content in the crude argon feed with: the column section only model (—) and with the integrated cold-box model (. . .); (b) fractional length of the superheated section in the heat exchanger.

or feed flow rate is used as manipulated/decision variables, such heat integration becomes critical. However, the model complexity increases once the PHX model is included due to the additional equations.

A Positive Step Change in Waste Nitrogen Stream Flow Rate

A positive step change is introduced to the waste N_2 stream flow rate while other system inputs remain constant. With the integrated cold-box model, this will lead to an increase in the cold stream flows in the HX. The fractional length of the superheated region of the PHX is expected to decrease. In addition, with an increase in waste N_2 stream, more N_2, together with the O_2 (i.e. impurity in the N_2 streams), are removed from the system. Hence, the O_2 profile in the UC is shifted upwards and the O_2 content in the argon feed stream

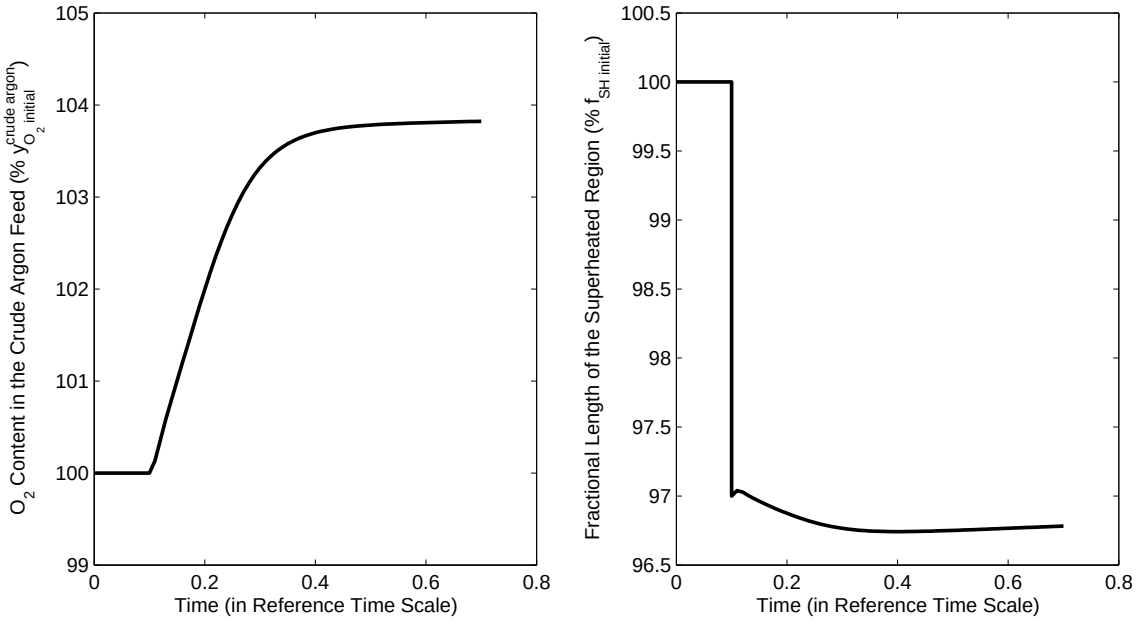

Figure 2.12: Dynamic response to a positive step change in the waste N_2 stream: (a) O_2 content in the crude argon feed; (b) fractional length of the superheated section in the heat exchanger.

should increase. Observations in the simulation results in Fig. 2.12 are consistent with these expectations.

A Pulse Change in Gas Oxygen Stream Flow Rate

In the simulation cases shown previously, the changes in the system inputs affect only the O_2 content in the crude argon feed stream without influencing the N_2 composition, as the lower section of the UC mainly involves separation of O_2 and Ar like binary distillation columns. The result of O_2 entering the argon section will result in increasing product impurity in the argon product (i.e. O_2 composition) and losing argon recovery, which is undesirable since argon is the most valuable product. The more severe case is when N_2 enters the argon section of the process. There is no exit for the N_2 in the argon section except the vent streams. Opening the vent hurts the argon recovery, but if the vent valve remains closed, N_2

accumulates in the argon section (i.e. the column becomes colder), causing the condenser pressure of the argon condenser to increase and the pressure driven crude argon feed stream to decrease. If no corrective actions are taken, the vapor rising through the argon columns (i.e. LRC and SSC in Fig. 1.1) becomes insufficient to support the liquid and all the liquid inventory in the argon section dumps into the upper column and the oxygen product, which is withdrawn from the bottom of the UC, is spoiled. Once argon section dumping occurs, it takes hours to re-establish the oxygen product purity and an even longer time to re-build the composition profile and bring the argon product on-spec. Hence, it is critical for the model to be able to capture these phenomena. In this section, we introduce a pulse change in the gas O_2 product stream (i.e. $F_{\text{base}} \rightarrow F_{\text{base}} + \Delta \rightarrow F_{\text{base}}$) to demonstrate. With an increase in the gas O_2 flow rate, the N_2 content in the crude argon feed increases, and as a result, the crude argon feed flow rate should decrease. Once the gas O_2 flow rate returns to the original level, the system should return to its initial steady state point. As shown in Fig. 2.13, simulation results with the integrated cold-box model are consistent with expectation. Since there is more cold stream in the PHX, the fractional length of the superheated section decreases. Inspection of the upper column N_2 composition and temperature profiles in response to the pulse change, shown in Fig. 2.14, shows that the N_2 profile is initially pulled downwards (the column gets colder) then restores.

A Negative Step Change in Vapor Air Feed Flow Rate

Due to electricity price deregulation, ASUs might need to perform loading and unloading in response to electricity price changes to reduce operating costs. It is ideal to maintain a given production level with the least amount of air feed. However, considering the high degree of integration in the multi-product ASUs, multiple system inputs should be adjusted simultaneously to achieve this goal. To demonstrate this, we introduce a negative step change in the vapor air feed stream into the LC. It is assumed that there is a ratio controller between the vapor air feed and the UC shelf (i.e. the portion of the condensed LC top sent to the

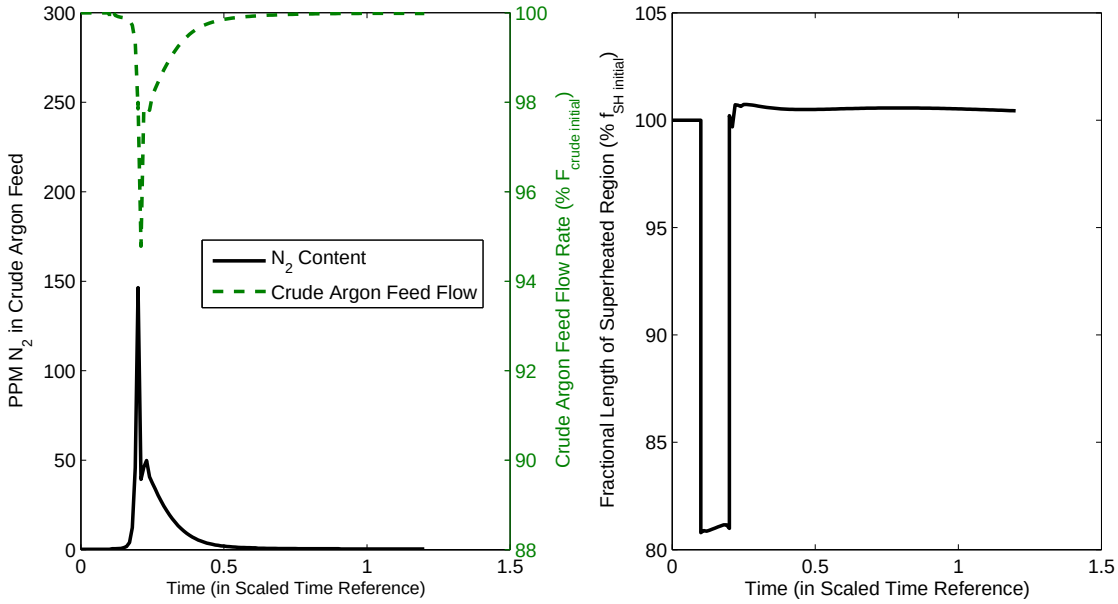

Figure 2.13: Dynamic response to a positive pulse change in the gas O_2 stream flow rate: (a) N_2 content in the crude argon feed (—) and crude argon flow rate (. . .); (b) fractional length of the superheated section in the heat exchanger.

UC; it acts as a reflux stream to the UC). Other system inputs are held constant. When the vapor air feed into the LC decreases, the flow rate of the vapor leaving the LC top, hence the condensed liquid from the main condenser, reduces. As a result, the reflux stream flow rates for both lower and upper column decrease. Additionally, the LC bottom liquid to the UC (manipulated by the LC sump level controller) is supplied at a reduced rate. These lead to a cutback in liquid flow down the UC and elevated O_2 content in the waste nitrogen stream (Fig. 2.15) and the crude argon feed. Without corrective control action, the liquid argon product purity will become off-spec, as explained previously, and result in economic loss for the plant. The liquid O_2 production rate also decreases as the result of the level controller manipulations.

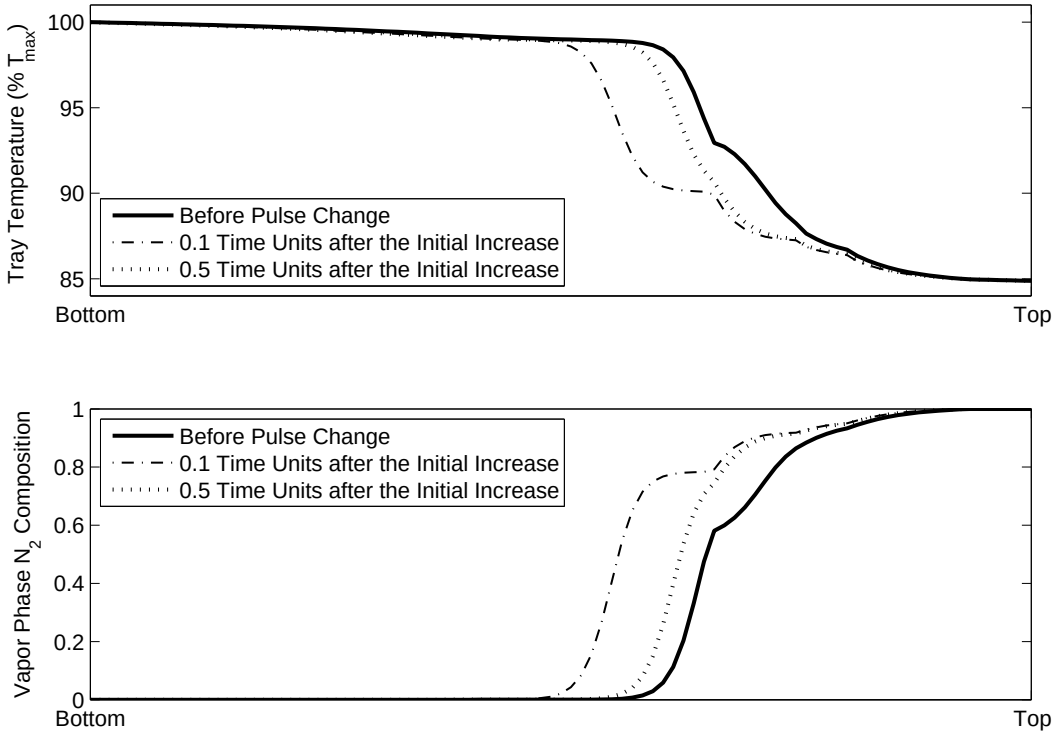

Figure 2.14: Dynamic response of upper column N_2 and temperature profile to a positive pulse change in the gas O2 stream flow rate

2.6 Conclusions

This study considered modeling of the cold-box section of a super-staged argon plant. In modeling the distillation columns, full order stage-wise models (FOSMs) with key process phenomena, heat leakage and stream pressure effects, were first proposed. Validation results show that the model can achieve high prediction accuracy. The FOSM has excellent agreement even for product purity at the ppm level. However, such large scale differential-algebraic equation systems ($>$ 1,000 differential variables) are likely to pose bottlenecks in dynamic optimization studies. To reduced the model size, a collocation-based model was derived. Application of the proposed model reduction approach to the LC, LRC and SSC shows that

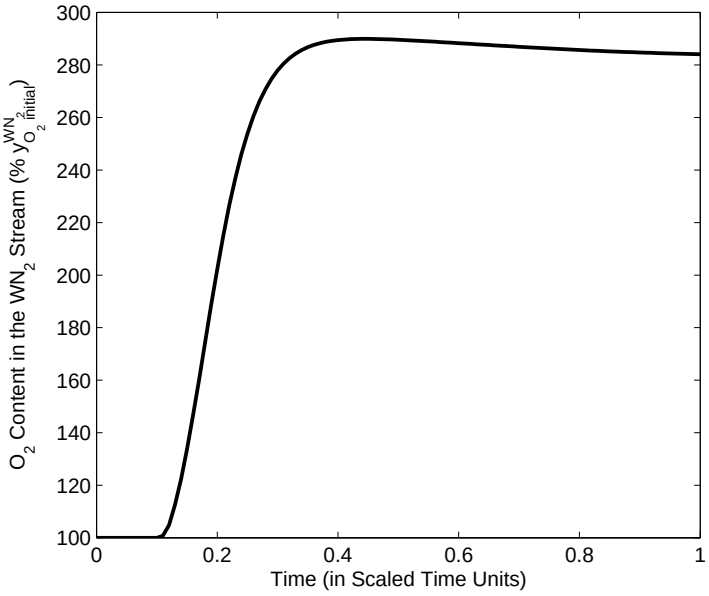

Figure 2.15: Dynamic response of O_2 content in the waste nitrogen stream in response to a negative step change in the vapor air feed to the LC.

with this approach, significant model size and simulation time reduction can be achieved with negligible prediction error in either steady state or dynamic simulations compared to the FOSM.

In the second section of this work, a novel moving boundary method for modeling a multi-stream heat exchange (MSHX) with one of the process streams experiencing a phase change was proposed. Applications to the primary heat exchanger demonstrate that the moving boundary model not only locates and tracks phase change, but also shows potential pinch points along the length of the heat exchanger. Similar to the column model, the collocation method was also used to reduce the model size. Dynamic simulation results with the column section and the integrated cold-box model illustrate the importance of capturing the thermal integration between the feed and product streams in accurately representing the plant behavior. Work is currently under way in applying the collocation based ASU model in dynamic optimization studies.

Bibliography

[1] Z. Chen et al. “Nonlinear model predictive control of high purity distillation columns for cryogenic air separation”. In: *IEEE Transactions on Control System Technology* 18.4 (2010), pp. 811 –821 (cit. on pp. 12, 15–17).

[2] Y. Zhu, S. Legg, and C. D. Laird. “A multiperiod nonlinear programming approach for operation of air separation plants with variable power pricing”. In: *AIChE Journal* 57.9 (2011), pp. 2421 –2430 (cit. on pp. 12, 15).

[3] J. Miller et al. “Improving agility of cryogenic air separation plants”. In: *Industrial & Engineering Chemistry Research* 47.10 (2008), pp. 394 –404 (cit. on pp. 12, 15, 19).

[4] U.S. Energy Information Administration. *Manufacturing energy consumptionsurvey*. Online. Available at: http://www.eia.gov/consumption/data.cfm. 2012 (cit. on p. 13).

[5] J. D. Figueroa et al. “Advances in CO_2 capture technology - The U.S. Department of Energy’s Carbon Sequestration Program”. In: *International Journal of Greenhouse Gas Control* 2.1 (2008), pp. 9 –20 (cit. on p. 13).

[6] Y. Cao, C. L. E. Swartz, and M. Baldea. “Design for dynamic performance: Application to an air separation unit”. In: *American Control Conference*. San Francisco, CA, USA, 2011, pp. 2683–2686 (cit. on p. 13).

[7] Y. Cao et al. “Optimization-based assessment of design limitations to air separation plant agility in demand response scenarios”. In: *Journal of Process Control* 33 (2015), pp. 37 –48 (cit. on pp. 13, 15).

[8] J. O. Trierweiler and S. Engell. “A case study for control structure selection: air separation plant”. In: *Journal of Process Control* 10.2 - 3 (2000), pp. 237 –243 (cit. on p. 14).

[9] T. Li et al. “Real time optimization of air separation plants”. In: *ISA Automation Week*. Mobile, Alabama, 2011 (cit. on p. 14).

[10] M. G. Ierapetritou et al. “Cost minimization in an energy-intensive plant using mathematical programming approaches”. In: *Industrial & Engineering Chemistry Research* 41.21 (2002), pp. 5262 –5277 (cit. on pp. 14, 15).

[11] A. R. Sirdeshpande et al. “Process synthesis optimization and flexibility evaluation of air separation cycles”. In: *AIChE Journal* 51.4 (2005), pp. 1190 –1200 (cit. on p. 14).

[12] J. Miller, W. L. Luyben, and S. Blouin. “Economic incentive for intermittent operation of air separation plant with variable power costs”. In: *Industrial & Engineering Chemistry Research* 47 (2008), pp. 1132 –1139 (cit. on pp. 14, 15).

[13] S. Mitra et al. “Optimal production planning under time-sensitive electricity prices for continuous power-intensive processes”. In: *Computers & Chemical Engineering* 38 (2012), pp. 171 –184 (cit. on pp. 14–16).

[14] S. Mitra, J. M. Pinto, and I. E. Grossmann. “Optimal multi-scale capacity planning for power-intensive continuous processes under time-sensitive electricity prices and demand uncertainty. Part I: Modeling”. In: *Computers & Chemical Engineering* 65.0 (2014), pp. 89 –101 (cit. on pp. 14, 15).

[15] B. Roffel, B. H. L. Betlem, and J. A. F. Ruijter. “First principles dynamic modeling and multivariable control of a cryogenic distillation process”. In: *Computers & Chemical Engineering* 24 (2000), pp. 111 –123 (cit. on pp. 15, 19).

[16] R. Huang, V. M. Zavala, and L. T. Biegler. “Advanced step nonlinear model predictive control for air separation units”. In: *Journal of Process Control* 19.4 (2009), pp. 678 –685 (cit. on p. 15).

[17] Y. Cao. “Design for Dynamic Performance: Application to Air Separation Unit”. MA thesis. Department of Chemical Engineering, McMaster University, Hamilton, 2011 (cit. on pp. 15, 19, 24, 30).

[18] Y. Zhu, S. Legg, and C. D. Laird. “Optimal design of cryogenic air separation columns under uncertainty”. In: *Computers & Chemical Engineering* 34.9 (2010), pp. 1377 –1384 (cit. on p. 15).

[19] Y. Zhu, S. Legg, and C. D. Laird. “Optimal operation of cryogenic air separation systems with demand uncertainty and contractual obligations”. In: *Chemical Engineering Science* 66.5 (2011), pp. 953 –963 (cit. on p. 15).

[20] A. W. Dowling and L. T. Biegler. “A framework for efficient large scale equation-oriented flowsheet optimization”. In: *Computers & Chemical Engineering* 72.0 (2015), pp. 3 –20 (cit. on p. 15).

[21] Y. Zhu, X. Liu, and Z. Zhou. “Optimization of cryogenic air separation distillation columns”. In: *6th World Congress on Intelligent Control and Automation*. Dalian, China, 2006, pp. 7702 –7705 (cit. on p. 16).

[22] S. Bian et al. “Compartmental modeling of high purity air separation columns”. In: *Computers & Chemical Engineering* 29.10 (2005), pp. 2096 –2109 (cit. on pp. 16, 17).

[23] S. Bian et al. “Nonlinear state estimation and model predictive control of nitrogen purification columns”. In: *Industrial & Engineering Chemistry Research* 44.1 (2005), pp. 153 –167 (cit. on p. 16).

[24] V. White, J. D. Perkins, and D. M. Espie. “Switchability analysis”. In: *Computers & Chemical Engineering* 20.4 (1996), pp. 469 –474 (cit. on p. 16).

[25] G. Y. Zhu, M. A. Henson, and L. Megan. “Low-order dynamic modeling of cryogenic distillation columns based on nonlinear wave phenomenon”. In: *Separation and Purification Technology* 24 (2001), pp. 467 –487 (cit. on p. 16).

[26] A. Kienle. “Low-order dynamic models for ideal multicomponent distillation processes using nonlinear wave propagation theory”. In: *Chemical Engineering Science* 55.10 (2000), pp. 1817 –1828 (cit. on p. 16).

[27] A. Benallou, D. E. Seborg, and D. A. Mellichamp. “Dynamic compartmental models for separation processes”. In: *AIChE Journal* 32.7 (1986), pp. 1067–1078 (cit. on p. 16).

[28] S. Khowinij et al. “Dynamic compartmental modeling of nitrogen purification columns”. In: *Separation and Purification Technology* 46 (2005), pp. 95 –109 (cit. on p. 16).

[29] R. R. Horton, B. W. Bequette, and T. F. Edgar. “Improvements in dynamic compartmental modeling for distillation”. In: *Computers & Chemical Engineering* 15.3 (1991), pp. 197 –201 (cit. on p. 16).

[30] K. T. Wong and R. Luus. “Model reduction of high-order multistage systems by the method of orthogonal collocation”. In: *Canadian Journal of Chemical Engineering* 58 (1980), pp. 382 –388 (cit. on p. 17).

[31] Y. S. Cho and B. Joseph. “Reduced-order steady-state and dynamic models for separation processes. Part I. Development of the model reduction procedure”. In: *AIChE Journal* 29.2 (1983), pp. 261–269 (cit. on p. 17).

[32] W. E. Stewart, K. L. Levien, and M. Morari. “Simulation of fractionation by orthogonal collocation”. In: *Chemical Engineering Science* 40.3 (1985), pp. 409 –421 (cit. on pp. 17, 22, 24).

[33] C. L. E. Swartz and W. E. Stewart. “A collocation approach to distillation column design”. In: *AIChE Journal* 32.11 (1986), pp. 1832–1838 (cit. on pp. 17, 24).

[34] P. Seferlis and A. N. Hrymak. “Optimization of distillation units using collocation models”. In: *AIChE Journal* 40.5 (1994), pp. 813–825 (cit. on p. 17).

[35] R. S. Huss and A. W. Westerberg. “Collocation methods for distillation design. 1. Model description and testing”. In: *Industrial & Engineering Chemistry Research* 35.5 (1996), pp. 1603 –1610 (cit. on pp. 17, 24).

[36] T. Damartzis and P. Seferlis. “Optimal design of staged three-phase reactive distillation columns using nonequilibrium and orthogonal collocation models”. In: *Industrial & Engineering Chemistry Research* 49.7 (2010), pp. 3275 –3285 (cit. on pp. 17, 33).

[37] C. L. E. Swartz and W. E. Stewart. “Finite-element steady state simulation of multiphase distillation”. In: *AIChE Journal* 33.12 (1987), pp. 1977–1985 (cit. on p. 17).

[38] M. M. F. Hasan et al. “Operational modeling of multistream heat exchangers with phase changes”. In: *AIChE Journal* 55 (2009), pp. 150 –171 (cit. on pp. 17, 18).

[39] R. S. Kamath, L. T. Biegler, and I. E. Grossmann. “Modeling multistream heat exchangers with and without phase changes for simultaneous optimization and heat integration”. In: *AIChE Journal* 58.1 (2012), pp. 190–204 (cit. on pp. 17, 18).

[40] J. S. Fossas. “Modelling of Multistream LNG Heat Exchangers”. MA thesis. Norwegian University of Science and Technology, 2011 (cit. on p. 17).

[41] M. M. F. Hasan et al. “Modeling and simulation of main cryogenic heat exchanger in a base-load liquefied natural gas plant”. In: *17th European Symposium on Computer Aided Process Engineering (ESCAPE-17)*. Ed. by V. Plesu and P. S. Agachi. ESCAPE. Bucharest, Romania: Elsevier, 2007 (cit. on pp. 18, 26).

[42] R. C. Pattison and M. Baldea. “Multistream heat exchangers: Equation-oriented modeling and flowsheet optimization”. In: *AIChE Journal* 61.6 (2015), pp. 1856–1866 (cit. on p. 18).

[43] V. Bansal, J. D. Perkins, and E. N. Pistikopoulos. “A case study in simultaneous design and control using rigorous, mixed-integer dynamic optimization models”. In: *Industrial & Engineering Chemistry Research* 41.4 (2002), pp. 760 –778 (cit. on p. 19).

[44] J. M. Smith, H. C. Van Ness, and M. M. Abbott. *Introduction to Chemical Engineering Thermodynamics*. 7th ed. McGRAW-HILL, 2005 (cit. on p. 20).

[45] Robert C. Reid, John M. Prausnitz, and Thomas K. Sherwood. *The Properties of Gases and Liquids*. 3rd ed. McGRAW-HILL, 1977 (cit. on p. 20).

[46] R. D. M. MacRosty and C. L. E. Swartz. “Dynamic optimization of electric arc furnace operation”. In: *AIChE Journal* 53.3 (2007), pp. 640–653. ISSN: 1547-5905. DOI: 10.1002/aic.11104. URL: http://dx.doi.org/10.1002/aic.11104 (cit. on p. 24).

[47] *gPROMS ModelBuilder Documentation*. Release 4.0.0. Process Systems Enterprise Limited. London, United Kingdom, 2014 (cit. on p. 30).

[48] J. E. Cuthrell and L. T. Biegler. “On the optimization of differential-algebraic process systems”. In: *AIChE Journal* 33.8 (1987), pp. 1257 –1270 (cit. on p. 32).

[49] S. Vasantharajan and L. T. Biegler. “Simultaneous strategies for optimization of differential-algebraic systems with enforcement of error criteria”. In: *Computers & Chemical Engineering* 14.10 (1990), pp. 1083 –1100 (cit. on p. 33).

[50] J. V. Villadsen and W. E. Stewart. “Solution of boundary value problems by orthogonal collocation”. In: *Chemical Engineering Science* 22 (1967), pp. 1483–1501 (cit. on p. 37).

[51] J. V. Villadsen and M. L. Michelsen. *Solution of Differential Equation Models by Polynomial Approximation*. Prentice-Hall, Englewood Cliffs, New Jersey, 1978 (cit. on p. 37).

Chapter 3

Optimal Dynamic Operation of a High Purity Air Separation Plant under Varying Market Conditions

3.1 Introduction 52
3.2 Process Model 56
3.3 Optimization Problem Formulation 59
3.4 Case studies: scheduling under time-varying prices and demand 68
3.5 Conclusion 86
References 87

In the air separation industry, distillation-based cryogenic separation is the dominant technology for large scale production of high purity nitrogen, oxygen, and argon products. The use of rigorous dynamic models in the design and operation of air separation units can provide insights into the plant operation to inform the development of economically beneficial designs and operating practices. In this study, we provide a comprehensive analysis on a liquid storage and vaporization strategy for air separation units following a two-tier multi-period formulation with a collocation based dynamic model. Economic incentives for collecting liquid, either directly as liquid product or by liquefaction of overproduced gas product, and then redistribution for meeting gas product demand or for use as additional reflux, are explored in a transient market environment. This includes different electricity price and/or demand profiles, operation costs, as well as product specifications. Operation bottlenecks due to process dynamics constrains the operation practice and hence influences the potential profitability.

Note, portions of this chapter were published in the journal article:

Y. Cao, C.L.E. Swartz and J. Flores-Cerrillo “Optimal Dynamic Operation of a High Purity Air Separation Plant under Varying Market Conditions”. In: *Industrial & Engineering Chemistry Research*, 2016. 55(37), 9956–9970.

3.1 Introduction

Air separation plants produce liquid or gaseous products by separating air into different components. Although there are alternative technologies, cryogenic distillation processes operating at extremely low temperatures still dominate the production of high-purity oxygen, nitrogen and argon products in large qualities. The first step of such a process is typically compression of ambient air to high pressures using a multi-stage compression system, which is very costly due to the amount of energy required [1]. In 2010, the industrial gas sector in U.S. consumed 19.4 TWh, which is sufficient for year-round electricity usage of 1.77 million homes (based on the 2014 average annual electricity consumption for a U.S. residential customer) [2]. Changes in market conditions that include electricity price deregulation, volatile demands and the general trend toward smart energy management, accelerate the transformation of the air separation industry and associated research towards more efficient/flexible process design and dynamic operation. However, complex plant configurations with slow process dynamics, and tight thermal and material integration characteristic of the cryogenic process, constrain the flexibility and agility of such plants [3]. This further motivates our research to closing the gap between the market needs and the process reality through assessing the design and operation of such plants under time-sensitive information with accurate representations of variable interactions and dynamics.

The changing landscape in power generation, distribution and management is of particular relevance to the present study. In order to balance the supply and demand of the power grid over time, energy providers encourage their customers to practice demand response (DR) operations through introducing time varying electricity pricing (e.g. time-of-use and

real-time pricing) and/or providing additional incentive payments (e.g. ancillary service and demand bidding/buyback programs) [4]. With DR activities, these end-users adjust their energy consumption patterns in accordance to the market conditions. With the price-based DR, customers plan out operations based on given or forecast electricity price information, which typically involves voluntarily reducing the consumption when the electricity price is at the peak. An example of such a strategy in air separation unit (ASU) operation is increasing production when the electricity price is low and storing excess product, and reducing production when the electricity price is high with stored product used to meet demand [5]. By storing products while price is low price, a portion of the production requirement (hence the demand for electricity) during the period of high price, is transferred/redistributed. On other hand, with the incentive-based DR, additional compensation is paid to the participating customers when load curtailments are called upon in situations such as electricity system contingencies [4]. Cryogenic energy storage (CES) for ASUs investigated by Zhang *et al.* [6] belongs to this category, where the stored liquid products are used to generate electricity which can be sold to the grid or participate as an ancillary service as reserves available on request.

Air separation units have been the subject of several studies on design and/or operation under changing market conditions. Some of these studies focus more on the operation aspects. The work by Ierapetritou and coworkers [7] considered operation schedules under varying and uncertain electricity prices. In the study, the plant switches between three pre-determined operation modes, and the economically optimal operation mode sequence is identified over the time period of interest. Mitra and coworkers [8] investigated cost-effective operation strategies under real-time electricity pricing, in which ASUs also transition between identified operation modes. For given liquid product storage capacity and demand, and electricity profile, practices of production or shutdown are optimized to reduce the total cost. Zhu and Laird [9] studied the trade-off between profitability and customer satisfaction level for an ASU producing liquid products. In the study, the operation strategies are subjected to

varying electricity price with constant or uncertain demands. This work is later extended to use liquid product storage to improve plant's overall profit [3].

Another branch of studies on ASUs also introduces modifications of the flowsheet in the consideration of single or multiple period operation problems. Miller and coworkers [10] proposed adding storage vessels to collect liquid during column shutdown, which can be re-introduced to the system as reflux during startup to improve plant's agility. The performance of the strategy was evaluated through dynamic simulations. Pattison and Baldea [11] considered the practice of collecting and vaporizing liquid product in a multi-scenario (i.e. off-peak and on-peak electricity price) design study of a nitrogen plant. In their study, steady-state operating conditions are optimized so that a specified constant customer demand can be satisfied, with the total liquid collected in the off-peak scenario available for use in the on-peak scenario. Dynamic transitions are not considered. In more recent work, Pattison *et al.* [5] explored the scheduling problem of an ASU producing gas nitrogen product with a storage-then-vaporization strategy with additional liquefier and storage units. All stored liquid comes from condensing over-produced gas product. The plant operation is subject to time-varying electricity price and demand. A key consideration is the inclusion of process dynamics in the problem formulation, for which a strategy for the identification of low-order data-driven dynamic models was proposed. Zhang *et al.* [6] also addressed the scheduling problem of ASUs by evaluating different utilization of the liquid product to minimize the net operation cost. In this study, the liquid product collected could be used to meet the gas product demand (i.e. vaporization), directly supply the customer or generate electricity (i.e. cryogenic energy storage). Operation mode sequencing together with the distribution of the collected liquid are optimized subject to varying electricity price. Cao *et al.* [12] investigated the use of stored liquid as additional reflux to the top section of the column during transitions to improve plant's agility for a single change in the production load under hourly varying electricity price.

It is well understood that process design, control and operability are highly interactive. Both sequential and simultaneous paradigms for integrated design and control require the proposed design to exhibit satisfactory dynamic performance [13, 14]. However, most of above mentioned studies on ASUs implemented either surrogate/empirical models or steady-state models. Moreover, the work by Pattison and coworkers [5] is the only one that solved multi-period problem with flowsheet modification using dynamic data-driven or detailed first principle models. In other studies with surrogate or empirical models to represent the slow dynamics of the process, assumptions such as fixed start-up time, minimum off-line time or pre-specified transition times between operation modes are commonly introduced [6–8]. Hence, the process dynamics, which may be critical when considering plant transitions [12, 15], are not accurately captured. Studies on ASUs with more accurate representation of the process dynamics though fundamental dynamic models have generally not focused on multi-period operation and/or design modifications. These works primarily consider controller performance [15–18] or operating profile determination targeting a specific load change [12, 19].

The study in this chapter intends to draw a more comprehensive picture for the operation strategy of storage-then-vaporization, as practiced in Pattison and coworkers [5] and Zhang *et al.* [6], using a high purity nitrogen plant with an additional liquid storage tank (design modification). One of the objectives is to understand the economic incentive of such a practice under different time-varying electricity and/or customer demand profiles with:

- alternative liquid collection approaches (i.e. direct liquid product production or liquefaction of over-produced gas product), and
- different stored liquid utilization practices (i.e. vaporization for gas product demand or treating as additional reflux).

Each of these options is assigned an additional operation cost. As the pattern of electricity price, costs of the additional operations, and/or product quality requirements vary, the plant

could adopt different practices. These external conditions are considered known in this study, resulting in deterministic formulations. The other objective is to reveal the bottlenecks posed by process dynamics that force the operation to trade profitability for feasibility. To the best of our knowledge no such studies have been done. The resulting multi-period dynamic optimization problems are solved using accurate collocation based reduced order dynamic models.

The chapter is organized as follows. A description of the plant model used in the study is first introduced in Section 3.2. The proposed two-tier optimization problem formulation involving economic optimization followed by move suppression, is discussed in detail in Section 3.3. Three alternative objective function formulations are presented for the move suppression tier of the problem. Optimization results under various market and operation conditions, as described in the previous paragraph, are documented in Section 3.4. In addition to the scenarios with the storage tank, cases of the current plant configuration are also solved as a benchmark for comparison purposes. Section 3.5 presents concluding remarks highlighting the contributions and recommendations for future studies.

3.2 Process Model

In this chapter, an ASU that produces nitrogen at very high purities (i.e. parts per million impurity) is considered. A typical process flow diagram is shown in Fig. 3.1. Ambient air is compressed and purified, then cooled in a primary heat exchanger (PHX) against the waste N_2 and gas N_2 product streams. A portion of the air feed is withdrawn from within the PHX. After expansion using a turbine, this air stream is fed as vapor into the bottom of the column. The remaining air stream is completely liquefied in the PHX and enters the column as liquid at a location above the vapor air feed. A detailed process description can be found in Cao *et al* [12].

The dynamic N_2 plant model implemented in the optimization studies is derived from the one presented in Cao *et al* [12], using further model formulation and reduction strategies. The distillation column model is a vapor-liquid equilibrium based first principles model. To ensure the prediction accuracy, non-idealities in thermodynamics, tray non-ideality and heat leakage between the cold box and surroundings are also considered. Instead of assuming a constant pressure drop, in this study column tray pressure varies as internal vapor flow rates and tray liquid heads change in the column; this results in an index-1 DAE system, obviating the need for index reduction as conducted in Cao *et al* [12]. Then, to reduce the model size, the stage-wise distillation and primary heat exchanger models are reformulated using the collocation strategy proposed in Cao *et al* [20] for a multi-product ASU. In this earlier study, significant model size reduction was achieved without sacrificing the desired prediction accuracy. In the collocation approach, modeling equation sets, including tray hydraulics, material and energy balances, as well as physical and thermal property equations, are required only at the collocation points instead of each stage. Profiles of the system's algebraic and differential states are approximated using low order polynomials constructed from information at the collocation points [20, 21].

In the present application, one finite element (FE) with 4 collocation points (CPs) is used for the section of the PHX before vapor air feed removal. In the column section, a grid of multiple FEs with 2 CPs per FE is adopted. After model reduction, the collocation based model is less than 40 % of the dimension of the equivalent full-order stagewise version. The execution time for conducting identical dynamic simulations is shortened by about 70 %. The numerical condition of the reduced model is also improved based on the number of corrector and error test failures during simulations as reported by `gPROMS 4.1.0`. This implies significant solution time reduction when optimization iterations are involved. However, a high level of prediction accuracy is maintained, consistent with results of our previous study[20]. For example, the difference in temperature predictions for the GN_2 stream leaving the PHX is less than 0.1 % between the collocation based and full order integrated plant model.

The integrated plant model used in this study consists of

- air feed compressor and turbine models – that take the form of algebraic equations (AEs)
- primary heat exchanger model – a collocation-based model with dynamic energy balances, which takes the form of a DAE system
- distillation column model – a reduced-order vapor-liquid equilibrium based model with dynamic material and energy balances, of DAE form
- integrated reboiler/condenser (IRC) model – dynamic model similar to a column tray with level controllers, of DAE form.

Additionally, since now we also consider product storage, a mathematical representation of the storage tank needs to be derived. Either a simplified model assuming constant liquid density, or a more rigorous model considering component material and energy balances could be used. However, due to the fact that the liquid collected comes from product streams having tight purity requirements at parts per million levels, the constant density assumption holds. This gives

$$\rho_{\text{storage}} \frac{dV_{\text{storage}}(t)}{dt} = \sum_{i=1}^{N_{in}} F_{in,i}(t) - \sum_{j=1}^{N_{out}} F_{out,j}(t) \tag{3.1}$$

where ρ_{storage} is the liquid density, V_{storage} is the liquid volume, and N_{in} and N_{out} represent the number of inlet and outlet streams, respectively. Evaluations of simplified and rigorous storage tank models through dynamic optimization studies confirm the validity of this assumption. Hence, Eqn. 3.1 is implemented to represent the liquid storage tank.

3.3 Optimization Problem Formulation

Constrained dynamic optimization problems solved in this study take the general form

$$\min_{\mathbf{u}(t)} \Phi(\mathbf{u}(t), t_f) \tag{3.2a}$$

$$\text{subject to:} \quad \mathbf{f}(\dot{\mathbf{x}}(t), \mathbf{x}(t), \mathbf{z}(t), \mathbf{u}(t), \mathbf{p}, t) = \mathbf{0} \tag{3.2b}$$

$$\mathbf{g}(\mathbf{x}(t), \mathbf{z}(t), \mathbf{u}(t), \mathbf{p}, t) = \mathbf{0} \tag{3.2c}$$

$$\mathbf{h}(\mathbf{x}(t), \mathbf{z}(t), \mathbf{u}(t), \mathbf{p}, t) \leq \mathbf{0} \tag{3.2d}$$

$$\mathbf{h}_j(\mathbf{x}(\bar{t}_j), \mathbf{z}(\bar{t}_j), \mathbf{u}(\bar{t}_j), \mathbf{p}, \bar{t}_j) \leq \mathbf{0}, \quad \forall j \in J \tag{3.2e}$$

$$\mathbf{h}_f(\mathbf{x}(t_f), \mathbf{z}(t_f), \mathbf{u}(t_f), \mathbf{p}, t_f) \leq \mathbf{0} \tag{3.2f}$$

$$\dot{\mathbf{x}}(t_0) = \mathbf{0} \tag{3.2g}$$

$$t_0 \leq t \leq t_f \tag{3.2h}$$

In the above equations, $\mathbf{x}$, $\mathbf{z}$, $\mathbf{u}$ and $\mathbf{p}$ represent differential states, algebraic states, control inputs and parameters vectors. $\mathbf{f}$ and $\mathbf{g}$ comprise the plant model equations in differential-algebraic form, and $\mathbf{h}$ includes variable bounds and operational constraints. The subscripts j and f denote the j^{th} interior point (at time $\bar{t}_j$) and endpoint (at t_f), respectively.

3.3.1 Decision Variables

The plant configuration used is shown in Fig. 3.1. The dashed lines in the diagram represent potential process streams that are available only with a proposed design modification of an external storage tank. Decision variables in this study are listed in Table 3.1. Dynamic trajectories for all these flows are optimized.

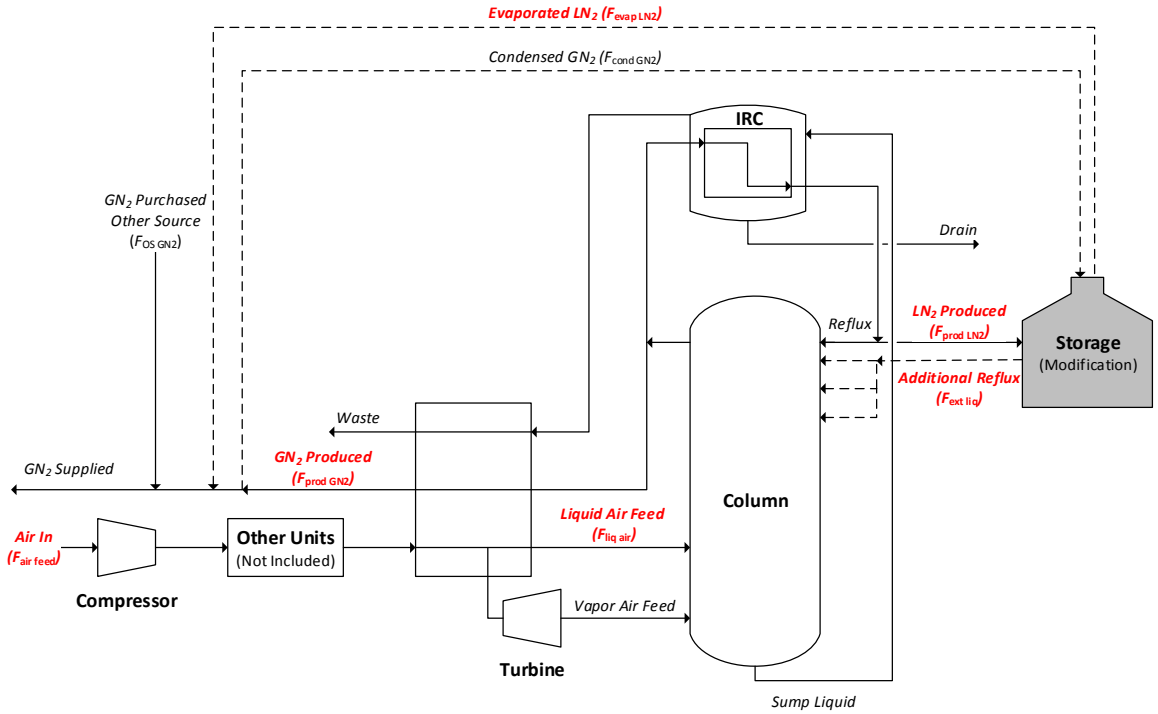

Figure 3.1: Case study ASU configuration (solid lines are existing streams with the base case plant design and dashed lines are streams available with design modifications).

Note that the condensed GN_2 stream, $F_{\text{cond GN}_2}$, is computed as

$$F_{\text{cond GN}_2}(t) = \max(0, F_{\text{prod GN}_2}(t) + F_{\text{evap LN}_2}(t) - D(t)) \tag{3.3}$$

due to the assumption that there is no market value for product that exceeds the specified demand (i.e. over supplied product has no selling value and can be condensed). It is also assumed that when the plant's production, $F_{\text{prod GN}_2}$, together with vaporized stored liquid, $F_{\text{evap LN}_2}$, cannot satisfy the demand, there is a high penalty for the unmet portion (due, for example, to purchase from other sources). Hence, GN_2 from other sources, $F_{\text{OS GN}_2}$, is calculated as:

$$F_{\text{OS GN}_2}(t) = \max(0, D(t) - (F_{\text{prod GN}_2}(t) + F_{\text{evap LN}_2}(t))) \tag{3.4}$$

Table 3.1: Potential decision variables.

Variable	Symbol	Plant Configuration
Air feed to the compressor	$F_{\text{air feed}}$	Original
GN_2 production rate	$F_{\text{prod GN}_2}$	Original
Liquid air feed to the column	$F_{\text{liq air}}$	Original
LN_2 production rate	$F_{\text{prod LN}_2}$	Original
Stored LN_2 evaporation rate	$F_{\text{evap LN}_2}$	Modified
Additional reflux	$F_{\text{ext liq}}$	Modified

Table 3.2: Piecewise constant control profile setup.

		# of Control Intervals	Decision Variable
Initial steady state (no parameter changes)		1	Specified
Change in parameters	Fast Transition	3	Optimized
	Settling Period	1	Optimized

where D is the customer demand.

The study in this chapter uses piecewise constant input profiles with the control interval duration time specified. The control intervals used are described in Table 3.2 and illustrated in Fig. 3.2. When the system encounters a transition in the market conditions (e.g. electricity price and/or demand change), the plant can adopt 3 fast adjustments, followed by a settling movement, in system inputs. This approach that uses non-equally spaced control intervals allows necessary transition control actions to be captured with fewer optimization variables.

3.3.2 Constraints

Constraints in the study comprise both endpoint and path constraints, and are summarized in Table 3.3. The resulting trajectories must guarantee feasible operation within equipment limitations, away from column flooding and compressor surge, while satisfying operational constraints such as liquid level and process stability. Off-spec product is not permitted and a safety margin on product purity is enforced, both during transition and at steady state, with a tighter margin at steady state (i.e. $\text{PPMO}_{ss}^{UB} < \text{PPMO}_{\text{trans}}^{UB}$, where PPMO signifies parts per

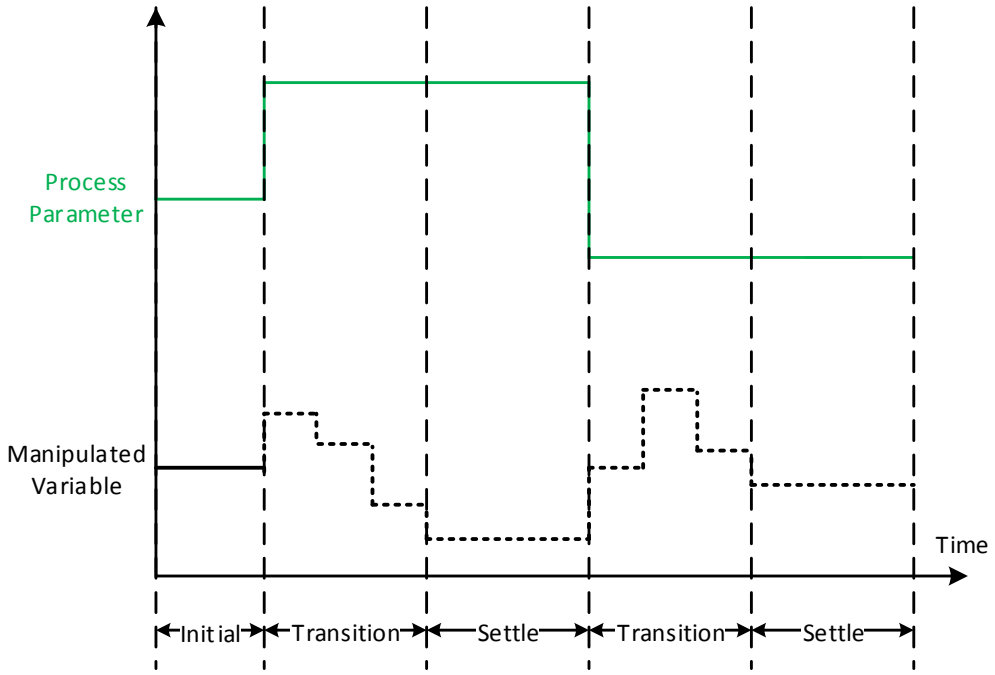

Figure 3.2: Illustration of the control profile

million oxygen) unless otherwise specified. Additional constraints requiring the turbine inlet and discharge streams to be above the dew point, and the column liquid air feed to be below its bubble point are imposed [12].

Each path constraint is converted into a combination of endpoint and interior point inequality constraints ($\mathbf{h}_j$ and $\mathbf{h}_f$ in Eqn. 4.2) [19]. For example, the reboiler liquid lower and upper bounds are expressed as

$$l_{\text{reb}}^{LB} \leq l_{\text{reb}}(t) \Rightarrow \begin{cases} \dfrac{d\epsilon_{\text{reb}}^{LB}(t)}{dt} = [\max(0, l_{\text{reb}}^{LB} - l_{\text{reb}}(t))]^2 \quad \text{and} \quad \epsilon_{\text{reb}}^{LB}(t_f) \leq \varepsilon_{\text{reb}} \\ l_{\text{reb}}^{LB} \leq l_{\text{reb}}(\bar{t}_j) \end{cases} \tag{3.5}$$

$$l_{\text{reb}}(t) \leq l_{\text{reb}}^{UB} \Rightarrow \begin{cases} \dfrac{d\epsilon_{\text{reb}}^{UB}(t)}{dt} = [\max(0, l_{\text{reb}}(t) - l_{\text{reb}}^{UB})]^2 \quad \text{and} \quad \epsilon_{\text{reb}}^{UB}(t_f) \leq \varepsilon_{\text{reb}} \\ l_{\text{reb}}(\bar{t}_j) \leq l_{\text{reb}}^{UB} \end{cases} \tag{3.6}$$

where $\epsilon_{\text{reb}}^{LB}$ and $\epsilon_{\text{reb}}^{UB}$ represent accumulated constraint violations, and ε_{reb} is a pre-determined

Table 3.3: Constraints in the study.

Constraint	Type	Expression
Final steady state (stability)	Endpoint	$-\varepsilon_{ss} \leq \frac{dx(t_f)}{dt} \leq \varepsilon_{ss}$
Steady state purity	Endpoint	$\text{PPMO}(t_f) \leq \text{PPMO}_{ss}^{UB}$
Final volume in storage tank	Endpoint	$V_{\text{final}}^{LB} \leq V_{\text{storage}}(t_f) \leq V_{\text{final}}^{UB}$
Purity constraint	Path	$\text{PPMO}(t) \leq \text{PPMO}_{\text{trans}}^{UB}$
Sump liquid level	Path	$l_{\text{sump}}^{LB} \leq l_{\text{sump}}(t) \leq l_{\text{sump}}^{UB}$
Reboiler liquid level	Path	$l_{\text{reb}}^{LB} \leq l_{\text{reb}}(t) \leq l_{\text{reb}}^{UB}$
Flooding constraint	Path	$\alpha_{\text{flood}}(t) \leq 1$
Dew point at turbine outlet	Path	$T_{\text{TB out}} \geq T_{\text{TB out}}^{\text{dew}} + \varepsilon_{\text{TB out}}$
Dew point at turbine inlet	Path	$P_{\text{TB in}}(t) \leq P_{\text{TB in}}^{\text{dew}} - \varepsilon_{\text{TB in}}$
Bubble point at liquid air feed	Path	$P_{\text{liq air}}(t) \geq P_{\text{liq air}}^{\text{bubble}}(t) + \varepsilon_{\text{liq air}}$
Storage volume constraint	Path	$V_{\text{storage}}^{LB} \leq V_{\text{storage}}(t) \leq V_{\text{storage}}^{UB}$

tolerance.

3.3.3 Objective Function

To obtain an economically optimal operation policy with a relatively smooth control profile, a two tiered approach is proposed. The first step is to solve a dynamic optimization problem with an economic objective function to minimize the accumulated operation cost over the time horizon of interest. The optimization problem takes the general form,

$$\min_{\mathbf{u}(t)} \int_{t_0}^{t_f} \varphi_{\text{econ}}(t)dt \tag{3.7a}$$

subject to
- DAE process model (3.7b)
- operational path and point constraints

where

$$\begin{aligned}\varphi_{\text{econ}}(t) = C_{\text{elec}}(t)W_{\text{comp}}(t) + C_{\text{cond}}(t)F_{\text{cond GN}_2}(t) + C_{\text{evap}}(t)F_{\text{evap LN}_2}(t) \\ + C_{\text{OS}}(t)F_{\text{OS GN}_2}(t) + C_{\text{ext liq}}(t)F_{\text{ext liq}}(t) - C_{\text{GN}_2}(t)F_{\text{sale}}(t)\end{aligned} \tag{3.8}$$

In the above equation, C_{cond}, C_{evap}, C_{OS} and $C_{\text{ext liq}}$ are costs associated with condensation, vaporization, penalty due to unfulfilled demand and using additional reflux, while $F_{\text{cond GN}_2}$, $F_{\text{evap LN}_2}$, $F_{\text{OS GN}_2}$ and $F_{\text{ext liq}}$ are corresponding stream flow rates. C_{elec} and C_{GN_2} are the electricity price and selling price of the GN_2 product, respectively. W_{comp} is the power consumption of the compressor system to process the air feed. Since over-produced product has no revenue associated with it, the GN_2 sold, F_{sale}, is defined as

$$F_{\text{sale}}(t) = \min(D(t), F_{\text{supplied GN}_2}(t)) \tag{3.9}$$

$$F_{\text{supplied GN}_2}(t) = F_{\text{prod GN}_2}(t) + F_{\text{GN}_2\text{ OS}}(t) + F_{\text{evap LN}_2}(t) - F_{\text{cond GN}_2}(t) \tag{3.10}$$

The solution of the first tier provides an achievable economic optimal point and an initial set of control trajectories. However, such input profiles may contain unnecessary oscillations, which are undesirable for implementation in the actual plant operations. Hence, a second tier dynamic optimization problem is solved to suppress the input movements:

$$\min_{\mathbf{u}(t)} \varphi_{\text{MS}} \tag{3.11a}$$

$$\text{subject to} \quad \bullet \text{ DAE process model} \tag{3.11b}$$

$$\bullet \text{ operational path and point constraints}$$

An additional constraint is introduced to ensure that the economic performance is maintained to within a specified tolerance:

$$\int_{t_0}^{t_f} \varphi_{\text{econ}}(t)dt \leq \varphi_{T1}^{*} + \varepsilon \tag{3.12}$$

where φ_{MS} represents the objective function for the move suppression, φ^*_{T1} is the value of the economic-based objective function at the solution of the tier 1 problem, and ε is a user-specified tolerance. A similar strategy for achieving optimal economics in dynamic optimization with reduced input variation was used in Balthazaar[22], and extended to multi-tiered optimization in Chong and Swartz[23]. An alternative approach is to append a move suppression penalty to the economic objective function, but this introduces an arbitrary weighting of the two objectives, which is avoided in the present approach.

Typically, the move suppression problem requires information of the control profile at specific points in time to minimize the summation of absolute or squared changes in the system inputs. However, when the dynamic optimization problem is solved following the sequential approach in a platform such as gPROMS, the user may have no direct access to such information. To address this issue, we propose three different formulations that could potentially mimic the original problem.

Formulation 1: *Trajectory tracking based*

From the solution of the first tier problem, a set of desired operation trajectories, $\overline{u}_i(t)$, can be determined. For example, operation points during the settling periods can be utilized to assemble target/reference trajectories for the system inputs. $\overline{u}_i(t)$ is then specified as operation parameters in the second tier of the problem and the objective function, Eqn. 3.11a, can be simply formulated as:

$$\min_{\mathbf{u}(t)} \varphi_{\text{MS}} = \min_{\mathbf{u}(t)} \int_{t_0}^{t_f} \sum_{i=1}^{N_{\text{MV}}} \left[u_i(t) - \overline{u}_i(t)\right]^2 dt \tag{3.13}$$

Formulation 2: *Approximation using time invariant variables with hyperbolic functions*

This formulation is inspired by applying hyperbolic tangent functions to approximate the discontinuity in a piecewise linear function. The basic concept is that the piecewise constant

time varying input profile can be approximated using a group of time invariant parameters:

$$\begin{aligned} u_i(t) =& 0.5[1+\tanh(s(\tau_1 - t))]a_{1,i} \\ &+ \sum_{k=2}^{N_{\text{CI}}-1} \{0.25[1+\tanh(s(\tau_k - t))][1-\tanh(s(\tau_{k-1} - t))]\}a_{k,i} \\ &+ 0.5[1-\tanh(s(\tau_{N_{\text{CI}}} - t))]a_{N_{\text{CI}},i} \end{aligned} \tag{3.14}$$

where τ_n is the ending time of control interval n and $a_{n,i}$ is the value of control variable i at control interval n. In the above equation, s is the steepness factor that guides the sharpness of the change; the larger the value for s is, the closer Eqn. 3.14 approximates a piecewise constant profile. For t in control interval n, $\tau_{n-1} < t < \tau_n$, with a large value for s,

$$1+\tanh(s(\tau_k - t)) \approx \begin{cases} 0, \text{for } k = 1, \ldots, n-1 \\ 2, \text{for } k = n, \ldots, N_{CI} \end{cases} \tag{3.15a}$$

$$1-\tanh(s(\tau_k - t)) \approx \begin{cases} 2, \text{for } k = 1, \ldots, n-1 \\ 0, \text{for } k = n, \ldots, N_{CI} \end{cases} \tag{3.15b}$$

and according to Eqn. 3.14,

$$u_i(t) = 0 + \{0.25 \times 2 \times 2\}a_{n,i} + 0 = a_{n,i}, \quad \tau_{n-1} < t < \tau_n \tag{3.16}$$

A trajectory with the hyperbolic tangent function approximation is illustrated in Fig. 3.3a. The objective function, Eqn. 3.11a, now simply takes the form

$$\min_{\mathbf{u}(t)} \varphi_{\text{MS}} = \min_{\mathbf{a}} \sum_{n=2}^{N_{\text{CI}}} \sum_{i=1}^{N_{\text{MV}}} (a_{i,n} - a_{i,n-1})^2 \tag{3.17}$$

where $\mathbf{a}$ is a composite vector of the $a_{i,n}$ coefficients.

Formulation 3: *Approximation using valve dynamics*

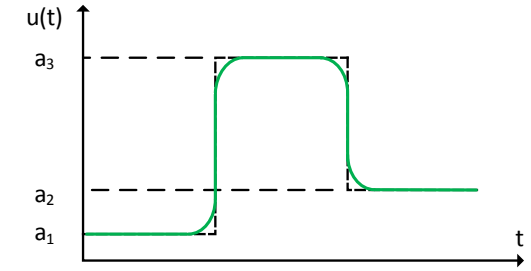

(a) Hyperbolic tangent function

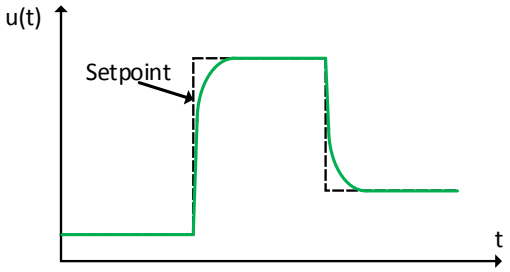

(b) Valve dynamic

Figure 3.3: Different approximations for piecewise constant input profile.

In this strategy, we penalize the rate of change of the inputs, which over a fixed time interval reflects the magnitude of the change. First, we introduce control valve dynamics,

$$\tau_{\text{valve}} \frac{du_i(t)}{dt} = u_i^{SP}(t) - u_i(t). \tag{3.18}$$

With small τ_{valve}, the piecewise constant control profile can be approximated, as shown in Fig. 3.3b. Noting that when the value of the system input, $u_i(t)$ reaches its setpoint, u_i^{SP}, $\frac{du_i(t)}{dt}$ takes a value of zero and makes no contribution to the accumulated rate of change. Hence, the move suppression problem, Eqn. 3.11a, is defined as

$$\min_{\mathbf{u}(t)} \varphi_{\text{MS}} = \min_{\mathbf{u}^{SP}(t)} \int_{t_0}^{t_f} \sum_{i=1}^{N_{\text{MV}}} \left[\left(\frac{du_i(t)}{dt} \right)^2 \right] dt. \tag{3.19}$$

The performance of these three formulations is presented in the next section.

3.4 Case studies: scheduling under time-varying prices and demand

As mentioned previously, the planning and scheduling studies on ASUs have traditionally been conducted with steady-state or simplified empirical models. Optimal plant operation in the face of varying electricity price and/or customer demand has not yet been fully analyzed using dynamic models. In response to electricity price fluctuations, the plant could follow the strategy of overproducing and liquefying the over-supplied product at low electricity price, then unloading the plant at high electricity price and vaporizing stored liquid product to meet constant and/or varying demand to seize the economic benefit. Such a store-then-vaporize practice was included in the work by Pattison and coworkers [5, 11], and Zhang *et al.* [6]. For a plant with both vapor and liquid production capability, the stored liquid could be collected (1) directly from liquid product or (2) through liquefying gas product. However, the amount of liquid product that can be directly extracted is typically limited by the plant and equipment design [24]. In this part of the study, assuming that the storage tank already exists, we would like to explore the following questions:

1. How could the practice of storage and vaporization benefit the plant operation and where should the liquid be collected?
2. How does the peak-to-minimum electricity price ratio ($P_{\text{elec}}^{\text{peak}}/P_{\text{elec}}^{\text{min}}$) affect the practice of storage and vaporization becoming a valid option for a given demand?
3. How should the collected liquid be utilized: vaporized to meet the demand or introduced as additional reflux, given the processing cost of the two options?

We note that the nitrogen plant on which the study is based originally focused on gas phase N_2 production, and assume that a liquefaction system is available to condense the over-produced gas product.

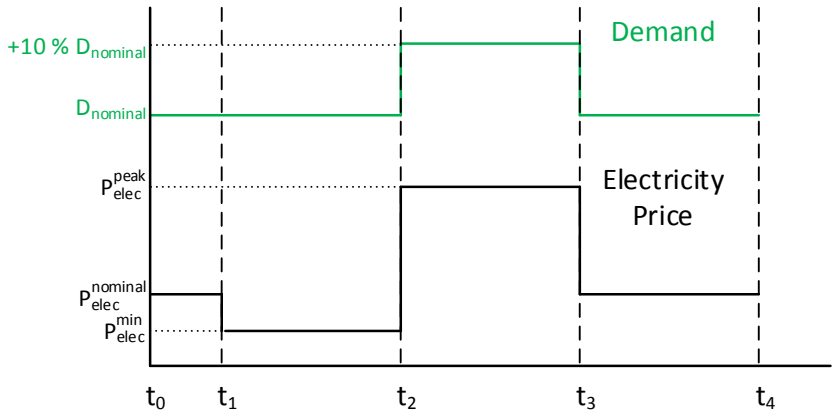

Figure 3.4: Example electricity and demand profile for the operational planning study. Two different sets of times, $\mathbf{t} = [t_0, t_1, t_2, t_3, t_4]$, are used in the study. The demand has a 10 % increase during the second change period unless otherwise specified. Starting from a nominal value ($P_{\text{elec}}^{\text{nominal}}$), the electricity price first decreases to ($P_{\text{elec}}^{\text{min}}$) then increases to ($P_{\text{elec}}^{\text{peak}}$) before returning to the nominal value.

3.4.1 Case 1: storage and vaporization only

In this part of the study, it is assumed that the stored liquid can be vaporized to meet customer demand as commonly practiced in the industry.[3, 5, 11] The demand and electricity price profile are given, as illustrated in Fig. 3.4. There are three changes in the electricity price following the initial period: off-peak (low), on-peak (high) and mid-peak. The off-peak electricity price is taken to be 40 % of the mid-peak value while multiple on-peak price values are considered. It is further assumed that when the electricity price is high, the customer also has an increase in the demand. Initially, the plant operates at a condition with low product impurity. Such operation is not economically optimal; however, it is practiced to keep a safety margin from the actual critical constraint.

Proportional controllers are implemented to regulate the liquid inventory in the reboiler and column sump liquid. The levels are controlled by adjusting the liquid discharge from the reboiler (i.e. drain) and the column (i.e. sump liquid). The expression for the proportional

control action is:

$$F_i(t) = F_i^{SS} + Kc_i \left(l_i(t) - l_i^{SS} \right), \quad i = \{\text{reb, sump}\} \tag{3.20}$$

where F_i and F_i^{SS} are the drain/sump liquid flow rate and their corresponding steady-state value, l_i and l_i^{SS} are the current level and set-point for the reboiler/column sump liquid inventory, and Kc_i is the controller gain.

It is hypothesized that the GN_2 liquefaction costs, the duration of the parameter change, as well as the electricity price peak-to-minimum ratio all affect the optimal operation policy decision. Hence, as shown in Table 4, a total of 8 dynamic optimization problems are solved here covering scenarios with different change duration ($\mathbf{t}$), operation cost (C_{evap} here) and peak-to-minimum ratios ($P_{\text{elec}}^{\text{peak}}/P_{\text{elec}}^{\text{min}}$). S1.1 and S1.2 in Table 3.4 are the benchmark cases and are solved for comparison purposes. In these reference cases, economically optimal operation is determined without consideration of the external storage. The change duration ($\mathbf{t}$ in Fig. 3.4) is $\mathbf{t} = [0, 1, 9, 17, 25]$ hours for S1.1, S1.3 and S1.5 – S1.8, and $\mathbf{t} = [0, 1, 3, 5, 8]$ hours for S1.2 and S1.4. In scenarios S1.3 – S1.6, operation optimization problems are solved with an external storage tank of a given capacity. In these studies, different values of the process parameters are used. Scenarios S1.7 and S1.8 are variants of earlier cases that further explore impacts related to stored liquid product. Decision variables in this part of the study consist of GN_2 production rate, LN_2 production rate, air feed flow rate, evaporation rate and liquid air flow rates. At the end of the time horizon, the plant needs to reach steady state and satisfy the demand without using liquid vaporization.

Remark The use of proportional-integral (PI) controllers to regulate the liquid levels, and the impact thereof on the optimization results were also investigated. However, for the same scenario, the optimal operation practices with P or PI controllers were found to be very similar, and for clarity only a single controller type (P-control) is considered in the sequel.

Table 3.4: Scenarios with different values of process parameters used in the vaporization study (Case 1)

Scenario	Time Set $\mathbf{t} = [t_0, t_1, t_2, t_3, t_4]$	Storage	$P_{\text{elec}}^{\text{peak}}/P_{\text{elec}}^{\text{min}}$	C_{cond} $(\%C_{GN_2})$	C_{evap} $(\%C_{GN_2})$	C_{OS} $(\%C_{GN_2})$
S1.1[†]	[0,1,9,17,25]	No	4	-	-	500 %
S1.2[†]	[0,1,3,5,8]	No	4	-	-	500 %
S1.3	[0,1,9,17,25]	Yes	4	5 %	5 %	500 %
S1.4	[0,1,3,5,8]	Yes	4	5 %	5 %	500 %
S1.5	[0,1,9,17,25]	Yes	4	5 %	50 %	500 %
S1.6	[0,1,9,17,25]	Yes	8	5 %	50 %	500 %
S1.7[‡]	[0,1,9,17,25]	Yes	4	-	5 %	500 %
S1.8[§]	[0,1,9,17,25]	No	8	-	-	500 %

[†] Benchmark scenarios: no storage (GN_2 condensation or LN_2 vaporization is not available).
[‡] Additional supporting case: similar setup as S1.3 but stored liquid is forced to be generated from LN_2 production only.
[§] Additional supporting case: similar setup as S1.6 but no storage is available.

Benchmark scenarios – no storage: S1.1 and S1.2

Fig. 3.5 shows the optimal profile for selected system variables for Scenario S1.2 at the solution of tier 1 (i.e. the economically optimal point). Variables are presented as scaled values. The electricity and demand profiles used are illustrated in Fig. 3.4. In these cases, the electricity price initially decreases to $P_{\text{elec}}^{\text{min}}$ when $t \in [t_1, t_2)$, then increases to $P_{\text{elec}}^{\text{peak}}$ when $t \in [t_2, t_3)$, and finally returns to $P_{\text{elec}}^{\text{nominal}}$ when $t \in [t_3, t_4]$. On the other hand, the GN_2 demand increased by 10 % during the period when $t \in [t_2, t_3)$, and returns to the nominal value for the rest of the time horizon. When there is no external storage available for storing the liquid, the plant loads and unloads as the demand changes. Optimal trajectories of GN_2 production in Fig. 3.5c coincide with the demand profile. Operations are pushed to the maximum allowable impurity level to increase the nitrogen recovery (Fig. 3.5e). Since the LN_2 product has no sale value (this is a gas plant, hence no customer for liquid product), the production of LN_2 is reduced to the minimum at the solution (Fig. 3.5d). When the air feed flow rate decreases, the compressor surge limit (minimum flow for required discharge

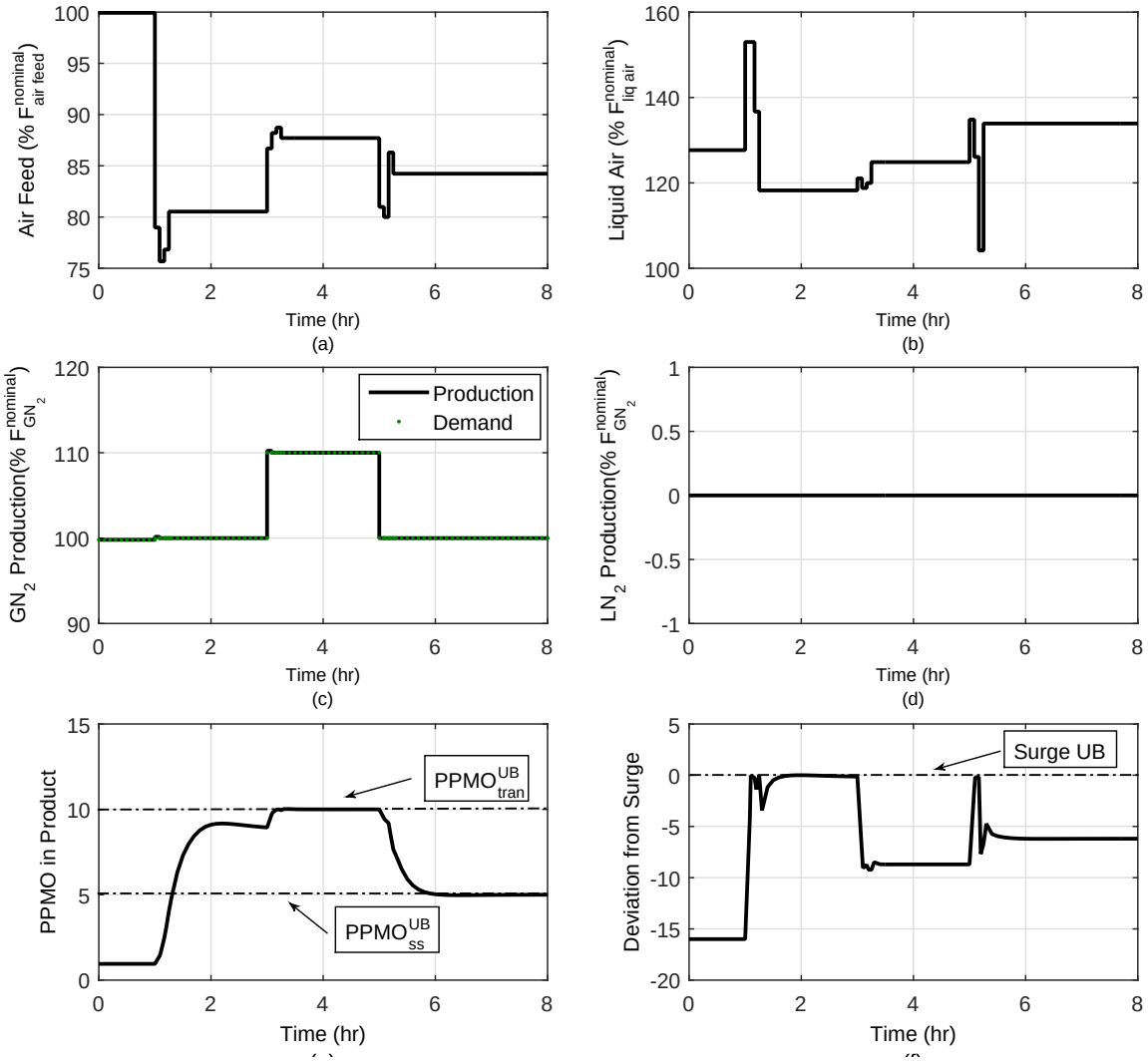

Figure 3.5: Optimal trajectories for selected variables in scaled values for Scenario S1.2 using economic objective function (tier 1).

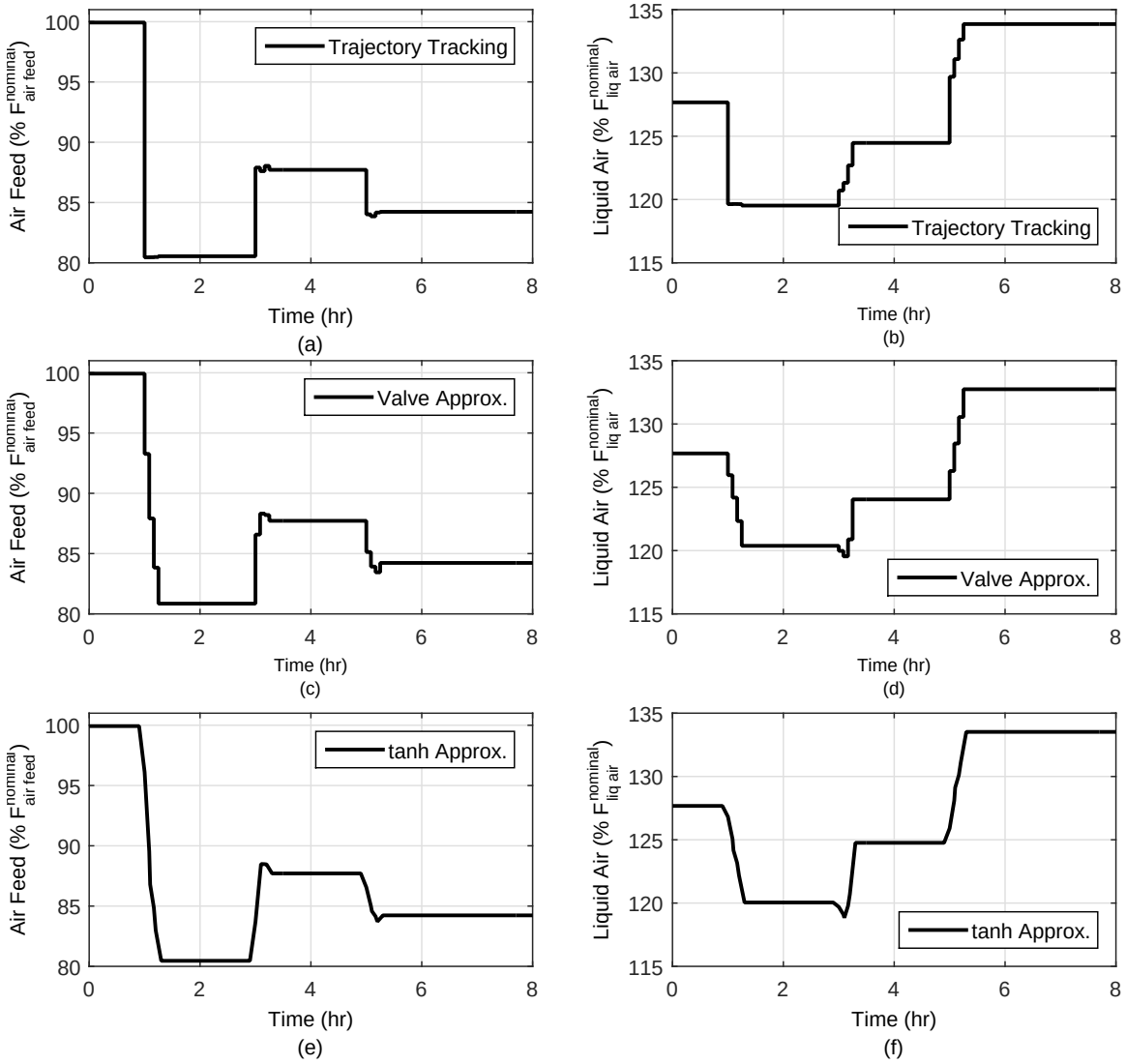

Figure 3.6: Optimal solution for Scenario S1.2 after move suppression (tier 2). Corresponding tier 1 solution is presented in Fig. 3.5.

pressure) is active, as indicated in Fig. 3.5f for $t \in [1, 3)$. In addition, the liquid air bubble point constraints at the PHX outlet are active during the operation. This means that these constraints limit the plant's overall performance and reconfiguring these units may improve plant's flexibility and agility. Such observations are consistent with the results obtained in our previous study.[12] Resulting trajectories for the benchmark scenarios, S1.1, show similar behavior and will not be repeated here. However, the solution of S1.1, together with that of S1.2, will be used as the comparison benchmark for later cases, where liquid storage becomes available.

As illustrated in Fig. 3.5, trajectories of the manipulated variables at the solution of the dynamic optimization problem with a pure economic-based objective function (tier 1) show periods of sharp variation/ocsillation, such as the total air feed flow (Fig. 3.5a) and liquid air flow (Fig. 3.5b). Such variations are undesirable in actual operating practice, thus a move suppression problem is solved to provide more suitable trajectories for plant implementation. Fig. 3.6 summarizes the resulting trajectories for the system inputs from the move suppression layer with all three forms of the objective function: trajectory tracking (Fig. 3.6a,b), valve approximation (Fig. 3.6c,d) and hyperbolic tangent function approximation (Fig. 3.6e,f). As shown, trajectories from the move suppression tier are smoother than those from the first tier of the optimization problem. There are slight differences between the results from the trajectory tracking formulation and the other two strategies: changes in the system input are more rapid than the other two cases. It is due to the fact that the deviations from the target trajectories are penalized with this formulation instead of the changes in the inputs. Among the three, the optimization problem with the hyperbolic based objective function tends to be more challenging to solve in `gPROMS` as it is observed that the resulting problems are more sensitive to the initial decision variable profiles supplied.

Remarks

1. For the remainder of this chapter, only the results from the move suppression tier

following the trajectory tracking formulation will be reported.

2. The execution time for solving the dynamic optimization problems presented in this study varies depending on the quality of the initial guesses supplied for the decision variables. For S1.2, gOPT converged to an optimal solution in about 1 hour for the economic optimization tier. At the move suppression tier, starting from the solution of Tier 1, the trajectory tracking and valve dynamic approximation formulations found optimal solutions in approximately 0.61 and 0.65 hours, respectively. The hyperbolic approximation problem is more challenging to solve; gOPT failed to claim an optimal solution with the same initial guess, but when initialized with the solution of the valve dynamic approximation, gOPT converged to an optimal solution in 0.45 hours. While the present detailed model and solution approach are appropriate for analysis, as in the present study, faster strategies would beneficial for real-time application.

Use of product storage and vaporization: S1.3, S1.4 and S1.7

Results for different scenarios with a storage tank available are tabulated in Table 3.5. In this section of the paper, the product storage option is evaluated with two sets of change duration, $\mathbf{t}$, as in the benchmark section. The optimization problems are still subject to the electricity and demand profiles shown in Fig. 3.4. For Scenarios S1.3 and S1.4, the optimal operation practice utilizes the storage and vaporization to gain improvements in economic performance. As indicated in Table 3.5, cost savings of 1.5 % and 1.3 % are realized for S1.3 and S1.4, respectively, relative to the corresponding base cases with the same change duration in electricity and demand profiles. Trajectories for liquefied GN_2 flow, LN_2 production rate, evaporation rate of stored liquid and storage volume for S1.3 and S1.4, together with the total air feed rate and product purity, are presented in Figs. 3.7 and 3.8, respectively. The bound on the product purity is active during transitions in both cases (Figs. 3.7b and 3.8b). Due to changes in the electricity price, even though the plant can

use production to meet the demand, as illustrated in S1.1 and S1.2, the optimal strategy involves storage and vaporization. When the electricity price is low, the plant gradually builds the liquid storage, indicated by the upward trend in the storage volume in Figs. 3.7f and 3.8f, either by LN_2 production or GN_2 liquefaction. Both mechanisms are practiced when the change duration is long, $\mathbf{t} = [0, 1, 9, 17, 25]$, as in Figs. 3.7c and 3.7d. When the change duration reduces, $\mathbf{t} = [0, 1, 3, 5, 8]$, only LN_2 production is utilized (Figs. 3.8c and 3.8d). The reason for practicing different mechanisms is explained in the next paragraph. When the electricity price is at the peak, the stored liquid is vaporized to meet the demand, hence, the storage volume decreases (Figs. 3.7f and 3.8f) and the LN_2 evaporation flow rate becomes non-zero (Figs. 3.7e and 3.8e).

Since the LN_2 product has no additional condensation cost, when the storage/vaporization strategy is practiced, direct liquid collection from LN_2 product is more economical than over-producing then liquefying the GN_2 product. LN_2 production should be utilized as the primary source for generating the stored liquid. This is confirmed by the optimization results for Scenario S1.4, where flow rates of the GN_2 condensation stream is negligible through out the entire control horizon, Fig. 3.8c. In this case, to prepare for the upcoming increase in the electricity price, LN_2 production becomes non-zero, but it only remains at the high level for 2 hours, i.e. $t \in [1, 3 \text{ hr})$. Note that the reboiler liquid level is approaching the lower bound at the end of the first settling period (i.e. $t = 3$ hr), Fig. 3.9d. Due to such dynamic behavior of the plant, increasing the LN_2 production could potentially lead to operation constraint violations. In the IRC, the vapor stream from the column top is condensed against the liquid holdup on the reboiler side. When more top vapor needs to be condensed in the IRC (such as in the case of collecting the liquid product), more reboiler liquid is boiled up, leading to a decrease in liquid level with potential constraint violation if this practice continues. In these situations, collecting liquid product via other means such as through GN_2 condensation becomes necessary. As illustrated in S1.3, to prevent violating the reboiler level lower bound (Fig. 3.9b), the LN_2 production rate needs to be reduced from about 10

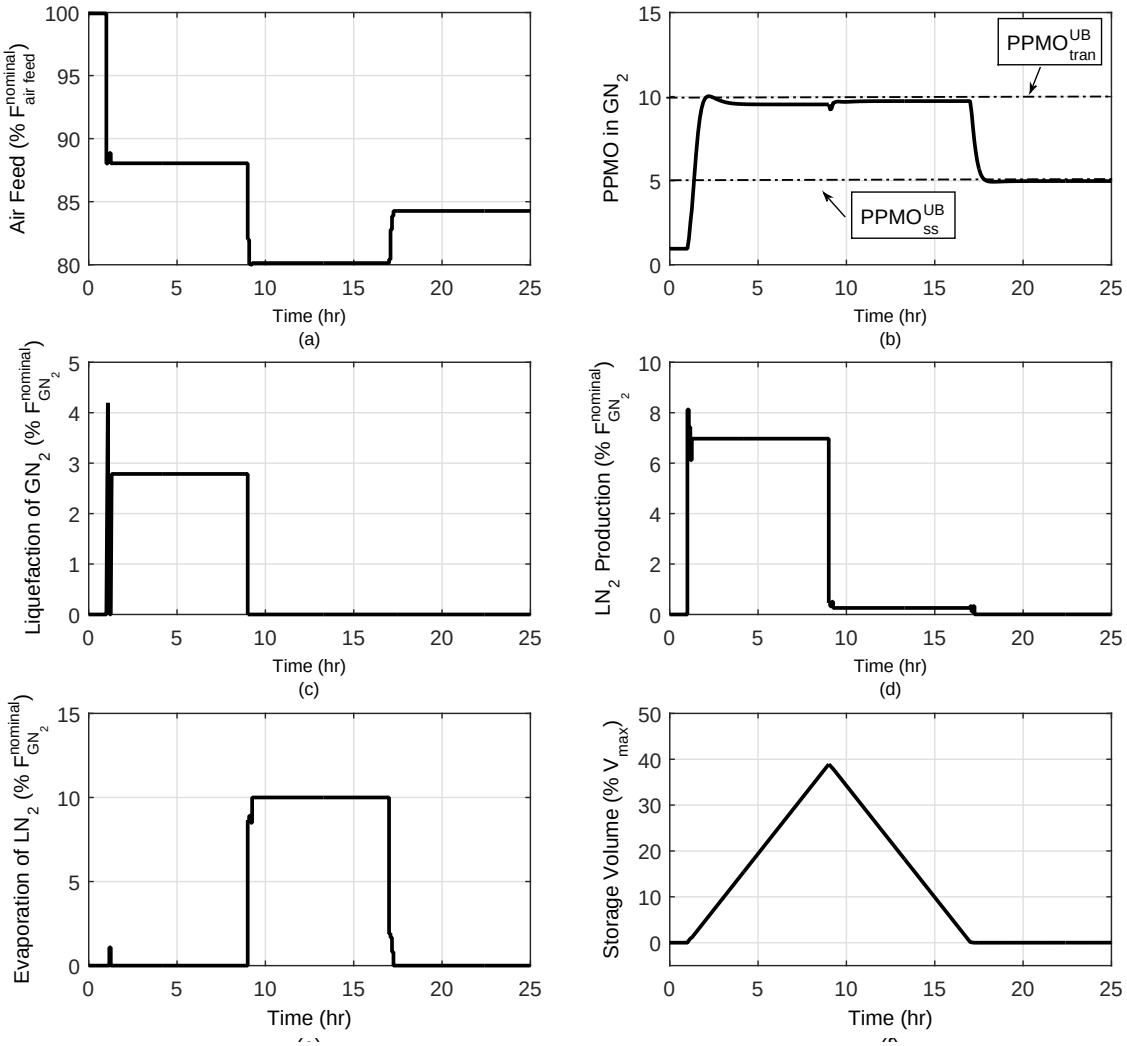

Figure 3.7: Optimal trajectories for selected variables in scaled values Scenario S1.3.

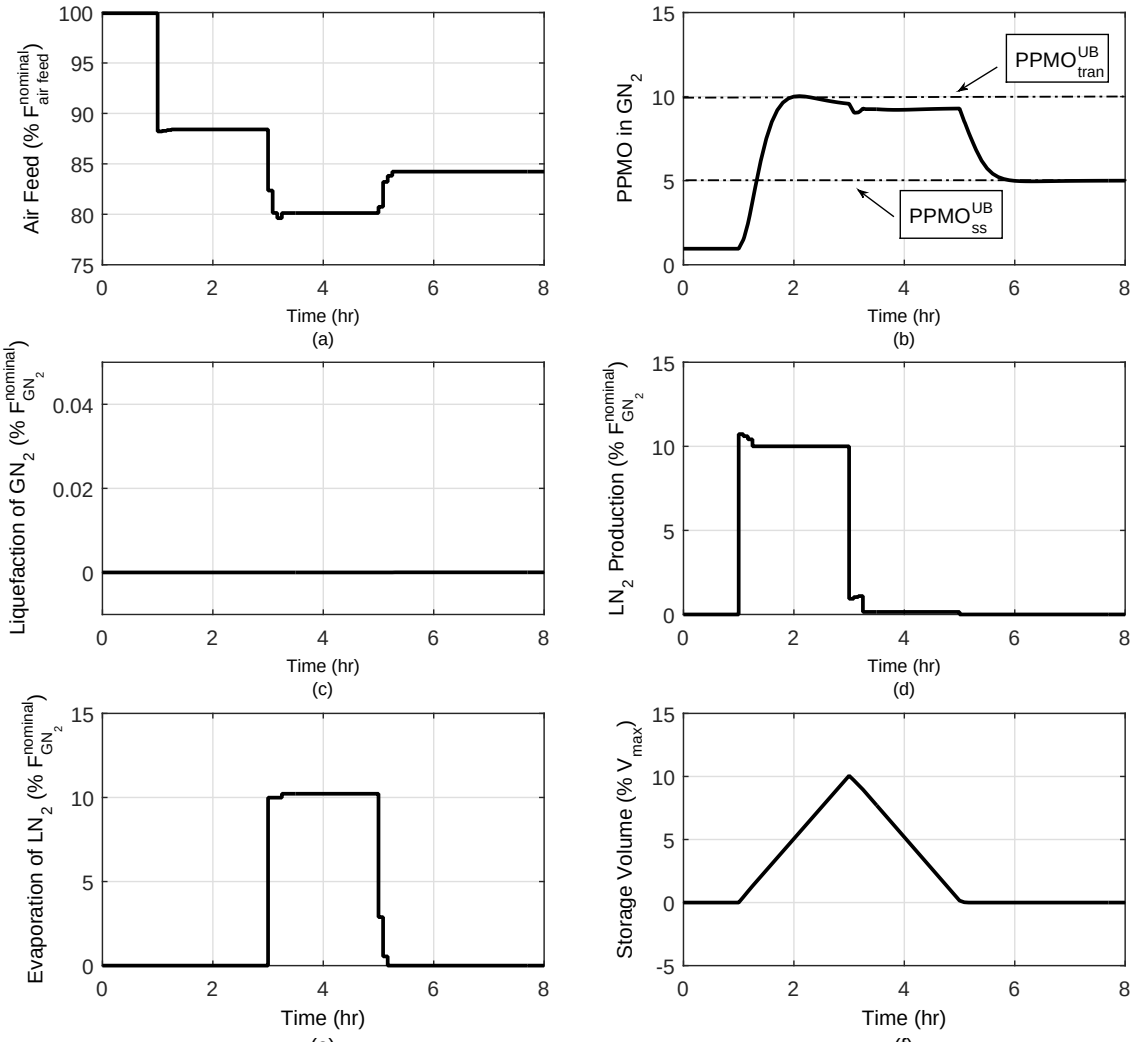

Figure 3.8: Optimal trajectories for selected variables in scaled values for Scenario S1.4.

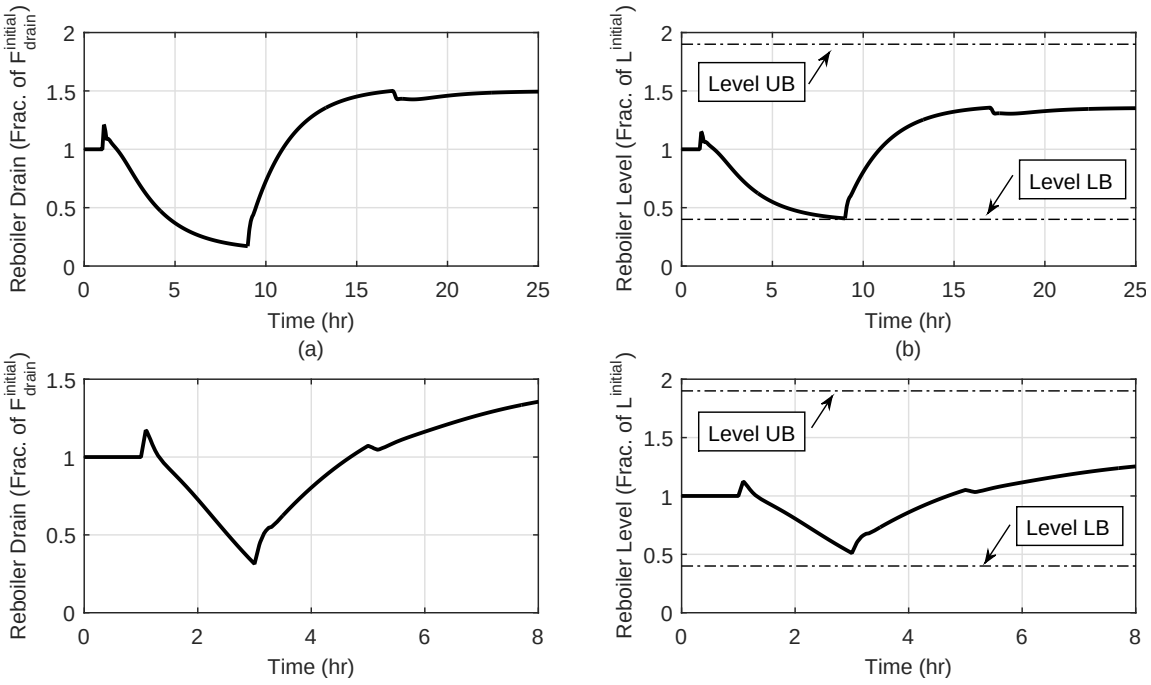

Figure 3.9: Reboiler drain flow rate and reboiler level for S1.3 (subfigs. a and b) and S1.4 (subfigs. c and d).

% of $F_{\text{GN2}}^{\text{nominal}}$ in S1.4 (Fig. 3.8d) to 7 % when the change duration increases (Fig. 3.7d). A portion of the stored liquid, i.e. about 3 % of the demand is collected from GN_2 liquefaction, Fig. 3.7c. We observed that in such situations, condensing over-produced GN_2 product could be an economically attractive option despite the additional cost. To further illustrate the point, an additional optimization problem is solved (S1.7 in Table 3.4), where all stored liquid is forced to come from the LN_2 production. As expected, when GN_2 liquefaction is not permitted as in this situation while LN_2 production is limited by the constraint, less liquid is collected (liquid volume peak at approx. 29 % compared to 40 % in S1.3) and available for vaporization; hence, the cost saving captured decreases to 1.2 % (Table 3.5).

Table 3.5: Optimization results for the vaporization scenarios with different values of process parameters compared to the corresponding reference cases (Table 3.4).

Scenario	Cost Saving†	Inventory Peak	Reference Case
S1.3	1.5 %	40 %	S1.1
S1.4	1.3 %	11 %	S1.2
S1.5	0 %	0 %	S1.1
S1.6	2.9 %	38 %	S1.8
S1.7	1.2 %	29 %	S1.1

† Calculated as $\frac{\varphi_{\text{econ}}^{\text{no storage}} - \varphi_{\text{econ}}}{\varphi_{\text{econ}}^{\text{no storage}}} \times 100\%$.

Incentives for product storage – effects of processing cost and $P_{\text{elec}}^{\text{peak}}/P_{\text{elec}}^{\text{min}}$ of electricity price: S1.5, S1.6 and S1.8

The cost saving realized from the practice of storage and vaporization is strongly affected by the additional processing costs (i.e. condensation and vaporization) and electricity price peak-to-minimum ratio. To demonstrate, two cases are solved with elevated LN_2 evaporation cost (S1.5 and S1.6 in Table 3.4). When the electricity price peak-to-minimum ratio is 4 (Scenario S1.5), under the increased operation costs, the optimizer converges to a solution of not practicing storage and vaporization. Compared to the benchmark case, S1.1, there is no improvement in the profitability. However, with the same processing cost, when the price peak-to-low ratio is increased to 8 (Scenario S1.6), over-producing and storing, then reducing the load while vaporizing becomes economically attractive. A 2.9 % improvement in the overall profit is realized at the solution of Scenario S1.6, compared to the corresponding case in which no storage is allowed (S1.8, Table 3.4). This observation suggests that the store-then-vaporize practice is beneficial for those plants experiencing significant variations in electricity price.

Table 3.6: Scenarios with different values of process parameters used in the reflux study (Case 2)

Scenario	Action[†]	Storage	$P^{\text{peak}}_{\text{elec}}/P^{\text{min}}_{\text{elec}}$	C_{evap} $(\%C_{GN_2})$	$C_{\text{ext liq}}$ $(\%C_{GN_2})$	$\text{PPMO}^{UB}_{\text{tran}}$
S2.1	R	Yes	4	- [♯]	5 %	5
S2.2	R	Yes	4	- [♯]	5 %	10
S2.3	R,E	Yes	4	5 %	5 %	10
S2.4[‡]	-	Yes	4	- [♯]	5 %	5
S2.5[‡]	R	Yes	4	- [♯]	5 %	5
S2.6	R	Yes	-[§]	- [♯]	5 %	5

[†] R = Reflux; E = Evaporation.
[♯] Evaporation action is not available.
[‡] Additional supporting case where there is no variations in the demand. S2.4, no storage; S2.5, storage is available.
[§] Additional supporting case where there is no variations in the electricity price.

3.4.2 Case 2: use of stored liquid as additional reflux

A prior study [12] illustrated that using stored liquid as additional reflux, even only during transitions, can lead to more agile operation with smaller safety margin requirements. In this part of the present study, the full potential of additional reflux is investigated. It is assumed that stored liquid can be used as reflux not only during transitions, but is available also during normal operation. However, when the plant settles at the final steady state, the use of stored liquid as additional reflux is not permitted. Similar to the vaporization case in this paper, different values of the process parameters, including the upper bound of product impurity are considered, as tabulated in Table 3.6. The condensation and vaporization cost will be held at 5 % of the sale price of GN_2. Stored liquid can be collected through GN_2 liquefaction or LN_2 production. Only the P controller is utilized for regulating the reboiler and column sump liquid levels, and the change duration is $\mathbf{t} = [0, 1, 3, 5, 8]$. To simplify the problem, the additional reflux is introduced only at the top column tray at this stage. Six scenarios are investigated in this section and the purpose is to understand in what circumstances using the stored liquid as additional reflux is a valid option from the operation prospective. Scenarios

Table 3.7: Optimization results for the reflux scenarios with different values of process parameters compared to the corresponding reference cases.

Scenario	$\text{PPMO}_{\text{tran}}^{UB}$	Cost Saving†	Inventory Peak	Reference Case
S2.1	5	0.7 %	10 %	S1.2(a): $\text{PPMO}_{\text{tran}}^{UB} = 10$
S2.2	10	1.5 %	10 %	S1.2(a)
S2.3	10	1.5 %	10 %	S1.2(a)
S2.5	5	1.4 %	10 %	S2.4

† Calculated as $\frac{\varphi_{\text{econ}}^{\text{no storage}} - \varphi_{\text{econ}}}{\varphi_{\text{econ}}^{\text{no storage}}} \times 100\%$.

S2.1–S2.3 are solved with electricity price and demand pattern shown in Fig. 3.4. In S2.1 and S2.2 stored liquid can be used only as additional reflux, while in S2.3, the optimizer can choose between the strategies of vaporization and adding reflux. Scenarios S2.4–S2.6 are additional supporting cases. Scenarios S2.4 and S2.5 are additional cases where the plant operation is subject to variations only in the electricity price. Scenario S2.6 is an additional case where the plant operation is subject to variations only in the product demand.

Optimization results for S2.1 and S2.2 are shown in Fig. 3.10. In these cases, the stored liquid is mainly utilized during the settling period when the electricity is high (i.e. $t \in [3, 5 \text{ hr}]$) as shown in Fig. 3.10c. During this period, to meet the demand, the fraction of the top vapor stream that is removed as GN_2 product increases. Hence, relatively less vapor is sent to the condenser side of the IRC and back to the column as reflux. The liquid collected is introduced to the column to make up for the missing reflux (Fig. 3.10c). This is further illustrated in Scenario S2.5, which has no demand changes. At the solution of S2.5, when the electricity price is at the peak, the same amount of GN_2 product is produced with a decreased air feed flow rate (i.e. compared to the no storage case S2.4) and the additional reflux stream has a non-zero flow rate, Fig. 3.11d. In addition, with the decreased vapor flow to the condenser, the reboiler liquid level upper bound becomes active towards the end of the second settling period in S2.1, S2.2 and S2.5. When the electricity price is high, the plant collects liquid from LN_2 production and the storage volume experiences initial accumulation followed by reduction, similar to S1.4.

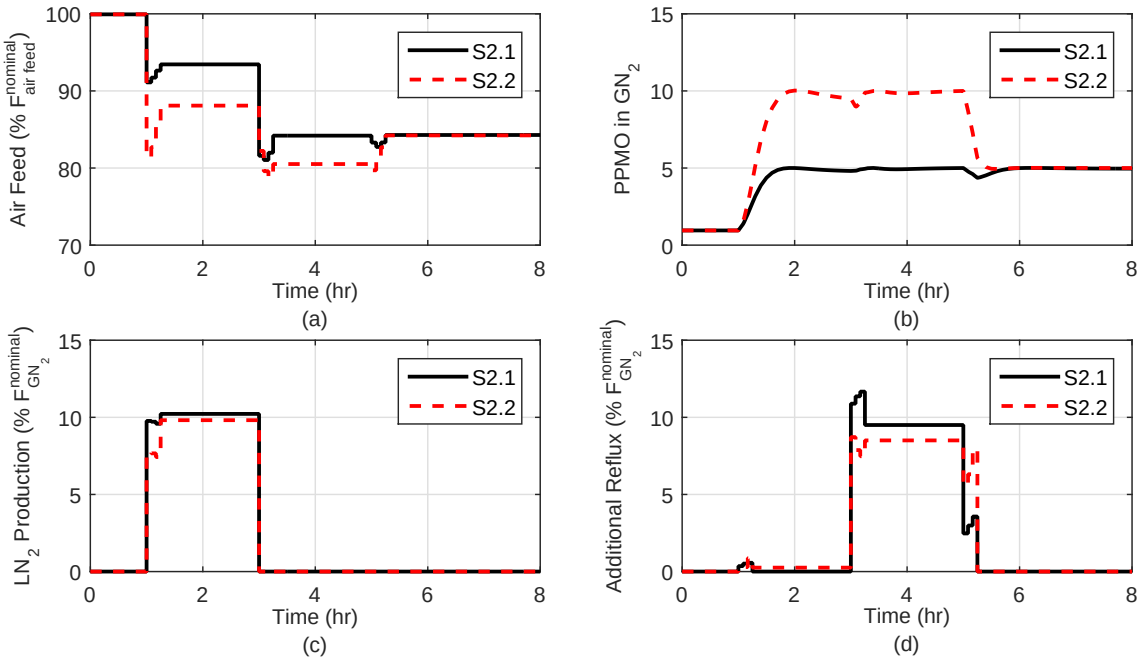

Figure 3.10: Optimal trajectories for selected variables in scaled values for Scenarios S2.1 and S2.2.

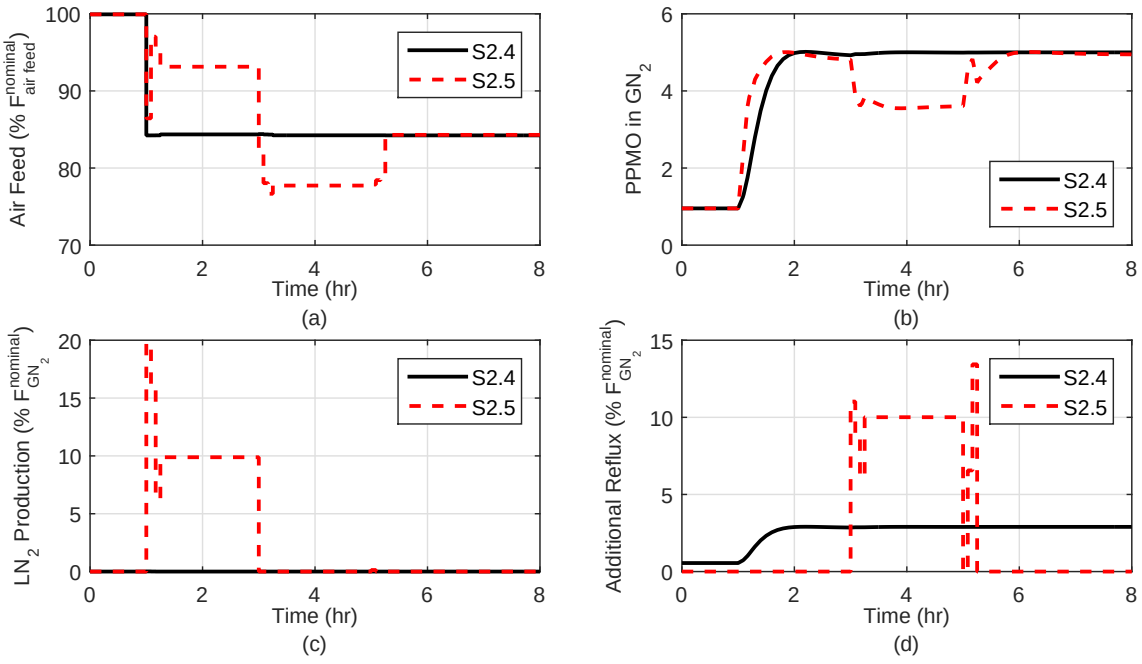

Figure 3.11: Optimal trajectories for selected variables in scaled values for Scenarios S2.4 and S2.5.

The cost saved by the introduction of additional reflux, compared to the corresponding reference cases, is tabulated in Table 3.7. In similar situations, when a tighter purity requirement is enforced (S2.1 vs. S2.2), to produce the same amount of GN_2 product, more air feed is required as illustrated by the higher air flow rate for the case with $PPMO_{tran}^{UB}$ = 5 PPMO compared to the 10 PPMO case (Fig. 3.10a). Consequently, the compressor surge constraint is active even during the settling period in S2.2, but is active only during transitions for S2.1. Hence, the cost of operating with tighter impurity limit is higher. However, when the storage is utilized, the operation can still be economically superior even with more restricted constraints (S2.1 vs. S1.2). The objective function value for Scenario 2.1 is 0.7 % better than that for the no storage scenario, S1.2. The improvement from the S2.2 case is about 1.5 %, which is slightly higher than 1.3 % attained in the corresponding vaporization case (S1.4). It is shown in Fig. 3.10 that with the additional reflux, the plant can cut closer to $PPMO_{tran}^{UB}$. Hence, while other expenses are the same, using stored liquid as additional reflux is more effective than the vaporization case. This can be further confirmed with the results from Scenario S2.3, where both vaporization and additional reflux actions are permitted at the same processing costs. At the solution point, the amount of liquid that is utilized as vaporized product is insignificant. The resulting trajectories for S2.3 are very similar to those in S2.2 and will not be repeated here. In S2.5, the storage with utilization as reflux strategy yields a 1.4 % improvement in the overall profit from the no storage case S2.4.

Electricity price fluctuations provide incentives for practicing the strategy of storing liquid for later use. When the electricity profile is constant and the changes in the demand requirement are within the plant capacity (Scenario S2.6), there is minimal motivation for storing liquid. As shown in Fig. 3.12, in this case additional reflux is mainly introduced during transitions. The maximum inventory held during the time period of interest is less than 0.1 % of the assigned storage capacity. With reflux options, the storage tank is only economically attractive when the plant operates under varying electricity price with large $P_{elec}^{peak}/P_{elec}^{min}$, especially considering the capital cost required.

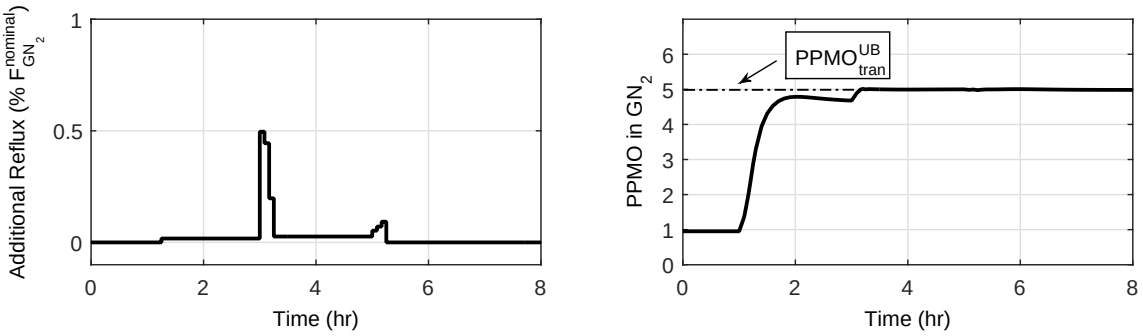

Figure 3.12: Optimal trajectories for selected variables in scaled values for Scenario S2.6.

3.5 Conclusion

In this chapter, we investigate multi-period dynamic operation of a nitrogen plant with a liquid storage tank under varying electricity price and customer demand. A high fidelity dynamic model based on the collocation approach is used. Questions regarding a storage-then-utilization strategy were posed, including the economic incentive, liquid collection strategy, and the impact of the peak-to-minimum electricity price ratio. When there are significant variations in the electricity price, use of stored liquid to meet the demand directly or to provide additional reflux to the column are valid options and economically attractive. However, the cost saving with additional reflux is slightly higher. The means of liquid collection are influenced by the operational bottlenecks. It is illustrated in the study that even though collecting liquid from LN_2 production is cheaper than liquefying over-produced GN_2, under certain scenarios, such as to prevent violating the reboiler level lower bound, GN_2 liquefaction is optimal. It is also revealed that production purity needs to be monitored closely during transitions. Such operational bottlenecks due to process dynamics impact the realizable profit and selection of operation strategies, and emphasize the importance of dynamic models in the exploration and evaluation of plant operating strategies.

To target the issue of unnecessary changes in input trajectories with a pure economic-based objective function, a second tier move suppression problem is solved. Three different objective

function formulations are proposed for solving this problem using a sequential dynamic optimization approach: trajectory-based, hyperbolic tangent function approximation and valve dynamic approximation. Optimization results with all three methods yield smoother input profiles compared to that with pure economic objective functions, without sacrificing the cost saving realized.

Future work will extend the formulation to consider process uncertainties, especially in electricity price and/or demand. We plan to conduct studies on design and operation under uncertainty following a multi-scenario based approach using the reduced dynamic nitrogen plant model. Our ultimate goal is to be able to improve plant flexibility and agility through process design modification and improved operation policies.

Bibliography

[1] A. R. Sirdeshpande et al. “Process synthesis optimization and flexibility evaluation of air separation cycles”. In: *AIChE Journal* 51.4 (2005), pp. 1190 –1200 (cit. on p. 52).

[2] U.S. Energy Information Administration. *Manufacturing energy consumptionsurvey*. Online. Available at: http://www.eia.gov/consumption/data.cfm. 2012 (cit. on p. 52).

[3] Y. Zhu, S. Legg, and C. D. Laird. “Optimal operation of cryogenic air separation systems with demand uncertainty and contractual obligations”. In: *Chemical Engineering Science* 66.5 (2011), pp. 953 –963 (cit. on pp. 52, 54, 69).

[4] US Department of Energy. *Benefits of demand response in electricity markets and recommendations for achieving them*. A Report to the United States Congress Pursuant to Section 1252 of the Energy Policy Act of 2005. 2006 (cit. on p. 53).

[5] R. Pattison et al. “Optimal process operations in fast-changing energy markets: Framework for scheduling with low-order dynamic models and an air separation application”. In: *Industrial & Engineering Chemistry Research.* 55.16 (2016), pp. 4562 –4584 (cit. on pp. 53–55, 68, 69).

[6] Q. Zhang et al. “Air separation with cryogenic energy storage: Optimal scheduling considering electric energy and reserve markets”. In: *AIChE J.* 61.5 (2015), pp. 1547–1558 (cit. on pp. 53–55, 68).

[7] M. G. Ierapetritou et al. “Cost minimization in an energy-intensive plant using mathematical programming approaches”. In: *Industrial & Engineering Chemistry Research* 41.21 (2002), pp. 5262 –5277 (cit. on pp. 53, 55).

[8] S. Mitra et al. “Optimal production planning under time-sensitive electricity prices for continuous power-intensive processes”. In: *Computers & Chemical Engineering* 38 (2012), pp. 171 –184 (cit. on pp. 53, 55).

[9] Y. Zhu, S. Legg, and C. D. Laird. “A multiperiod nonlinear programming approach for operation of air separation plants with variable power pricing”. In: *AIChE Journal* 57.9 (2011), pp. 2421 –2430 (cit. on p. 53).

[10] J. Miller et al. “Improving agility of cryogenic air separation plants”. In: *Industrial & Engineering Chemistry Research* 47.10 (2008), pp. 394 –404 (cit. on p. 54).

[11] R. C. Pattison and M. Baldea. “Optimal Design of Air Separation Plants with Variable Electricity Pricing”. In: *Proceedings of the 8 International Conference on Foundations of Computer-Aided Process Design*. Ed. by M. R. Eden, J. D. Siirola, and G. P. Towler. Computer Aided Chemical Engineering. Cle Elum, WA, USA: Elsevier, 2014, pp. 393 –398 (cit. on pp. 54, 68, 69).

[12] Y. Cao et al. “Optimization-based assessment of design limitations to air separation plant agility in demand response scenarios”. In: *Journal of Process Control* 33 (2015), pp. 37 –48 (cit. on pp. 54–57, 62, 74, 81).

[13] M. C. Georgiadis et al. “The interaction of design, control and operability in reactive distillation systems”. In: *Comput. Chem. Eng.* 26 (2002), pp. 735 –746 (cit. on p. 55).

[14] M. J. Mohideen, J. D. Perkins, and E. N. Pistikopoulos. “Optimal design of dynamic systems under uncertainty”. In: *AIChE J.* 42 (1996), pp. 2251 –2272 (cit. on p. 55).

[15] R. Huang, V. M. Zavala, and L. T. Biegler. “Advanced step nonlinear model predictive control for air separation units”. In: *Journal of Process Control* 19.4 (2009), pp. 678 –685 (cit. on p. 55).

[16] B. Roffel, B. H. L. Betlem, and J. A. F. Ruijter. “First principles dynamic modeling and multivariable control of a cryogenic distillation process”. In: *Computers & Chemical Engineering* 24 (2000), pp. 111 –123 (cit. on p. 55).

[17] S. Bian et al. “Compartmental modeling of high purity air separation columns”. In: *Comput. Chem. Eng.* 29.10 (2005), pp. 2096 –2109 (cit. on p. 55).

[18] Z. Chen et al. “Nonlinear model predictive control of high purity distillation columns for cryogenic air separation”. In: *IEEE Transactions on Control System Technology* 18.4 (2010), pp. 811 –821 (cit. on p. 55).

[19] V. White, J. D. Perkins, and D. M. Espie. “Switchability analysis”. In: *Computers & Chemical Engineering* 20.4 (1996), pp. 469 –474 (cit. on pp. 55, 62).

[20] Y. Cao et al. “Dynamic modeling and collocation-based model reduction of cryogenic air separation units”. In: *AIChE J.* 62.5 (2016), pp. 1602–1615 (cit. on p. 57).

[21] W. E. Stewart, K. L. Levien, and M. Morari. “Simulation of fractionation by orthogonal collocation”. In: *Chemical Engineering Science* 40.3 (1985), pp. 409 –421 (cit. on p. 57).

[22] A. K. S. Balthazaar. *Dynamic Optimization of Multi-Unit Systems under Failure Conditions*. Master’s thesis, McMaster University, Canada, 2005 (cit. on p. 65).

[23] Z. Chong and C. L. E. Swartz. “Optimal operation of process plants under partial shutdown conditions”. In: *AIChE J.* 59.11 (2013), pp. 4151–4168 (cit. on p. 65).

[24] F. G. Kerry. *Industrial gas handbook: gas separation and purification*. CRC Press Taylor & Francis Group, 2007 (cit. on p. 68).

Chapter 4

Reactive and Preemptive Responses in the Operation of Cryogenic Air Separation Units

4.1 Introduction 92
4.2 Operational Studies on Air Separation Units 95
4.3 Process Model 97
4.4 Optimization Problem Formulations 99
4.5 Results and Discussion 104
4.6 Conclusion 124
References 125

As markets become more competitive and dynamic, manufacturing plants are undergoing transitions towards flexible, agile and low costs operations. Appropriate coordination within the supply chain is an important factor in manufacturing systems' performance. In this study, the impact of preemptive control action in advance of an upcoming demand change on the economic performance of a cryogenic air separation unit is investigated. The effects of various factors are explored through optimization formulations utilizing a high fidelity collocation based dynamic process model. This includes the amount of lead time, choice of manipulated inputs, direction of demand change, and liquid product market conditions. Plant performance is evaluated and analyzed through a comprehensive multi-part case study.

Note, portions of this chapter were submitted to the AIChE Journal:

Y. Cao, C.L.E. Swartz and J. Flores-Cerrillo "Preemptive Dynamic Operation of Cryogenic Air Separation Units". In: *AIChE Journal* (Submitted).

4.1 Introduction

Over the past few decades, traditional operating strategies of manufacturing plants, such as supply driven production and the practice of mainly steady-state operations, have been challenged by an increasingly transient and competitive market. To address this new operating environment, the adaptability of such processes needs be improved, as well as coordination/cooperation of different subsystems of a supply chain through information sharing. A high degree of adaptability can be achieved, according to Backx and co-workers [1], through either improving process operations (for given plant configurations) or re-engineering the flowsheet of the process. They also identified critical issues facing manufacturing plants as quality control, process transitions (time, cost and reproducibility) and production predictability (rate and product grade/type). An air separation unit (ASU) is a prime example of the above mentioned manufacturing plants, whose traditional operation practice involves infrequent load changes and is currently susceptible to dynamic markets. Since electricity deregulation in the 1990s, ASUs have been facing frequent and large variations in electricity price due to real-time pricing [2]. In addition, ASUs' gaseous products are commonly supplied to customers through pipelines [3], hence, on-time delivery of on-spec products despite the demand changes is one of the key factors for the business success.

Cryogenic air separation plants based on distillation technology, an example of which is shown in Fig. 1.1, are the primary means to produce large quantities of high purity nitrogen, oxygen and argon products. Customers of these plants include many industrial sectors such as energy, food processing, refinery, electronics, pharmaceutical, chemical and aerospace industries [4, 5]. Even though ASUs have some variation in configuration due to differences in product type and grade, the general operation principle and critical equipment are typically the same. Ambient air is compressed, purified and cooled before being separated through distillation. Key operation units consist of multi-stream heat exchangers, distillation columns operating at cryogenic conditions, multi-stage compressor system and integrated

reboiler/condensers. Cryogenic ASUs utilize the difference in components' boiling points to separate air into various products. These products are then collected at specific locations within the process. For the ultra high purity multi-product plant in Fig. 1.1, the Ar product is collected in liquid form from the super-staged column, while O_2 is removed from the bottom of the upper column and N_2 is withdrawn from the top of upper and lower columns. Detailed process descriptions are given in Miller *et al.* [6] and Zhu *et al.* [7]. Due to the operating conditions and process complexity, ASUs typically encounter three operational issues that make such plants deviate from the flexible, agile and low cost processes, favored by current environments:

- Costly compression – Atmospheric air is first compressed to a high pressure before being purified in the prepurifier, cooled in the primary heat exchanger and separated in the distillation columns into various products. Operation of the multi-stage compression system consumes a significant amount of electricity, at an annual cost of approximately $ 1 billion to industrial gas producers in the U.S. [8].

- Low flexibility – Due to the cryogenic operating conditions of the process, different process streams are utilized to recover heat/refrigeration within the system. For example, in the main condenser, the O_2 rich liquid at the bottom of the upper column is used to condense the N_2 rich vapor leaving the top of the lower column. Such arrangements introduce high degrees of thermal integration and remove process degrees of freedom in an already complex flow network and separation system.

- Inadequate agility – To achieve the high purity requirements, large distillation columns with significant numbers of stages are needed. The liquid holdup in these columns introduces prolonged delays in response dynamics.

The study in this chapter is motivated by an industrial need with the overall objective of seeking means to improve responsiveness/adaptability of ASUs towards factors such as fluctuating demand, real-time/time-of-use electricity prices and daily/seasonal disturbances. This

paper focuses on process operation aspects to improve the system's adaptability, especially in process transitions. In most of the operation studies in the literature (discussed in the next section), adjustments in the operation schemes are driven by the electricity market (the supply side of the equation). In this study, the demand side comprising the manufacturer and customer subsystem of the supply chain is analyzed. Currently, communications between ASUs and pipeline customers are very limited, and more frequently, the plant receives notification from the customer only when major changes in the operation, such as shutdowns, are anticipated in the near future. Here, incentives for active communication are assessed through solving dynamic optimization problems. Demand changes in both directions are studied. In response to gas oxygen demand fluctuation, plant operators can take two types of action. In the reactive case, system inputs are adjusted when changes in the external parameters are realized. Such scenarios are likely to occur when there is no on-going communication. On the other hand, with information on the upcoming demand change gathered through active information sharing, the plant can take action ahead of time. For liquid product demands, two scenarios are considered: whether or not the liquid customers have limits on the amount of products they are willing to purchase. While optimizing the plant control practices, in addition to system inputs already utilized in the daily operations, i.e. feed and production rates, the internal liquid inventory, including liquid holdups in the lower column bottom and argon condenser reboiler, are also considered.

The remainder of this chapter is organized as follows. First, we briefly review plant operation studies, particularly in the field of ASUs and explain the process model used in this study. This is followed by the proposed optimization problem formulation. Optimization results for selected case studies are documented and analyzed. Finally, concluding remarks on our current work that highlight the benefits of the proposed approach are presented.

4.2 Operational Studies on Air Separation Units

Motivated by the transient and competitive environment, operational issues, including operating mode transitions, short term scheduling and long term planning of ASUs have been presented in the literature.

Agility during transitions

In order to improve plant dynamic performance to take advantage of varying market conditions, transitional behavior of ASUs needs to be fully understood in terms of feasibility and speed. White and co-workers [9] conducted a switchability analysis for the column section of an ASU producing gaseous oxygen, where the plant was required to change from one load to another in a timely manner using a dynamic optimization approach. They concluded that even though the final results showed no limit to the speed at which the production rate could be changed, the product purity requirements affected the resulting trajectories of manipulated variables. Later, Miller and co-workers [6] addressed the start-up problem of an argon system. Through trial-and-error dynamic simulations, the authors concluded that collecting/redistributing liquid from/to the argon column could reduce the lengthy startup time by about 80 %. The slow plant startup is mainly due to the significant number of separation stages, low concentration of Ar in the air and high purity requirement. In the study by Cao *et al.* [10], the authors identified operational bottlenecks that limit rapid transitions between operation points in response to demand and electricity price fluctuations for a nitrogen plant following a two-tiered optimization framework. They also proposed design modifications, such as introducing pre-stored liquid as additional reflux, to help improve the plant's agility.

Short term scheduling

While research on agility has focused on the dynamic response to single step changes in system parameters, planning and scheduling studies emphasize operating strategies involving

multiple time periods. When the time horizon considered is short (a few hours to a couple of days), operating the plant within its capacity with continuous action is practiced. This includes plant loading and unloading, as well as utilizing storage and vaporization. Discrete events, such as shutdown and startup, are typically not considered due to the slow recovery of the process from such disruptions. Restoring the product purity to within the specifications after a shutdown could take a few hours to a day for a large-scale multi-product plant [6, 7]. The dynamic response of the process is still captured to a certain degree in scheduling studies through the use of ramping inputs with steady state models [7], or simplified/full rigorous dynamic models [11]. Zhu and Laird [7] investigate the trade-off between profitability and customer satisfaction level for an ASU producing liquid products. As the electricity price varies during the 24 hours horizon following a time-of-use pattern (i.e. on-peak, off-peak and mid-peak), the plant adjusts the amount of air feed and the production rate for different products under constant/uncertain demand to minimize the cost associated with power usage. This work is later extended to use the liquid product storage to improve the overall profit of the plant [12]. Pattison and co-workers [11] consider operation of a nitrogen plant under hourly varying electricity price over a 3-day scheduling period. In their study, besides using production, the plant can liquefy and store over-produced gas product for satisfying future demand. Results of the study demonstrated the economic incentive for using storage to buffer changes in the time-sensitive electricity price.

Long term planning

When long term strategies for weekly, monthly or even yearly operations are planned, practices of full/partial shutdown/startup of the plant may be economically beneficial under time-varying market conditions. The majority of the works on this subject for ASUs aim to determine the operation mode sequence. Minimum mode duration (e.g. downtime $\geq$ X hrs) and/or operation mode transition duration are imposed to capture rudimentary process dynamic behavior [13–15]. Ierapetritou and coworkers [13], determine the cost-optimal sequence of operation modes (i.e. regular, shutdown and assist) under varying

and partially uncertain electricity price are determined through a two-stage stochastic optimization framework. During the time period of interest (i.e. 5 to 8 days), demand variations are also considered. Karwan and Keblis [14] investigated a planning problem of ASUs for weekly or monthly operation under different electricity price situations of real-time pricing (RTP), or time-of-use pricing (TOU) by solving mixed-integer problems. The plant selects among defined operation slates of specific production rates and power consumption to minimize the accumulated operation costs. Mitra and coworkers [15] also investigated cost-optimal operating strategies under RTP scenarios where plant operations are represented by various previously identified operation modes. For given product demand and storage capacity, schedules of operation modes are determined to minimize the total cost. This study was further extended to include uncertainty in electricity price [16], and later to a multi-scale framework that evaluates operating practices with a flowsheet modification of an additional liquefier over a planning horizon of several years under varying electricity price and uncertain demand [17]. A more recent work from the same research group by Zhang *et al.* [3] evaluated the benefit of adding cryogenic energy storage to an ASU to minimize the net operating cost. In the study, as the electricity price varies, the plant can collect and utilize liquid to meet gas/liquid product demand or generate electricity and sell it back to the market.

4.3 Process Model

This chapter builds on our previous work on modeling and simulation of an ultra-high purity argon plant [18]. The process model in the optimization study is a dynamic model with the plant configuration shown in Fig. 1.1. The key process units captured are highlighted in the dashed box. The mathematical representation for the distillation columns comprises vapor-liquid equilibrium based first principles dynamic models. Some of the features include dynamic material balances, pseudo steady-state energy balances, Margules equation activity

coefficient estimation, tray efficiency, varying pressure drop, heat leakage and elevation-induced partial vaporization in liquid process streams. Models for the lower column (LC), lower-ratio column (LRC) and super-stage argon column (SSC) are collocation-based (multiple finite elements grids with two collocation points per finite element), while the model for the upper column (UC) is full-order stage-wise. The primary heat exchanger (PHX) is a multi-stream heat exchanger with process streams undergoing phase change. The PHX is represented using a moving boundary model with further model reduction through the collocation approximation. Considering the faster dynamics compared to the columns, the PHX is modeled under a pseudo steady-state assumption. Models for the integrated reboiler/condenser (i.e. main and argon condensers) are similar to that of a column stage with the addition of a liquid level controller for the reboiler side. Details for the process modeling approach can be found in Cao *et. al.* [18]. Fig. 4.1 highlights key process streams and process unit models used in this part of the study.

The multi-stage compressor model is not included in the integrated plant model, but the power consumption is required in the estimation of the plant's profitability. To calculate the compressor energy usage, historical data of a similar plant is used. It is assumed that the compressor power, W_{comp}, is proportional to the volumetric flow rate of the total air feed at standard conditions, $\dot{V}_{\text{air, std}}$:

$$W_{\text{comp}} = \alpha \dot{V}_{\text{air, std}} \tag{4.1}$$

The value for α is obtained through regression of historical plant data.

Remark

Even with model reduction, due to the prediction accuracy requirement for this ultra high purity system, the resulting plant model still contains more than 500 ordinary differential equations. As a consequence, the optimization problems in this paper are large-scale nonlinear dynamic optimization problems with a high degree of variable interaction.

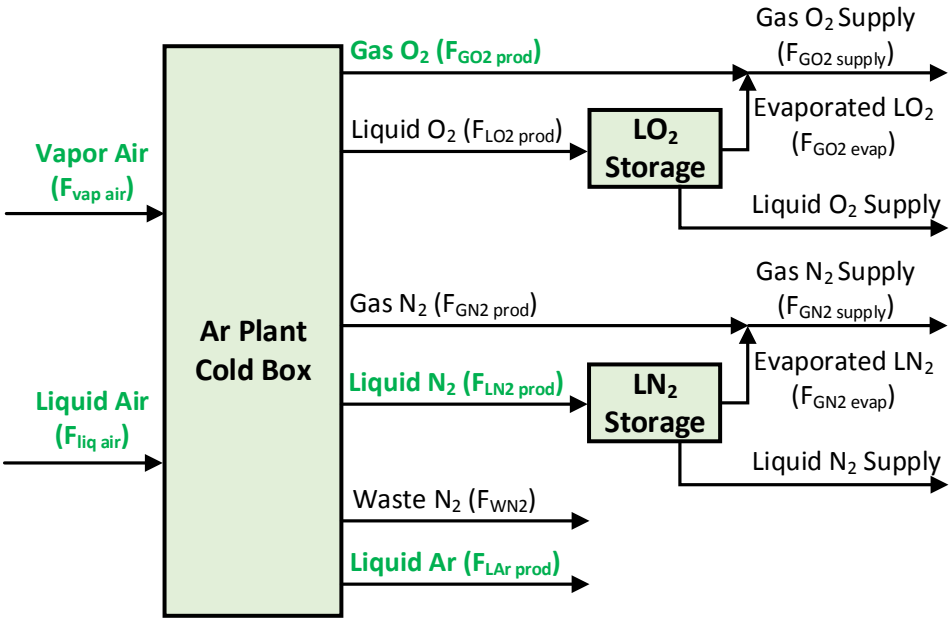

Figure 4.1: Simplified process diagram with system inputs and outputs used in the optimization study. Detailed argon plant configuration is shown in Fig. 1.1.

4.4 Optimization Problem Formulations

Constrained dynamic optimization problems solved in this study are of the general form

$$\min_{\mathbf{u}(t)} \Phi(\mathbf{u}(t), t_f) \tag{4.2a}$$

$$\text{subject to:} \quad \mathbf{f}(\dot{\mathbf{x}}(t), \mathbf{x}(t), \mathbf{z}(t), \mathbf{u}(t), \mathbf{p}, t) = \mathbf{0} \tag{4.2b}$$

$$\mathbf{g}(\mathbf{x}(t), \mathbf{z}(t), \mathbf{u}(t), \mathbf{p}, t) = \mathbf{0} \tag{4.2c}$$

$$\mathbf{h}(\mathbf{x}(t), \mathbf{z}(t), \mathbf{u}(t), \mathbf{p}, t) \leq \mathbf{0} \tag{4.2d}$$

$$\mathbf{h}_j(\mathbf{x}(\bar{t}_j), \mathbf{z}(\bar{t}_j), \mathbf{u}(\bar{t}_j), \mathbf{p}, \bar{t}_j) \leq \mathbf{0}, \quad \forall j \in J \tag{4.2e}$$

$$\mathbf{h}_f(\mathbf{x}(t_f), \mathbf{z}(t_f), \mathbf{u}(t_f), \mathbf{p}, t_f) \leq \mathbf{0} \tag{4.2f}$$

$$\dot{\mathbf{x}}(t_0) = \mathbf{0} \tag{4.2g}$$

$$t_0 \leq t \leq t_f \tag{4.2h}$$

where $\mathbf{x}$, $\mathbf{z}$, $\mathbf{u}$ and $\mathbf{p}$ are vectors of differential states, algebraic states, control inputs and parameters, respectively. $\mathbf{f}$ and $\mathbf{g}$ comprise the plant model equations in differential-algebraic form, and $\mathbf{h}$ includes variable bounds (i.e. for $\mathbf{x},\ \mathbf{z},\ \mathbf{u}$), operational constraints, product specification constraints and constraints required in the model. $\mathbf{h}_j$ and $\mathbf{h}_f$ represent interior point and endpoint constraints with $\bar{t}_j$ and t_f defined as the time corresponding to the jth interior point and endpoint, respectively. In the study, the process starts at steady state as reflected in the initial condition. All optimization problems are solved using `gOPT 4.1.0` using a sequential approach.

4.4.1 Decision variables

Main decision variables, according to plant operating procedures, include flow rates of vapor and liquid air feed streams, as well as production rates of LN_2, GO_2 and LAr products (i.e. highlighted in Fig. 4.1). Additional decision variables, such as liquid level set-points at selected locations in the system, are also introduced when exploring alternative operating policies. In this study, the system inputs are captured using piece-wise constant profiles with specified control interval duration.

4.4.2 Objective function

An economic based objective function is used in most of the case studies. It takes into account the power consumption of processing the feed to the system and the revenue from selling different products:

$$\min_{\mathbf{u}(t)} \ \Phi_{\text{econ}} = \phi_{\text{cost}}(t_f) - [\phi_{\text{rev}}^{\text{gas}}(t_f) + \phi_{\text{rev}}^{\text{liq}}(t_f)] \tag{4.3}$$

where $\phi_{\text{cost}}(t_f)$ is the accumulated cost, and $\phi_{\text{rev}}^{\text{gas}}(t_f)$ and $\phi_{\text{rev}}^{\text{liq}}(t_f)$ are the total revenues from gas and liquid products. Since gas O_2 and N_2 products (i.e. GO_2 and GN_2) are supplied to the customer through pipelines, no unmet demands are permitted and the portion that cannot

be satisfied through production (either due to capacity limits or economic reasons) will be supplied through vaporizing the corresponding liquid products. Based on this assumption, the overall operation cost combines the cost due compressor power consumption and liquid product vaporization:

$$\phi_{\text{cost}}(t_f) = \int_{t_0}^{t_f} C_{\text{elec}}(t) W_{\text{comp}}(t) dt + \sum_{j \in \mathcal{J}} \int_{t_0}^{t_f} C_{j,\,\text{evap}} F_{j,\,\text{evap}}(t) dt, \quad \mathcal{J} = \{\text{GN}_2, \text{GO}_2\} \tag{4.4}$$

In above equations, C_{elec} and $C_{j,\,\text{evap}}$ are the unit price of electricity and cost of vaporizing the liquid, respectively. $F_{j,\,\text{evap}}$ is the flow rate of a liquid product vaporized to meet the demand for its corresponding gas product, D_j, and is calculated as:

$$F_{j,\,\text{evap}}(t) = \max(0, D_j(t) - F_{j,\,\text{prod}}(t)), \quad j \in \mathcal{J} \tag{4.5}$$

where $F_{j,\,\text{prod}}$ is the production rate of gas product j.

To estimate the revenue from the gas products, it is assumed that since an on-site liquefier is not within the scope of the study, instead of being condensed and stored for later use, the over-supplied gases will be vented and cannot generate additional revenue. This gives

$$\phi_{\text{rev}}^{\text{gas}}(t_f) = \sum_{j \in \mathcal{J}} \int_{t_0}^{t_f} C_{j,\,\text{prod}} D_j(t) dt \tag{4.6}$$

As mentioned previously, different scenarios for the liquid product market are considered. Under the assumption of no maximum saleable amount for liquid products, all LN_2, LO_2 and LAr produced within the storage capacity can be sold at given sale prices to current or new liquid customers. Then, the revenue from liquid products is accounted for at the end of the control horizon and estimated as

$$\phi_{\text{rev}}^{\text{liq}}(t_f) = \sum_{k \in \mathcal{K}} C_{k,\,\text{prod}} ST_k(t_f), \quad \mathcal{K} = \{\text{LN}_2, \text{LO}_2, \text{LAr}\} \tag{4.7}$$

where $ST_k(t_f)$ is the accumulated amount of liquid produced at the end of the control horizon. ST_k is calculated according to

$$\frac{dST_{\text{LO}_2}(t)}{dt} = F_{\text{LO}_2\text{ prod}}(t) - F_{\text{GO}_2\text{ evap}}(t) \tag{4.8}$$

$$\frac{dST_{\text{LN}_2}(t)}{dt} = F_{\text{LN}_2\text{ prod}}(t) - F_{\text{GN}_2\text{ evap}}(t) \tag{4.9}$$

$$\frac{dST_{\text{LAr}}(t)}{dt} = F_{\text{LAr prod}}(t) \tag{4.10}$$

ST_k is defined to be nonnegative throughout the time period of interest, which means that at any point in time, you cannot consume more than what you have collected. Even though most of the plants have non-zero initial liquid holdup, here we account for profit over the time horizon and have $ST_k(t_0) = 0$.

The other liquid market scenario assumed is that a maximum level exists on the amount of liquid that customers are willing to purchase, $\overline{ST}_k$, e.g. in a saturated/over-supplied market. Then the potential revenue from liquid is constrained by the demand and becomes

$$\phi^{\text{liq}}_{\text{rev}}(t_f) = \sum_{k\in\mathcal{K}} C_{k,\text{ prod}}[\min(ST_k(t_f), \overline{ST}_k)] \tag{4.11}$$

In above equations $C_{k,\text{ prod}}$ is the sale price of different liquid products. Detailed pricing information is not provided due to confidentiality requirements of the partner company.

4.4.3 Constraint sets

Operation constraints addressed in the optimization problems are summarized in Table 4.1. The superscripts UB and LB represent upper and lower bounds. Critical quality control constraints include product purity requirements, given as parts per million O_2 for GN_2, parts per million O_2 and N_2 for LAr and percentage O_2 in GO_2. Other operational constraints, including O_2 content in the crude argon feed, $y_{\text{O2, crude}}$, and temperature measurements at

selected trays in the upper column, are also considered in the optimization study. The drifting of the temperature profile is an indicator for movement of the composition profile [18], which is critical for identifying issues such as N_2 getting into the argon section. Note that for the temperature constraints in Table 4.1, the “Top",“Middle" and “Bottom", indicates approximate locations of the selected tray, rather than the exact position in the column. These trays are selected as practiced in the plant.

In addition, we also require that the system approaches stability at the end of the horizon. The argon section has the most prolonged response to input changes. Hence, the rate of change of O_2 and N_2 content at the LAr removal location, $\frac{dm_{\text{O2,LAr Tray}}}{dt}$ and $\frac{dm_{\text{N2,LAr Tray}}}{dt}$, are selected and required to be within a small tolerance, essentially at steady state, at the end of the time horizon. One may argue against the necessity of the final steady state constraint since the time scale of parameter changes could be significantly smaller than that of the process dynamics. This means that the plant could be required to adopt a new operating policy before reaching the steady state. However, if the final change in the demand is expected to be sustained, from the feasible operation perspective, the last action a plant undertakes should not lead to foreseeable instability.

Each path constraint is converted into a combination of endpoint and interior point inequality constraints, where the integral of the constraint violation is checked at the end of the time horizon and the bounds are enforced at each interior point [9, 19]. For example, the GO_2 product purity constraint is implemented as

$$y^{LB}_{\text{GO2}} \leq y_{\text{GO2}}(t) \Rightarrow \begin{cases} \dfrac{d\epsilon_{\text{GO2}}(t)}{dt} = [\max(0, y^{LB}_{\text{GO2}} - y_{\text{GO2}}(t))]^2 \quad \text{and} \quad \epsilon_{\text{GO2}}(t_f) \leq \varepsilon_{\text{GO2}} \\ y^{LB}_{\text{GO2}} \leq y_{\text{GO2}}(\bar{t}_j) \end{cases} \tag{4.12}$$

where ε_{GO2} is a pre-determined threshold and $\bar{t}_j$ represents the time corresponding to the jth interior point.

Table 4.1: Optimization Problem Constraints

Constraint	Type	Expression
System stability	Endpoint	$\left\|\frac{dm_{\text{O2,LAr Tray}}(t_f)}{dt}\right\| \leq \epsilon, \left\|\frac{dm_{\text{N2,LAr Tray}}(t_f)}{dt}\right\| \leq \epsilon$
GN_2 endpoint purity	Endpoint	$\text{PPMO}_{\text{GN2}}(t_f) \leq \text{PPMO}^{UB}_{\text{GN2 ep}}$
LAr endpoint purity	Endpoint	$\text{PPMO}_{\text{LAr}}(t_f) \leq \text{PPMO}^{UB}_{\text{LAr ep}}$
GN_2 purity constraint	Path	$\text{PPMO}_{\text{GN2}}(t) \leq \text{PPMO}^{UB}_{\text{GN2 trans}}$
LAr purity constraint (O_2)	Path	$\text{PPMO}_{\text{LAr}}(t) \leq \text{PPMO}^{UB}_{\text{LAr trans}}$
LAr purity constraint (N_2)	Path	$\text{PPMN}_{\text{LAr}}(t) \leq \text{PPMN}^{UB}_{\text{LAr trans}}$
GO_2 purity constraint	Path	$y_{\text{GO2}}(t) \geq y^{LB}_{\text{GO2}}$
O_2 content in crude Ar feed	Path	$y^{LB}_{\text{O2, crude}} \leq y_{\text{O2, crude}}(t) \leq y^{UB}_{\text{O2, crude}}$
UC tray temperature (Top)	Path	$T^{LB}_{\text{Top}} \leq T_{\text{Top}}(t) \leq T^{UB}_{\text{Top}}$
UC tray temperature (Middle)	Path	$T^{LB}_{\text{Middle}} \leq T_{\text{Middle}}(t) \leq T^{UB}_{\text{Middle}}$
UC tray temperature (Bottom)	Path	$T^{LB}_{\text{Bottom}} \leq T_{\text{Bottom}}(t) \leq T^{UB}_{\text{Bottom}}$
Liquid product storage	Endpoint	$ST_k^{\min} \leq ST_k(t_f) \leq ST_k^{\max}$

4.5 Results and Discussion

The study in this chapter intends to illustrate the idea of implementing reactive and preemptive control action and the benefit of cooperative operation of supply chain subsystems. Reactive operation allows the plant to adjust manipulated variable values only when an external change (e.g. demand and/or electricity price increase/decrease) reaches the plant. This means that system input trajectories are optimized only after the process parameter variation in a dynamic optimization (DO) calculation. On the other hand, with preemptive control, the plant can prepare for the change ahead of time such that input trajectories both before and after the external change are optimized. A prerequisite for adopting a preemptive control strategy is that the different supply chain segments share information about pricing and demand. However, key questions are: (1) how much time in advance such information should become available; (2) what the economic incentives are with preemptive control action; and (3) whether the improvements in the economic performance diminishes as the "preparation" time extends (as shown in Fig. 4.2).

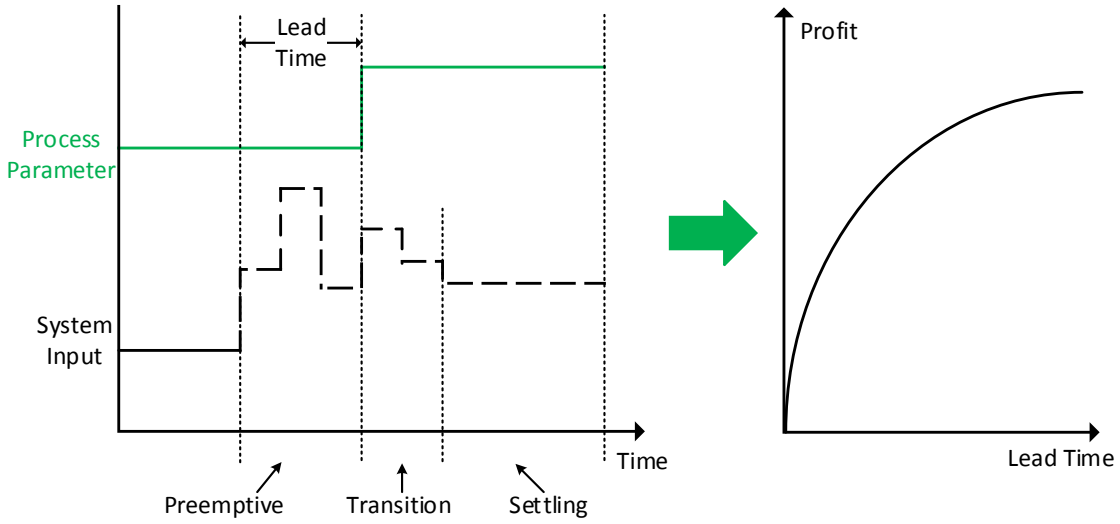

Figure 4.2: Input action categorization and lead-time definition.

In this study, we address these questions through solving dynamic optimization problems with positive and negative step changes in the GO_2 demand. For the demand increase case, operation strategies (1) with current manipulated variables (MVs), (2) with additional degrees of freedom from changing liquid level set-points during transitions, and (3) without changing the feed into the system are investigated. In case of the demand decrease, the full set of system MVs (excluding the inventory set-points) is utilized assuming either that the liquid market is under supplied or saturated. The entire control horizon can be categorized into preemptive, transition and settling periods, as illustrated in Fig. 4.2. When the optimization problem is solved with a nonzero lead time, the plant can take one or multiple actions during the preemptive period. In addition, regardless of the control action taken in preparation, when the external change occurs, the plant immediately responds by implementing rapid adjustments during the transition period. This is followed by a settling period, where the control inputs remain constant so that a new steady state can be reached. For all scenarios considered here, the plant operation starts from a reference point selected based on available plant data. Process flow rates presented in the remainder of this paper are scaled based on this point.

4.5.1 Preemptive Actions for an Increase in GO_2 Demand

With current operation degrees of freedom (full flexibility)

In this part of the study, starting from the reference point, the plant needs to compensate for a 10 % increase in the GO_2 demand without violating process constraints. Liquid and vapor air feed flow rates together with GO_2, LN_2 and LAr production rates are operational degrees of freedom and potential optimization variables (Fig. 4.1). The GN_2 demand remains unchanged at the reference value and all the liquids produced can be sold at given sale prices (Eqn. 4.7 is used).

With reactive control (RC), the duration of the preemptive period is zero (i.e. lead time, LT, equals 0). The solution of the RC case is used as a benchmark for comparison purposes (Benchmark Scenario 1) and is presented in Fig. 4.3. As shown, the plant is able to meet the GO_2 demand solely by direct production and no LO_2 product is consumed/vaporized due to the higher sale price. In order to meet the GO_2 demand while maintaining the high liquid production levels, the total air into the system increases. This led to GN_2 being produced at surplus at the final steady state. As soon as the plant is allowed to move, a significant amount of LAr production is withdrawn from the plant during the transition period, corresponding to the peak in the LAr impurity level during the transition (i.e. hitting the upper bound). In addition, the lower bound on the O_2 content in the crude argon feed is also active during transition.

When the GO_2 demand information is available in advance, the plant can take a single action (SA) or multiple changes (MA) during the preemptive period. In this study, the lead time increases with a constant increment, Δt (1 reference time unit $= 60\Delta t$). For example, when the duration of the entire preemptive period is $6\Delta t$, the plant can take 6 control actions with MA policy but only 1 adjustment with the SA operation. Fig. 4.4 summarizes the percentage profit improvements (PPI; reported as percentage of the hourly profit at the

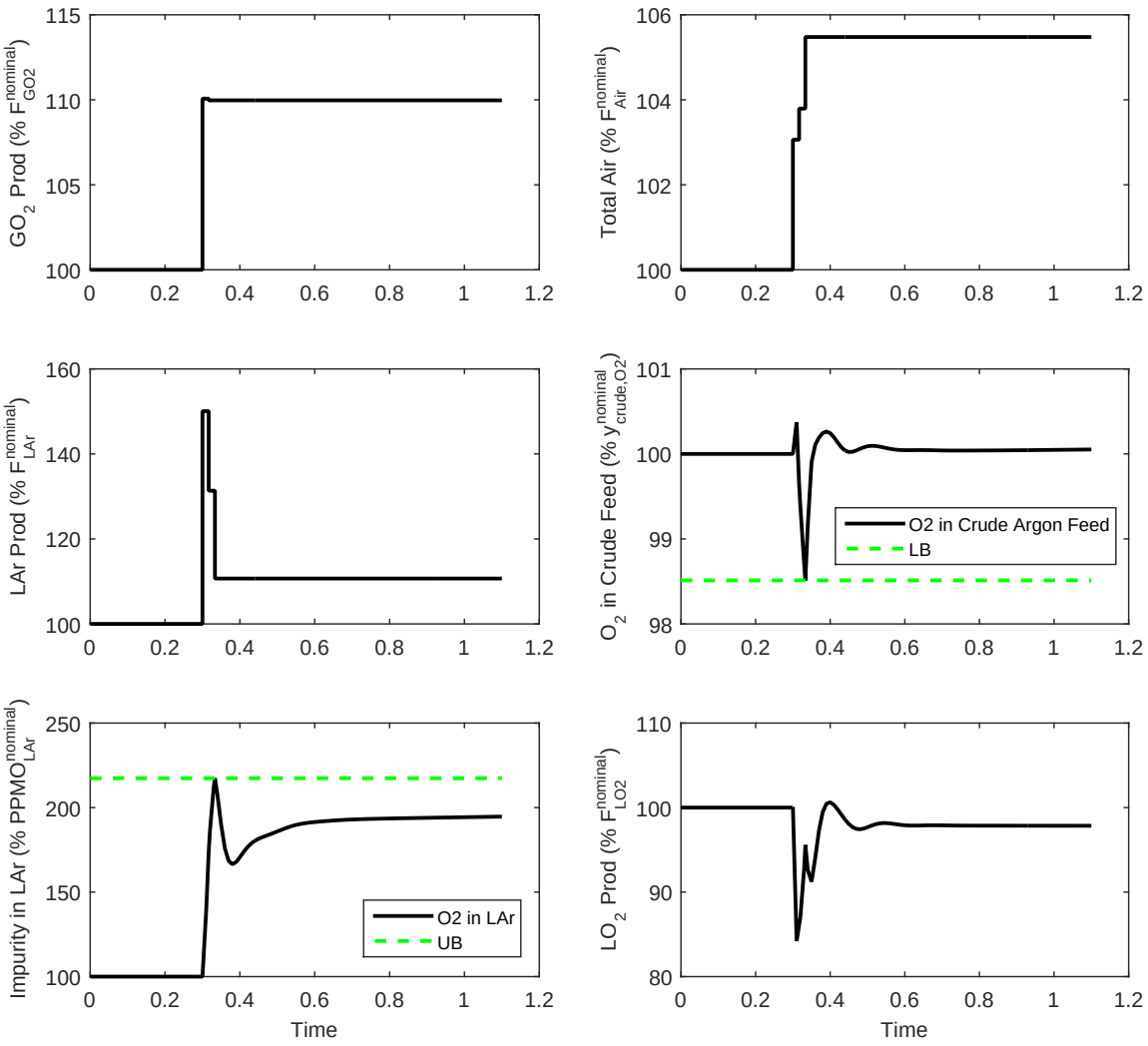

Figure 4.3: Trajectories of selected variables for the reactive case under a 10 % GO_2 demand increase, reported in scaled values.

reference condition) of the MA and SA cases at different LT levels. The plant's profit with preemptive control (PC) is better than that with the reactive control (RC), as indicated by the positive PPI. This means that there is an economic incentive for implementing PC. As the duration of the preemptive period extends, the plant's economic performance improves, but exhibits a diminishing trend. In addition, values of the objective function, i.e. accumulated profit, are higher in the MA case compared to the corresponding SA one, especially when the LT is longer (from 0 % at LT $= 2\Delta t$ to 0.4 % at LT $= 6\Delta t$). Fig. 4.5 shows input and response trajectories under preemptive action with a lead time of LT $= 5\Delta t$ for both SA and MA scenarios. The flexibility in operations due to multiple adjustments allows the plant to get closer to the bounds faster without violating the constraints. For example, it can be seen in Fig. 4.5 that with MA, more LAr is drawn from the process initially, leading to a rapid increase in the LAr impurity level to its limit. On the other hand, in the SA case, a less drastic action is taken, so that the LAr impurity approaches the bound slowly. The drawback of implementing the MA strategy is more oscillations in the resulting trajectories.

Similar to the RC case, the GO_2 demand is satisfied with production and there is no overproduction during the preemptive period with both SA and MA policies. When GO_2 demand increases, the optimization results suggest that the operator should load the plant: the air feed into the system increases. By doing so, LO_2 production does not need to be sacrificed as in the "liquid split" scenario presented later in this paper. At the end of the control horizon, compared to the result of acting reactively, preemptive actions lead the system settling at operation points having lower rates of air feed and LO_2 production (Fig. 4.3 vs. Fig. 4.5). Meanwhile, the LN_2 removal rate increases and the amount of over-supplied GN_2 reduces. Note that all the internal liquid inventory in the system (i.e. liquid holdup in the reboiler of main condenser and argon condenser, as well as liquid sump at lower column and super-stage column) all return to their set-points under PI control at the solution. The lower bound on the O_2 content in the crude argon feed is also active with PC. The impurity levels in LAr product hit the upper bound during transition and the constraint on the LAr PPMO remains

active at the final steady state with PC. These observations suggest that preemptive action indeed allows the plant to prepare for upcoming changes in process parameters so that improved economic performance can be achieved considering the dynamic response of the process. The differences in the final steady state are a result of the preparation and finite time horizon: when the GO_2 demand change happens, the plant is at different conditions, and when the accumulated profit is considered, the subsequent actions taken by the plant over the defined time horizon may be different. An additional dynamic optimization study is solved next to further illustrate the point.

A supporting DO problem is solved for LT $= 3\Delta t$ with the objective of maximizing the overall profit and an extra constraint to enforce the LO_2 production rate to be no less than that in the RC case at the end of the control horizon

$$\min_{\mathbf{u}(t)} \ \Phi_{\text{econ}} \tag{4.13a}$$

$$\text{subject to:} \quad \text{Process Model + Constraints} \tag{4.13b}$$

$$F_{\text{LO2}}^{\text{LT}=3\Delta t}(t_f) \geq F_{\text{LO2}}^{RC*}(t_f) - \epsilon \tag{4.13c}$$

where $F_{\text{LO2}}^{RC*}(t_f)$ is the final LO_2 production in Benchmark Scenario 1. The problem converged to a final steady state with system inputs settling at values close to those in Benchmark Scenario 1. The PPI realized here is smaller (i.e. 2.5 %) than that in the case without the LO_2 production constraint (Eqn. 4.13c), which is active at the solution. The results demonstrate that differences in the final steady state are the result of an economic decision (1) made based on the trade-off among different products and the operation cost, and (2) permitted by taking preemptive action. Even when forced to reach a similar final steady state, PC still can achieve better economic performance than RC.

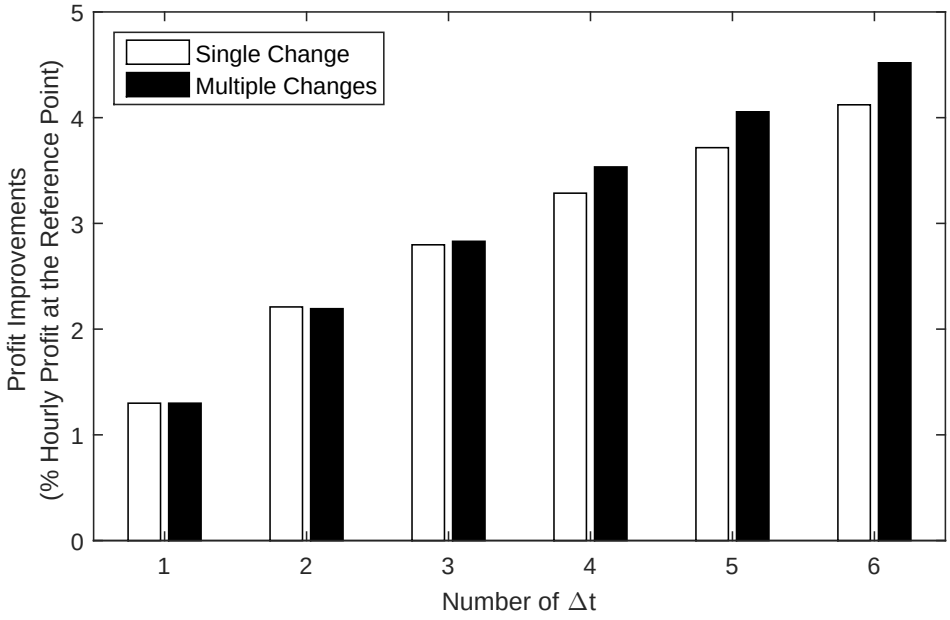

Figure 4.4: Improvement in the profitability with increasing lead time. Single action - one set of sustained preemptive actions regardless of the length of the lead time. Multiple actions - multiple actions with one set of control actions per Δt during the preemptive period. Lead time = 0 represents the result from the reactive controls (Benchmark Scenario 1).

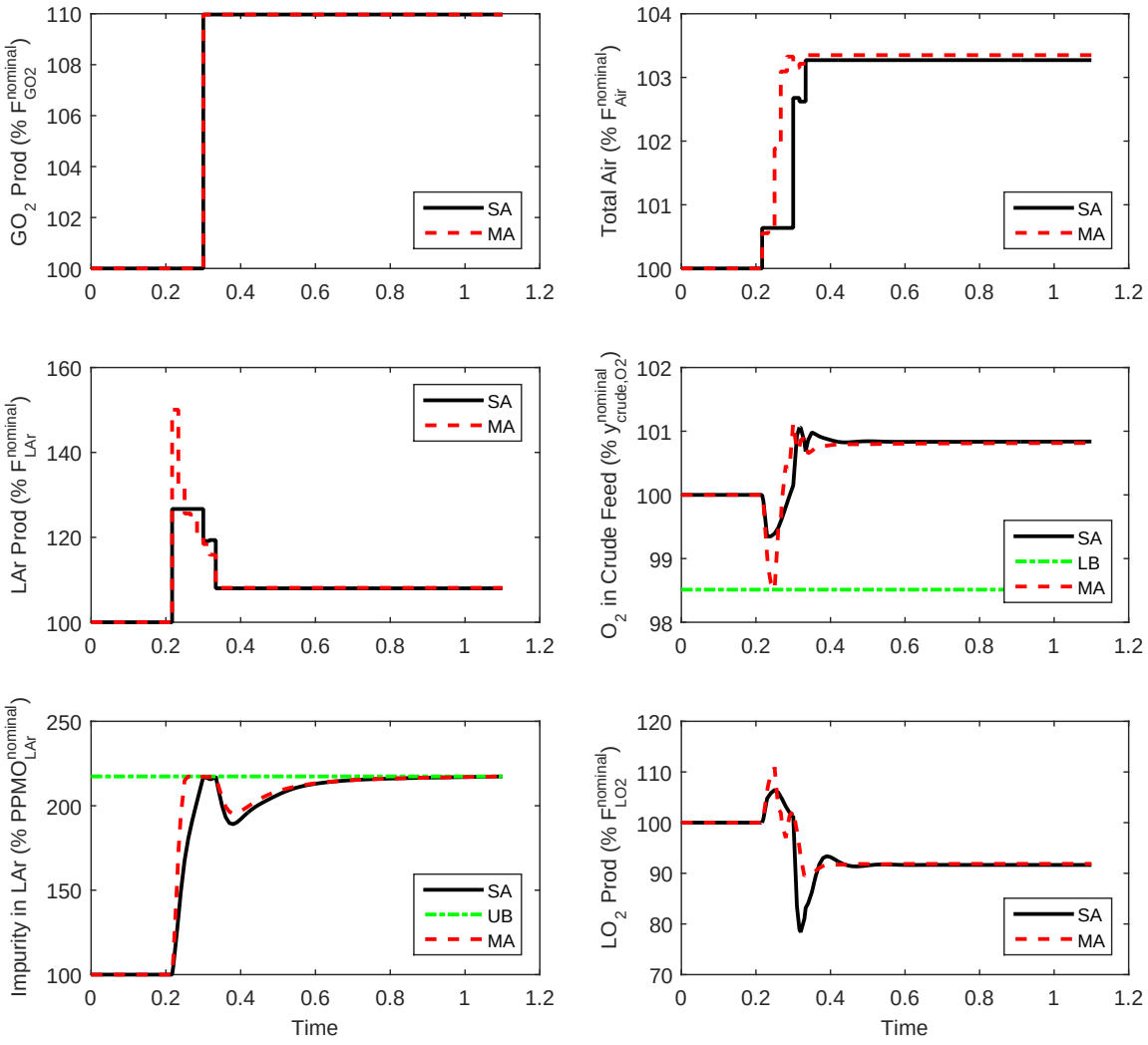

Figure 4.5: Trajectories of selected variables for the preemptive case with LT $= 5\Delta t$ under a 10 % GO_2 demand increase, reported in scaled values. SA = single set of preemptive actions; MA = multiple sets of preemptive actions; LB = lower bounds; UB = upper bounds.

Adding internal liquid inventory set-points (internal liquid)

A multi-product ASU has a significant amount of internal liquid inventory at different locations of the plant, such as inside the column and on the reboiler side of the integrated reboiler condenser (Fig. 1.1). Such liquid holdups lead to delays in the dynamic response of the process. However, when utilized properly, they might also have the potential to improve the plant's performance during transition. In this part of the study, the liquid level set-points for the LC sump and the reboiler side of the argon condenser are introduced as additional optimization variables. Different from other system inputs, changes in the level set-points only happen during preemptive and transition periods and need to return to the nominal value when the system settles. The performance of the proposed control strategy is compared to the solution for Benchmark Scenario 1 in the "full flexibility" section when the full set of operational degrees of freedom can be used.

As expected, the preemptive actions outperform the benchmark reactive case (Benchmark Scenario 1). At the solutions for all 6 lead time levels, the PPIs realized are higher with liquid level set-points compared to the corresponding case without (Fig. 4.6). The difference is more noticeable when the lead time is small and gradually diminishes as the preemptive period increases as shown in Fig. 4.6. This means that when the plant needs to respond to external changes at short notice, more flexible operation policies are favored. However, as the lead time increase, even with fewer handles, more actions can be taken to prepare the plant for the upcoming demand change. After a certain point, the economic benefits achieved through introducing flexibility through additional operation degrees of freedom and control intervals diminish and level out.

Optimal trajectories of selected variables when LT $= 2\Delta t$ are presented in Fig. 4.7 (solid line). Simulation results with constant liquid level set-points but keeping other inputs as in the optimal solution are shown by the dashed line in Fig. 4.7. Note that argon condenser liquid level set-point is increased initially during the transition. The liquid level in the reboiler

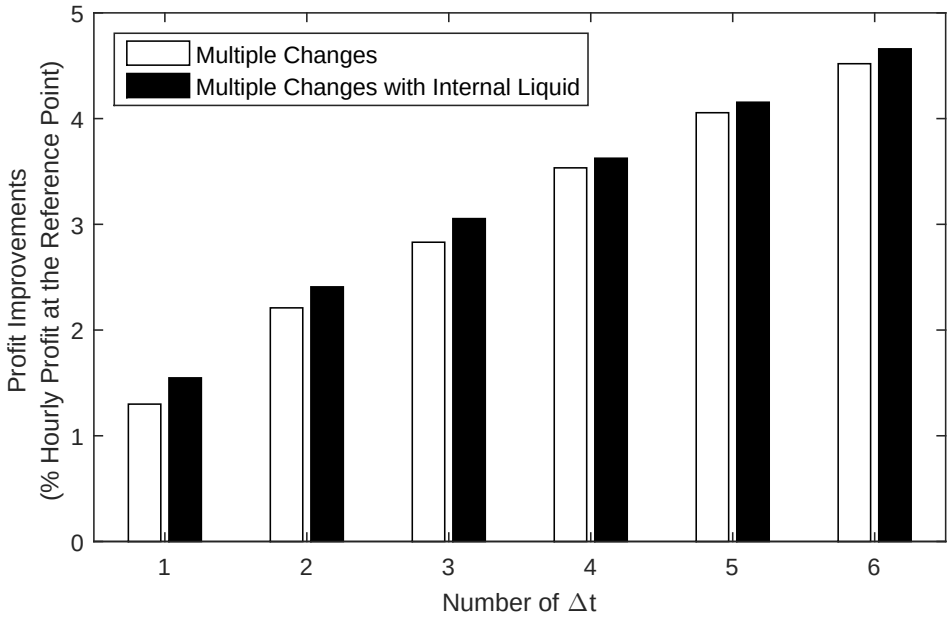

Figure 4.6: Improvement in the profitability with increasing lead time, with and without inventory set-point manipulation. Lead time = 0 represents the result from the reactive controls (Benchmark Scenario 1).

side of argon condenser (AC) is controlled by manipulating the amount of lower column (LC) bottom liquid entering: a increasing set-point means elevated liquid inlet and more super-stage top vapor can be condensed (i.e. reflux) to assist the LAr production peak. Such behavior is illustrated when comparing trajectories of the AC liquid inlet flow for the optimal and simulation solutions. As vapor is being condensed, the pressure on the condenser side of the AC drops, leading the pressure driven argon feed to increase. However, as more LC bottom liquid is being sent to the AC reboiler, the level in the LC sump drops. Since the LC sump level is controlled by adjusting the liquid outlet to the upper column (UC), the flow rate of this stream will drop. The strategy found at the optimal solution tries to overcome the problem by decreasing the level set-point (note the initial increase in the UC liquid inflow); however, this leads to noticeable oscillations in the flow rate of the liquid stream to the UC.

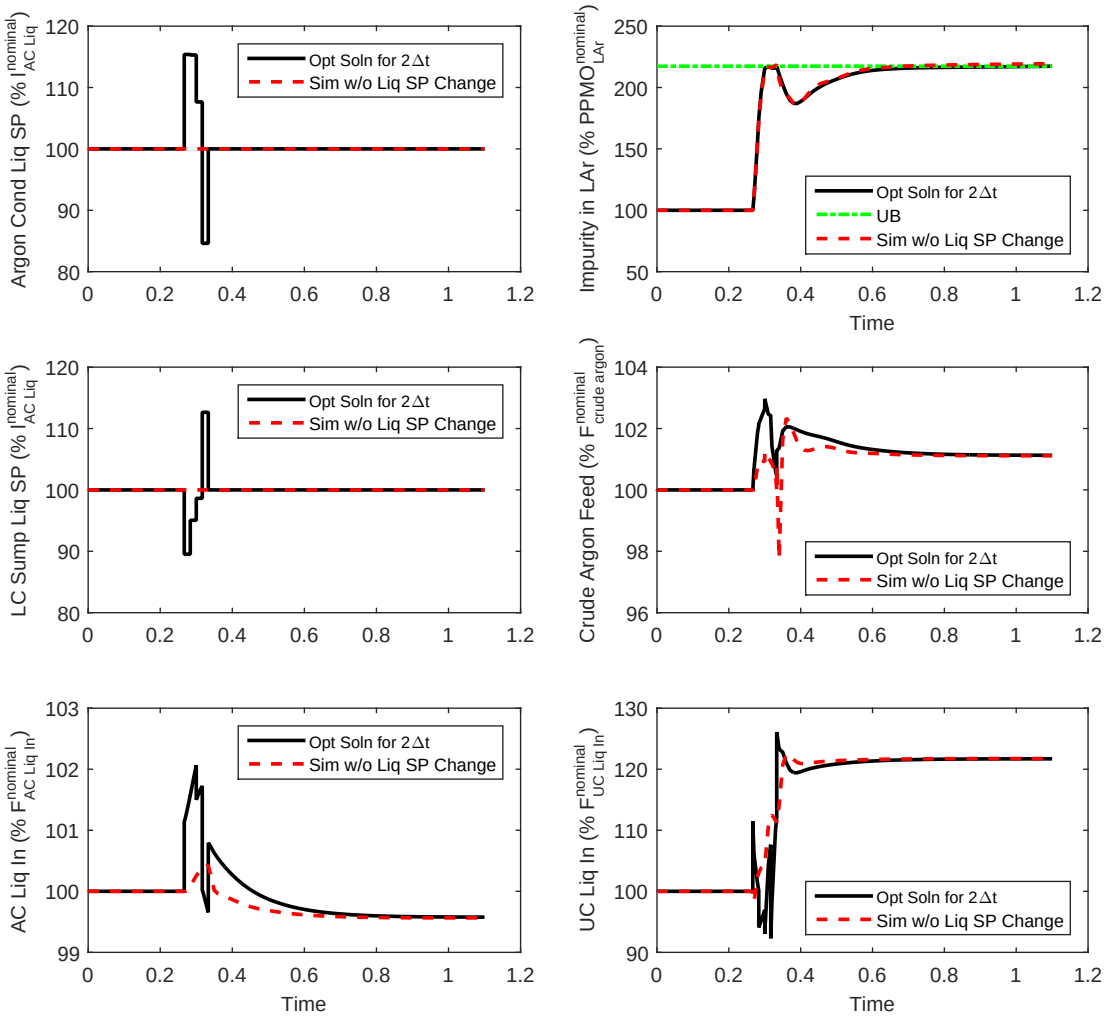

Figure 4.7: Trajectories of selected variables for the preemptive case (MA with LT $= 2\Delta t$) under a 10 % GO_2 demand increase, reported in scaled values. The optimal solution is indicated by the solid line (–). The dashed line (- -) shows the simulation result with the optimal solution except for use of constant liquid level set-points.

Without changing the feed stream flow rate (liquid split)

Sometimes, the plant needs to accommodate a GO_2 demand increase without loading the plant. This could be due to a strategic decision made based on forecasted electricity price, plant capacity, or operating practice such as maintaining a stable air feed rate. With a constant feed into the system, the rate of O_2, N_2 and Ar molecules entering the system is constant. Hence, in order to ramp up the GO_2 production, the LO_2 production rate is reduced when the system stabilizes at the new steady state. To prevent overcooling the system due to refrigeration accumulation (now a smaller amount of O_2 leaves the system as "cold" liquid), the amount of "cold" LN_2 entering the UC needs to be reduced. As shown in Fig. 1.1, the condensed N_2 stream from the MC is split into LN_2 product and LN_2 to the UC, hence, the LN_2 production rate needs to be increased. This will lead to decreased flows of the gas phase N_2 streams (i.e. WN_2 and GN_2) through the overall N_2 material balance. In other words, the "liquid split" of the plant needs to be changed from LO_2 to LN_2 mode. Here, the benefit of preemptive action is evaluated under this operation paradigm.

Since changes in the feed are not allowed, a trajectory tracking problem is solved first for the 10 % GO_2 demand increase:

$$\min_{\mathbf{u}(t)} \ \Phi_{\text{traj}} = \int_{t_0}^{t_f} \left[\frac{F_{\text{GO2, prod}}(t) - D_{\text{GO2}}(t)}{D_{\text{GO2}}(t)} \right]^2 dt \tag{4.14}$$

with decision variables consisting of production rates of GO_2, LN_2 and LAr. The purpose is to check how closely the produced GO_2 flow can track the demand change. The optimal solution shows that such a demand change can be achieved essentially instantaneously by production, which means that in the absence of an economic objective, no liquid vaporization is needed. This also indicates that when the problem is solved with the objective of maximizing profit, any vaporized LO_2 usage is due solely to economic considerations.

The reactive control case is solved with the economic-based objective function to obtain

a benchmark solution (Benchmark Scenario 2). The same processing cost is assigned to the vaporization of LO_2 and LN_2 products. Resulting trajectories of selected variables are shown in Fig. 4.8. During the transition, there is a period that GO_2 production does not meet the 10 % demand increase. As the demand has to be satisfied through either production or vaporization, this means that LO_2 vaporization must be practiced. As expected, LO_2 is produced at a reduced rate when the system reaches the new steady state (i.e. approximately 15 % smaller than that in the reactive “full flexibility" case). Meanwhile, more LN_2 is withdrawn from the system (i.e. approximately 54 % higher than the initial value), leading to a corresponding lower GN_2 production rate (i.e. 2.6 % less). Since here the GN_2 demand is assumed to correspond to the nominal production rate, LN_2 product needs to be vaporized. These observations are consistent with operation expectations. During transitions, the bound on the LAr product impurity is active. Although the compression cost here is smaller in comparison to Benchmark Scenario 1 in the “full flexibility" section, due to reduced production of LO_2 and GN_2, the overall profit is lower (LO_2 is more expensive than LN_2).

Preemptive action also yields positive PPIs in all 6 cases evaluated (reported relative to the result of Benchmark Scenario 2). However, for the same amount of lead time, the profit for the fixed air case is lower than that for the corresponding “full flexibility" case. A diminishing trend is also observed as the preemptive period expands (Table 4.2). As shown in Fig. 4.9, with preemptive action, GO_2 production follows the demand change exactly (i.e. no LO_2 driox is used). The LAr impurity level stays closer to the bound for the majority of time in the horizon. When the system settles at the solution, all liquid levels return to the set-points. The various paths taken during the preemptive period lead to different process dynamics and subsequent control actions. Hence, determining operating policies without considering process dynamics can lead to less desirable strategies.

Remark

Three operation setups are evaluated: (1) full flexibility, (2) with additional internal liquid, and (3) liquid split. Regardless of the choice of operation setup, taking preemptive control

Table 4.2: Profitability vs Lead Time for 10 % Increase in GO_2 Demand without Feed Flow Rate Changes

Lead Time (Number of Δt)	Profit Improvement (% of Hourly Profit at the Reference Condition)
0 †	0
1	1.09
2	2.03
3	2.76
4	3.37
5	3.90
6	4.39

† Lead time = 0 corresponds to the reactive control case without loading the plant.

action is shown to improve the plant's profitability. While a significantly long lead time in notifying the demand increase may not be necessary as the benefit diminishes over time, it is beneficial for ASUs and customers to share production plans and demand requirements in advance. When the operation flexibility is high (more MVs), a shorter preemptive period is required to achieve the same PPI. This means that the plant should identify and leverage additional operational degrees of freedom when it is required to react to the change within a short time period.

4.5.2 Preemptive Actions for a Decrease in GO_2 Demand

Through the previous sets of case studies, it is shown that preemptive action yields economic benefits when the plant faces GO_2 demand increases. In this section, the plant is subject to a 10 % decrease in the GO_2 demand, while the GN_2 demand is assumed to be constant at 60 % of the nominal production rate. As demands for gaseous product decrease, the operator could unload the plant to reduce the electricity consumption and the operation costs. However, according to the analysis in the "liquid split" scenario, if the feed rate is maintained at the current level, more LO_2 could be produced. Hence, the most cost-effective operation depends on the liquid product market situation.

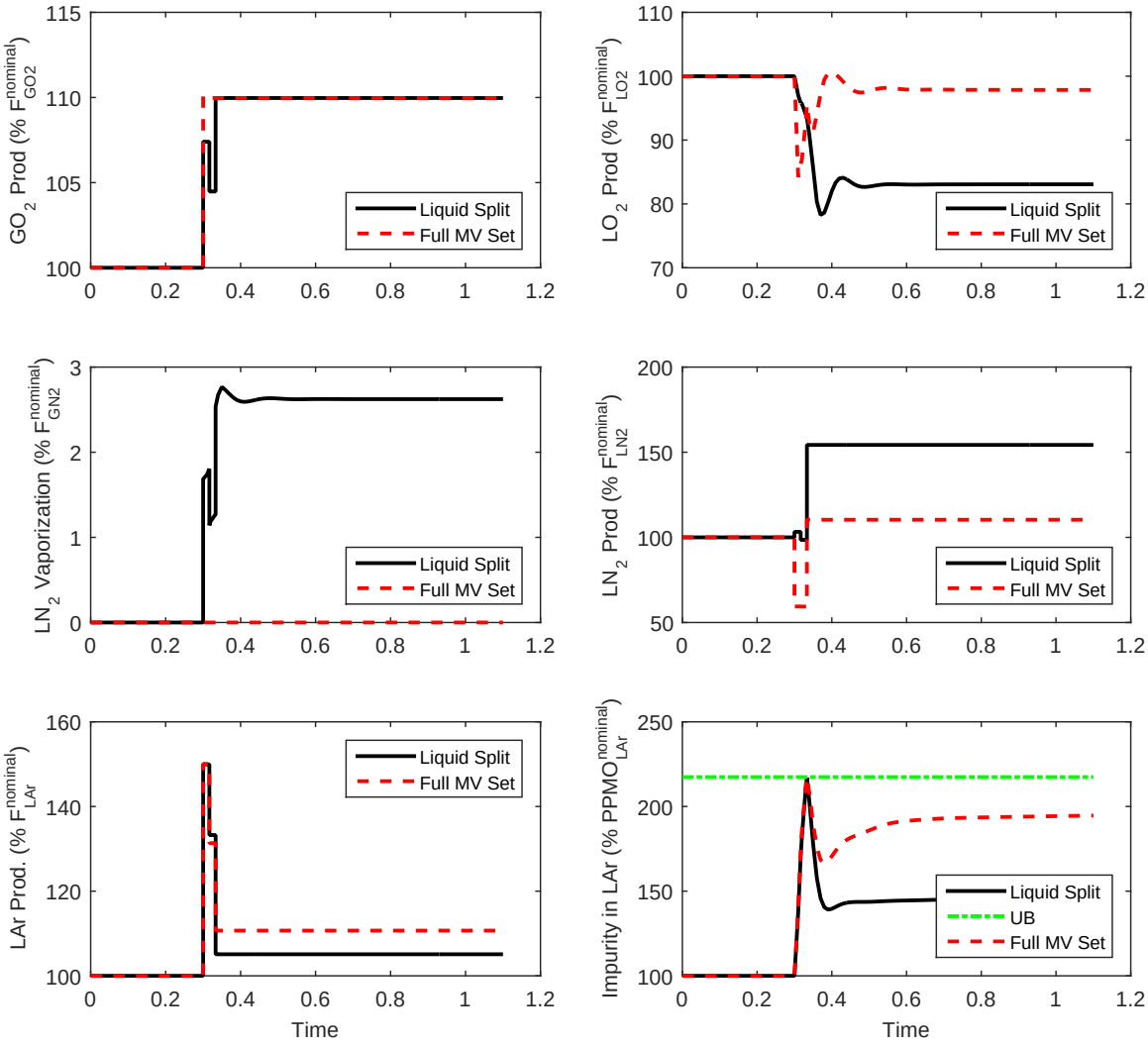

Figure 4.8: Trajectories of selected variables for reactive case under a 10 % GO_2 demand increase, reported in scaled values with and without feed rate changes. Liquid split = without feed flow rate changes.

Under supplied LO_2 market

If the overall LO_2 market is unsaturated or under-supplied, customers (current or new) are capable of absorbing the potential increase in the liquid production. In other words, all product generated can be sold at the given price. Hence, Eqn. 4.7 is used to estimate

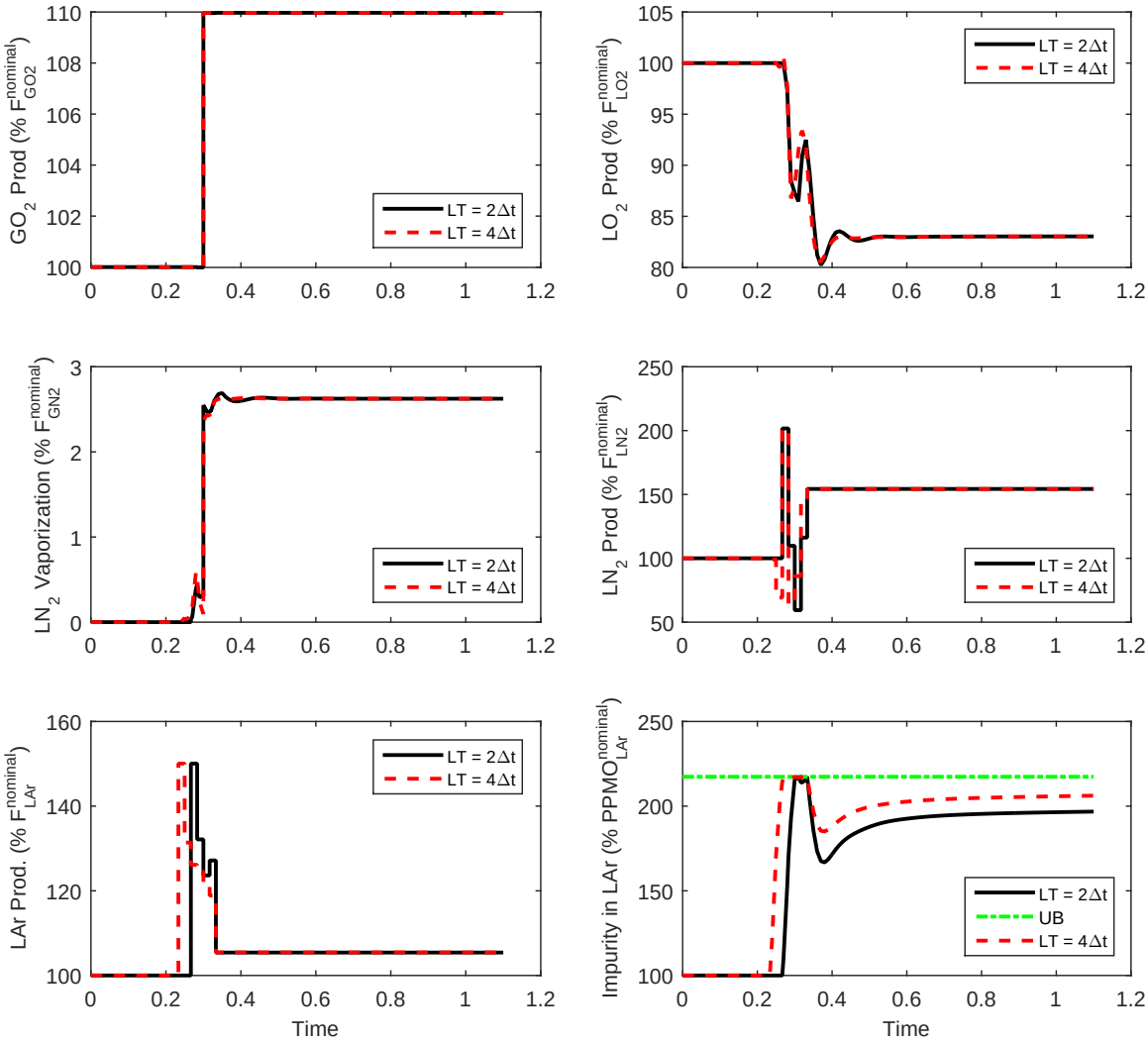

Figure 4.9: Trajectories of selected variables for preemptive cases under a 10 % GO_2 demand increase without feed flow rate change, reported in scaled values.

Table 4.3: Profitability vs Lead Time for 10 % Decrease in GO_2 Demand in Under-Supplied LO_2 Market

Lead Time (Number of Δt)	Profit Improvement (% of Hourly Profit at the Reference Condition)
0 †	0
1	1.58
2	2.96
3	4.05
4	5.07
5	5.82
6	6.41

† Lead time = 0 corresponds to the reactive control case solved under the same set of assumptions.

the revenue from liquid products. Seven dynamic optimization problems are solved here: one reactive and six preemptive action cases. PPIs realized at solutions of these cases are summarized in Table 4.3. As in the demand increase cases, preemptive control is also seen to yield economic improvement when the plant is facing a decrease in the GO_2 demand. The PPI increases with the lead time but experiences a diminishing trend.

Trajectories of GO_2 and LO_2 production, total air feed and O_2 content in the crude feed with reactive and preemptive control (LT = $6\Delta t$) are presented in Fig. 4.10. Similar to the demand increase case, the plant production follows the GO_2 demand closely: demand is satisfied solely with production. However, with reactive control there is a small amount of over-supply. Since all the LO_2 produced is sold at the given price, more liquid is generated: LO_2 production increased by more than 16 % when settled. Meanwhile, the final value of the total air feed is very close to that at the reference point (Fig. 4.10). The LAr production rate peaks during transition and eventually settles at a value higher than that at the reference point. The LAr product purity constraint is active during transition and remains active at the final steady state in the PC case. During the transition, the lower bound on the O_2 content in the crude feed is active (Fig. 4.10).

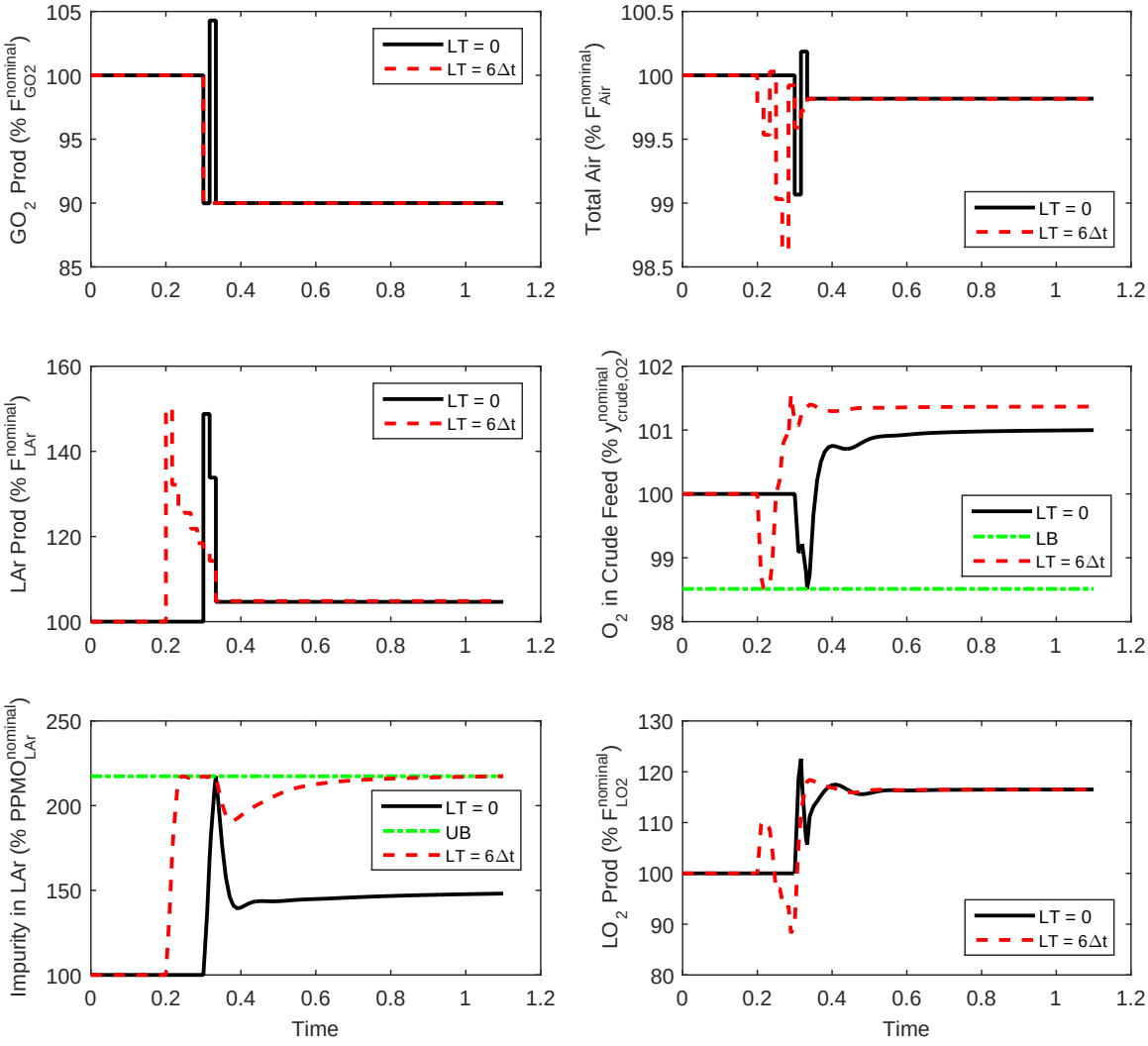

Figure 4.10: Trajectories of selected variables with preemptive controls (LT = $6\Delta t$) in response to a 10 % GO_2 demand decrease (under-supplied liquid market), reported in scaled values.

Saturated LO_2 market

When the liquid market is saturated, the customer cannot absorb the product supplied at surplus. Hence, the economic value of the liquid product is realized through either direct sale (up to the demand level) or vaporized to meet the gaseous demand (less feed needs to be processed). In this case, the revenue from selling liquid is calculated using Eqn. 4.11. The accumulated LO_2 produced is the main concern, hence, $\overline{ST}_{\mathrm{LO2}}$ demand is constrained to be $\int_0^{t_f} F_{\mathrm{LO2}}^{\mathrm{nominal}}(t)dt$, where t_f is the duration of the entire control horizon. Demands for LN_2 and LAr are not limited here. PPIs realized at solutions of 1 reactive and 6 preemptive cases are summarized in Table 4.4. Similar trends are also observed in this part of the study.

Trajectories of total air feed, LO_2 production, vaporization of LO_2 and LAr production rate are shown in Fig. 4.11 for reactive and preemptive (LT $= 6\Delta t$) control. In both cases, the total air feed into the system decreases significantly (in contrast to the case with an under-supplied LO_2 market). Meanwhile the production rate of LO_2 returns to a point close to its nominal value after some oscillations during transition. There is a noticeable peak in the LO_2 production with the reactive action. Since the oversupplied LO_2 cannot directly lead to increased revenue, at the solution, a portion of the liquid is vaporized for the GO_2 demand, with a corresponding temporary decrease in GO_2 production, as can be seen in Fig. 4.11. Note that for negative step changes, the demand can always be met by production. In addition, in the reactive case the final LO_2 is approximately 0.7 % lower than the nominal rate under the saturated market assumption. However, as the plant is able to take more preparatory action to assist the transition in the preemptive case, the large peak in LO_2 production does not occur and the GO_2 demand is met solely by GO_2 production, without liquid vaporization as in the reactive case. The LAr purity constraint, together with the LB on O_2 content in crude argon feed are active during the transition.

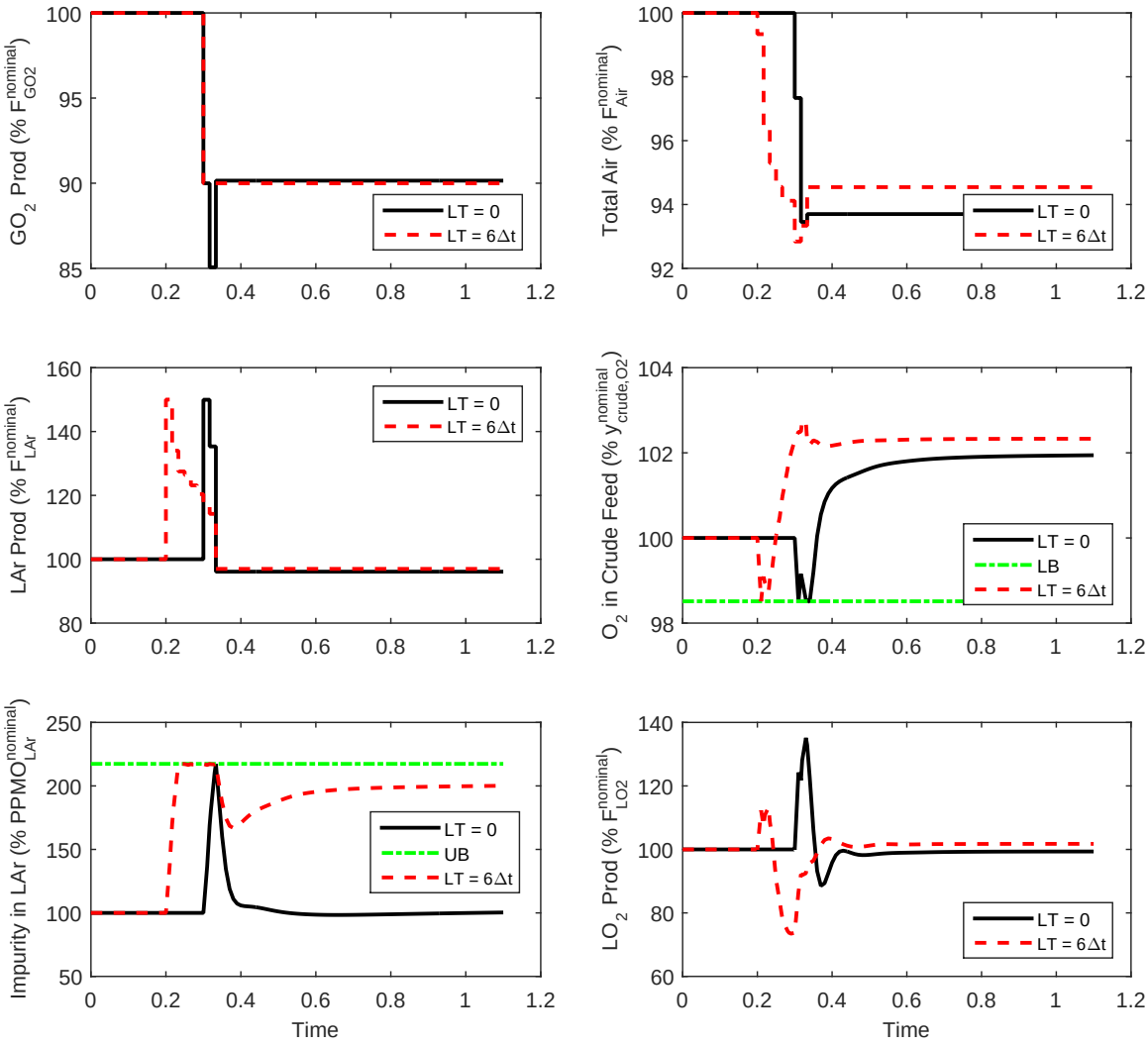

Figure 4.11: Trajectories of selected variables with reactive and preemptive control in response to a 10 % GO_2 demand decrease (saturated liquid market), reported in scaled values.

Table 4.4: Profitability vs Lead Time for 10 % decrease in GO_2 demand in Saturated Liquid Market

Lead Time (Number of Δt)	Profit Improvement (% of Hourly Profit at the Reference Condition)
0 †	0
1	2.87
2	4.46
3	5.91
4	7.33
5	8.72
6	10.02

† Lead time = 0 corresponds to the reactive control case solved under the same set of assumptions.

4.6 Conclusion

This study compares the economic performance of preemptive and reactive operations for a multi-product air separation unit in response to GO_2 demand changes. A high fidelity dynamic model based on the collocation approach is embedded in the optimization formulation to represent the plant. It is shown that there are economic incentives for taking preemptive action, with such a strategy leading to higher profit. As the lead time increases, more cost effective operation can be achieved. However, a very long lead time is not necessary as the improvements gradually diminish. These observations are consistent in all cases presented in this paper, regardless of the direction of the GO_2 demand change, whether manipulated variables are added or removed, and assumptions with respect to the liquid market. When the lead time is small, the plant performs better if more system inputs can be leveraged, but the difference reduces as the duration of the preemptive period increases. In addition, preemptive controls tend to result in operations that push the system closer to the operation bounds. LAr product purity, UC tray temperatures at selected locations and the O_2 content in the crude feed need to be carefully monitored to ensure feasible operation. Even when the differences in the values of manipulated variables between the reactive and preemptive cases are negligible at the final steady state, the system could respond differently during

transitions.

Bibliography

[1] T. Backx, O. Bosgra, and W. Marquardt. “Towards intentional dynamics in supply chain conscious process operations”. In: *Proceedings of Third International Conference on Foundations of Computer-Aided Process Operations*. Ed. by J. F. Pekny, G. E. Blau, and B. Carnahan. American Institute of Chemical Engineers. Snowbird, Utah, 1998, pp. 5–20 (cit. on p. 92).

[2] G. Y. Zhu, M. A. Henson, and L. Megan. “Low-order dynamic modeling of cryogenic distillation columns based on nonlinear wave phenomenon”. In: *Separation and Purification Technology* 24 (2001), pp. 467 –487 (cit. on p. 92).

[3] Q. Zhang et al. “Air separation with cryogenic energy storage: Optimal scheduling considering electric energy and reserve markets”. In: *AIChE J.* 61.5 (2015), pp. 1547–1558 (cit. on pp. 92, 97).

[4] J. D. Figueroa et al. “Advances in CO_2 capture technology - The U.S. Department of Energy’s Carbon Sequestration Program”. In: *International Journal of Greenhouse Gas Control* 2.1 (2008), pp. 9 –20 (cit. on p. 92).

[5] Z. Chen et al. “Nonlinear model predictive control of high purity distillation columns for cryogenic air separation”. In: *IEEE Transactions on Control System Technology* 18.4 (2010), pp. 811 –821 (cit. on p. 92).

[6] J. Miller et al. “Improving agility of cryogenic air separation plants”. In: *Industrial & Engineering Chemistry Research* 47.10 (2008), pp. 394 –404 (cit. on pp. 93, 95, 96).

[7] Y. Zhu, S. Legg, and C. D. Laird. “A multiperiod nonlinear programming approach for operation of air separation plants with variable power pricing”. In: *AIChE Journal* 57.9 (2011), pp. 2421 –2430 (cit. on pp. 93, 96).

[8] U.S. Energy Information Administration. *Manufacturing energy consumptionsurvey*. Online. Available at: http://www.eia.gov/consumption/data.cfm. 2012 (cit. on p. 93).

[9] V. White, J. D. Perkins, and D. M. Espie. “Switchability analysis”. In: *Computers & Chemical Engineering* 20.4 (1996), pp. 469 –474 (cit. on pp. 95, 103).

[10] Y. Cao et al. “Optimization-based assessment of design limitations to air separation plant agility in demand response scenarios”. In: *Journal of Process Control* 33 (2015), pp. 37 –48 (cit. on p. 95).

[11] R. Pattison et al. “Optimal process operations in fast-changing energy markets: Framework for scheduling with low-order dynamic models and an air separation application”. In: *Industrial & Engineering Chemistry Research.* 55.16 (2016), pp. 4562 –4584 (cit. on p. 96).

[12] Y. Zhu, S. Legg, and C. D. Laird. “Optimal operation of cryogenic air separation systems with demand uncertainty and contractual obligations”. In: *Chemical Engineering Science* 66.5 (2011), pp. 953 –963 (cit. on p. 96).

[13] M. G. Ierapetritou et al. “Cost minimization in an energy-intensive plant using mathematical programming approaches”. In: *Industrial & Engineering Chemistry Research* 41.21 (2002), pp. 5262 –5277 (cit. on p. 96).

[14] M. H. Karwan and M. F. Keblis. “Operations planning with real time pricing of a primary input”. In: *Computers & Operations Research* 34.3 (2007), pp. 848 –867 (cit. on pp. 96, 97).

[15] S. Mitra et al. “Optimal production planning under time-sensitive electricity prices for continuous power-intensive processes”. In: *Computers & Chemical Engineering* 38 (2012), pp. 171 –184 (cit. on pp. 96, 97).

[16] S. Mitra et al. “Robust Scheduling under Time-sensitive Electricity Prices for Continous Power-intensive Processes”. In: *FOCAPO 2012: Foundations of Computer-Aided Process Operations*. Foundations of Computer-AidedProcess Operations. Savannah, Georgia January 8 - 11, 2012 (cit. on p. 97).

[17] S. Mitra, J. M. Pinto, and I. E. Grossmann. “Optimal multi-scale capacity planning for power-intensive continuous processes under time-sensitive electricity prices and demand uncertainty. Part I: Modeling”. In: *Computers & Chemical Engineering* 65.0 (2014), pp. 89 –101 (cit. on p. 97).

[18] Y. Cao et al. “Dynamic modeling and collocation-based model reduction of cryogenic air separation units”. In: *AIChE J.* 62.5 (2016), pp. 1602–1615 (cit. on pp. 97, 98, 103).

[19] V. S. Vassiliadis, R. W. H. Sargent, and C. C. Pantelides. “Solution of a class of multistage dynamic optimization problems. 2. Problems with path constraints”. In: *Industrial & Engineering Chemistry Research* 33.9 (1994), pp. 2111–2122 (cit. on p. 103).

Chapter 5

Conclusions and Future Work

5.1 Concluding Remarks 129
5.2 Future Work 131

In this final chapter, the main contributions of this thesis are summarized and further directions are noted.

5.1 Concluding Remarks

In this work, we studied dynamic modeling and optimization of air separation units with the objective of assisting the transition of such a process towards the high adaptability desired by current dynamic and competitive markets.

In Chapter 2, we explained the modeling efforts involved, focusing on the cold-box section of a super-staged argon plant. The first aspect is the two different approaches for representing distillation columns: full order stage-wise models and collocation based reduced order model. Despite its large size and nonlinearity, the vapor liquid equilibrium based, first principles model is shown to achieve the prediction accuracy comparable to that of the high fidelity model, provided by the industrial collaborator. Collocation based model reduction was then performed and proven to be an effective solution due to significant model size and simulation time reduction without sacrificing desired accuracy. The second issue addressed in this part of the study is deriving a mathematical representation for the primary heat exchanger, a multi-stream heat exchange with phase change. A novel stage-wise moving boundary model is proposed and its ability to track the occurrence of phase change is demonstrated. Collocation based approximation is later applied to reduce the size of this model. Dynamic

simulation results showed consistent results with operation expectation. This modeling work is the foundation of the entire study.

In Chapter 3, we investigated the multi-period dynamic operation of a nitrogen plant with a liquid storage tank. An integrated plant model based on the collocation approach described in Chapter 2 is used. Under varying electricity price and customer demand, the plant can collect liquid through direct liquid production or gas product liquefaction, and choose to either vaporize the liquid for meeting the gas demand or introduce the liquid back to the column as additional reflux. It is shown that operational bottlenecks due to process dynamics (captured through the dynamic model) indeed impact the realizable profit and selection of operation strategies. Due to the constraint on reboiler level, it could be more economical to collect liquid through the more expensive gas product liquefaction. It is also illustrated that the storage-then-utilization strategy is economically attractive when there are significant variations in electricity price. In the move suppression layer, three objective function formulations, trajectory tracking, hyperbolic function and valve dynamics approximations, are proposed and demonstrated as being effective in obtaining smooth operation trajectories.

In Chapter 4, we evaluated the economic performance of preemptive action in the context of demand changes, assuming the gas customer shares such information with the plant. The problem is solved for an ASU producing three liquid and two gasesous products. Through the study, it is illustrated that there certainly is economic incentive for practicing preemptive control yielding a positive percentage profit improvement, compared to the corresponding reactive solution. However, for the same scenario, the improvement in the overall profit experiences a diminishing trend as the lead time extends. These observations are consistent regardless of the problem setup: the direction of the demand change, the set of the operational inputs used and the assumption of market conditions. In addition, the number of operational degrees of freedom has more impact when the lead time is short. LAr purity constraints are identified as critical bounds in operation of the plant, while, the O_2 content

in the crude feed needs to be carefully monitored during transitions.

5.2 Future Work

Aspects for further work are noted here.

- The dynamic optimization formulation for the multi-period scheduling problem can be extended to consider design decisions including storage tank sizing and the feed location of the additional reflux. Uncertainties in electricity price and demand could be considered in the detailed financial analysis following a multi-scenario based approach, with design parameters and operation trajectories as the first and second stage decisions, respectively. Considering the potential size of the problem, the nitrogen plant with the collocation based model is recommended for this work.

- Another topic is optimal operation policy under disturbances, such as variations in ambient temperature, T_{amb}. Changes in T_{amb} affect process efficiency through the air inlet, cooling water in the multi-stage compressor system and the heat leakage in the cold-box. Note that the heat leakage term is readily captured in both the nitrogen and multi-product plants, and the nitrogen plant also has a detailed compressor model.

- The third topic could be operations with control structure included. Issues such as variable interaction due to control loop pairing and valve saturation might introduce additional complexity in the plant operation, but the control logic should also help to stabilize the system, leading to different operation policies. Under this topic, the control loop pairing together with the tuning parameters can also be optimized.

- The last topic is optimization assisted plant startup. In order to address this issue, modeling efforts need to be invested at the initial stage of the project so that process behavior can be captured. This task is challenging, but improvements in the startup agility could lead to significant savings. In addition, the plant could be more responsive

towards changes in electricity price/demand: more frequent startup and shutdown in addition to loading and unloading. Note that accurate representations of such discrete events have not been used in scheduling and planning studies.

When a longer control time horizon is considered (i.e. a couple of days) under the above identified subjects, to reduce the computational effort, a different time discretization grid can be implemented as time proceeds. For example, an hourly grid may be used for the immediate 12 hours and four-hour intervals afterwards.

Notation

Acronyms	Meaning
AC	argon condenser
ASU	air separation unit
CES	cryogenic energy storage
CP	collocation point
DAE	differential algebraic equation (AE)
DO	dynamic optimization
DR	demand response
FE	finite element(s)
FOSM	full-order stage-wise model
GO_2, GN_2	gas oxygen and nitrogen
HX	heat exchanger
IRC	integrated reboiler-condenser
LAr, LO_2, LN_2	liquid argon, oxygen and nitrogen
LB	lower bound(s)
LC	lower column
LRC	lower-ratio column
LT	lead time
MA	multiple sets of preemptive actions
MSHX	multi-stream heat exchanger
MV	manipulated variable
NMPC	nonlinear model predictive control
NWT	nonlinear wave theory
ODE	ordinary differential equation
OTS	operator training simulator
PC	preemptive control
PHX	primary Heat Exchanger
PI	proportional integral
PPI	percentage profit improvements
PPMN, PPMO	parts per million nitrogen and oxygen
RC	reactive control
RTP	real-time pricing
SA	single set of preemptive actions
SC	subcooled
SH	superheated
SSC	super-staged column
TB	turbine
TOU	time-of-use pricing
TP	two-phase
UB	upper bound(s)
UC	upper column